



applied sciences

Cartilage Repair and Regeneration

Focus on Multi-Disciplinary Strategies

Edited by

Marta Anna Szychlinska and Giuseppe Musumeci

Printed Edition of the Special Issue Published in *Applied Sciences*

Cartilage Repair and Regeneration: Focus on Multi-Disciplinary Strategies

Cartilage Repair and Regeneration: Focus on Multi-Disciplinary Strategies

Editors

Marta Anna Szychlinska

Giuseppe Musumeci

MDPI • Basel • Beijing • Wuhan • Barcelona • Belgrade • Manchester • Tokyo • Cluj • Tianjin



Editors

Marta Anna Szychlinska
University of Palermo
Italy

Giuseppe Musumeci
University of Catania
Italy

Editorial Office

MDPI
St. Alban-Anlage 66
4052 Basel, Switzerland

This is a reprint of articles from the Special Issue published online in the open access journal *Applied Sciences* (ISSN 2076-3417) (available at: https://www.mdpi.com/journal/applsci/special-issues/cartilage_repair_regeneration).

For citation purposes, cite each article independently as indicated on the article page online and as indicated below:

LastName, A.A.; LastName, B.B.; LastName, C.C. Article Title. <i>Journal Name</i> Year , <i>Volume Number</i> , Page Range.
--

ISBN 978-3-0365-3939-3 (Hbk)

ISBN 978-3-0365-3940-9 (PDF)

© 2022 by the authors. Articles in this book are Open Access and distributed under the Creative Commons Attribution (CC BY) license, which allows users to download, copy and build upon published articles, as long as the author and publisher are properly credited, which ensures maximum dissemination and a wider impact of our publications.

The book as a whole is distributed by MDPI under the terms and conditions of the Creative Commons license CC BY-NC-ND.

Contents

About the Editors	vii
Preface to “Cartilage Repair and Regeneration: Focus on Multi-Disciplinary Strategies”	ix
Marta Anna Szychlinska Cartilage Repair and Regeneration: Focus on Multi-Disciplinary Strategies—Highlight on Magneto-Responsive Techniques Reprinted from: <i>Appl. Sci.</i> 2021 , <i>11</i> , 11092, doi:10.3390/app112311092	1
Angeliki Dimaraki, Pedro J. Díaz-Payno, Michelle Minneboo, Mahdiah Nouri-Goushki, Maryam Hosseini, Nicole Kops, Roberto Narcisi, Mohammad J. Mirzaali, Gerjo J. V. M. van Osch, Lidy E. Fratila-Apachitei and Amir A. Zadpoor Bioprinting of a Zonal-Specific Cell Density Scaffold: A Biomimetic Approach for Cartilage Tissue Engineering Reprinted from: <i>Appl. Sci.</i> 2021 , <i>11</i> , 7821, doi:10.3390/app11177821	5
Agnes Berta, Matthew S. Shive, Andrew K. Lynn, Alan Getgood, Saara Totterman, Grahame Busby, Jerome Hollenstein, Gábor Vásárhelyi, Imre Kéki and László Hangody Follow-Up Study Evaluating the Long Term Outcome of ChondroMimetic in the Treatment of Osteochondral Defects in the Knee Reprinted from: <i>Appl. Sci.</i> 2020 , <i>10</i> , 5642, doi:10.3390/app10165642	19
Stefano Zaffagnini, Angelo Boffa, Luca Andriolo, Davide Reale, Maurizio Busacca, Alessandro Di Martino and Giuseppe Filardo Mosaicplasty versus Matrix-Assisted Autologous Chondrocyte Transplantation for Knee Cartilage Defects: A Long-Term Clinical and Imaging Evaluation Reprinted from: <i>Appl. Sci.</i> 2020 , <i>10</i> , 4615, doi:10.3390/app10134615	31
Giovanna Desando, Livia Roseti, Isabella Bartolotti, Dante Dallari, Cesare Stagni and Brunella Grigolo Histopathological Signatures of the Femoral Head in Patients with Osteonecrosis and Potential Applications in a Multi-Targeted Approach: A Pilot Study Reprinted from: <i>Appl. Sci.</i> 2020 , <i>10</i> , 3945, doi:10.3390/app10113945	45
Silvia Ravalli, Marta Anna Szychlinska, Giovanni Lauretta and Giuseppe Musumeci New Insights on Mechanical Stimulation of Mesenchymal Stem Cells for Cartilage Regeneration Reprinted from: <i>Appl. Sci.</i> 2020 , <i>10</i> , 2927, doi:10.3390/app10082927	59

About the Editors

Marta Anna Szychlińska entered the international doctoral course in “Basic and Applied Biomedical Sciences” and she obtained her PhD in 2017 at the University of Catania, Italy. During her PhD studies, she was visiting scientist at the AO Research Institute Davos (Switzerland) in the Musculoskeletal Regeneration Program. She was University Researcher and Assistant Professor in Human Anatomy at the Department of Biomedical and Biotechnological Sciences at University of Catania, Italy, until 2021. She is currently a University Researcher and Assistant Professor in Human Anatomy at the Department of Biomedicine, Neuroscience and Advanced Diagnostics at the University of Palermo, Italy. She is a member of the editorial boards of international journals and national scientific Councils. Her leading research line regards musculoskeletal disorder studies with particular regard to tissue engineering applied to osteochondral regeneration. She is particularly interested in development of 3D in vitro models as technological platforms for the study and screening of degenerative diseases such as osteoarthritis. In this field she is author of more than 60 peer-reviewed papers on international journals.

Giuseppe Musumeci carried out his research activity at the Department of Biomedical Engineering and Orthopedic Surgery, Johns Hopkins University, Baltimore (Maryland, USA), the AO Research Institute, Davos (Switzerland) and the Department of Orthopedic Surgery, Medical University of Graz (Austria). Currently, he works as Full Professor of Exercise and Sport Sciences at the University of Catania, Italy. He is also Adjunct Professor at the Temple University’s College of Science and Technology, Philadelphia, Pennsylvania, USA and the Vice Director of the Faculty of Sport Sciences of the Fujian Normal University, China. Prof. Musumeci is the Director of the Research Center on Motor Activities (CRAM), the Director of the master’s Program, School of Posturology and Physical Exercise Sciences, the Dean of the Exercise and Sport Sciences School, the Head of the Movement Innovation PosturaLab and the Director of the Anatomy Museum at the University of Catania. He is a member of different Italian and international association of Anatomy, Histology, Kinesiology, Sports Medicine and Exercise. Since 2002 until today, he has been a Peer Reviewer in national and international scientific projects from 15 different countries and the European Community and in several international scientific journals. Moreover, he is an Editor in different international peer-reviewed journals, Founder and Editor-in-Chief of the Journal of Functional Morphology and Kinesiology (MDPI—Q2 journal ranking) and Section Editor-in-Chief in Heliyon Clinical research (Cellpress—Q1 journal ranking). Giuseppe Musumeci research interests are on morphological, molecular, and biochemical aspects of osteoarthritis and musculoskeletal disorders and the relative effects of tissue engineering, mechanobiology, diet, ageing and physical activity.

Preface to “Cartilage Repair and Regeneration: Focus on Multi-Disciplinary Strategies”

As widely demonstrated and known, adult articular cartilage exhibits a very poor self-healing capacity once injured. This is due to the complex multilayered morphological structure and an avascular, aneural, and hypocellular nature that characterize this tissue. A minimal damage or lesion may lead to cartilage tissue degeneration and osteoarthritis (OA) development, resulting in significant pain and disability.

Several approaches centered on cell-based therapies and cartilage engineering techniques have attempted to repair chondral or osteochondral defects that still remain a significant challenge in clinical practice. The failure in the use of these techniques is often due to the improper mechanical properties of newly formed cartilage-like tissue, the early entrance of the lately differentiated chondrocytes in hypertrophic stage, characterized by a senescent-associated secretory-like phenotype, or the insufficient insertion into the host tissue, often characterized by the inflammatory, osteoarthritic milieu.

While several advances have been made in recent decades, the complexity and the multifactorial aspect of articular cartilage degeneration and a consequent, apparently unstoppable OA onset and progression suggest that a multidisciplinary approach will likely be optimal to address the challenge of preserving the articular cartilage in early stages and/or developing a functional cartilage replacement in advanced degenerative stages. This kind of approach is based on a combination of several disciplines, such as biomechanics and mechanobiology (bioreactors/moderate physical activity, etc.), innovative biomaterials functionalized with growth factors, exogenous enhancers and biomolecules exploiting pharmacological activities, cells from different sources (adult stem cells, chondrocytes, co-cultures), epigenetic modifications, functional foods, etc.

In the context of developing cartilage repair and regeneration strategies, the main goal of the present Special Issue was to invite original contributions, review articles, communications, and concept papers that address these challenges. The suggested focus and the goal of a multidisciplinary strategy is to realize a clinically relevant tool for cartilage repair or regeneration that is more likely to be successful, obtained by controlling both the formation of a new suitable tissue replacements and the damaged joint tissues environment on the local and systemic level.

The articles published within the present *Special Issue* deal with the innovative multi-disciplinary therapeutic approaches for musculoskeletal diseases, starting from advanced 3D bioprinting technology to obtain a scaffold with different zonal cell densities, biphasic scaffold (ChondroMimetic) construction, passing through the comparison of different techniques for cartilage regeneration such as mosaicplasty and matrix-assisted autologous chondrocyte transplantation (MACT) and histopathological features of osteochondral units, and ending with the considerations regarding development of bioreactors able to mimic the biomechanical load on chondrocytes in vitro, giving some interesting insights in this specific scientific field.

In the end, we would like to take this opportunity to express our most profound appreciation to the MDPI Book staff, the editorial team of Applied Sciences journal, especially Mr. Steph Ke, the assistant editor of this Special Issue, talented authors, and hardworking and professional reviewers.

Marta Anna Szychlińska and Giuseppe Musumeci
Editors

Editorial

Cartilage Repair and Regeneration: Focus on Multi-Disciplinary Strategies—Highlight on Magneto-Responsive Techniques

Marta Anna Szychlinska

Department of Biomedicine, Neuroscience and Advanced Diagnostics (BiND), Human Anatomy Section, University of Palermo, 90127 Palermo, Italy; marta.sz@hotmail.it

Abstract: This editorial focuses on the interesting studies published within the present *Special Issue* and dealing with the innovative multi-disciplinary therapeutic approaches for musculoskeletal diseases. Moreover, it highlights the noteworthy magneto-responsive technique for a cartilage regeneration scope and reports some interesting studies and their outcomes in this specific field.

Keywords: tissue engineering; 3D bioprinting; ChondroMimetic; cartilage regeneration; osteochondral repair; mosaicplasty; matrix-assisted autologous chondrocyte transplantation; magneto-responsive techniques; biomechanical stimuli; multi-disciplinary approach

1. Introduction

The articular cartilage represents an incredibly complex multi-layered tissue, characterized by avascular and aneural structure, which limits its regenerative properties. Once injured, cartilage leads to its progressive degeneration with severe consequences such as the onset of chronic degenerative disorders like osteoarthritis (OA). The latter determines articular pain and stiffness, until the total disability of the joint in advanced stages [1]. Until now, no therapeutic strategy exists for this complex disease and the necessity to find the optimal approach for the cartilage regeneration still represents a big challenge.

Recently, a lot is known concerning the onset and the triggering factors of OA, as well as the main events at the base of its progression. It is well known that this severe disorder represents a multifactorial, progressively degenerating pathologic event that, principally, affects the cartilage tissue, but that expands to all the tissues of the joint [2]. It appears evident that the most promising therapeutic strategy for this complex disorder, is represented by a multi-disciplinary and multi-targeted approach.

2. Highlights on the Studies Published in the Present Special Issue: Emerging Therapies for Osteochondral Regeneration

The most promising approach for osteochondral repair is certainly represented by the tissue engineering, which aim is to create a cartilage and bone tissues able to replace the injured ones. This technique seems very encouraging, if it were not for the fact that the articular cartilage tissue has a multilayered complex structure, where every layer possesses its own spatial heterogeneity, different cell distribution and different mechanical properties [1]. With the advancement of the 3D bioprinting, the engineered grafts and the fabrication of the gradient scaffolds, enhanced their biomimicry and, consequently, their functionality and efficacy. In an interesting study by Dimaraki et al. [3] the authors bioprinted a scaffold with different zonal cell densities to mimic the organization of the complex three-layered articular cartilage structure. They observed a successful formation of a new cartilage-like tissue with a cell-density dependent zonal gradient. In another study by Berta et al. [4] a cell-free biphasic scaffold (ChondroMimetic) was evaluated for long-term outcomes in the treatment of osteochondral defects. The authors observed a cartilage-like repair tissue formation and clinical improvement at 7.9 years post-implantation. Zaffagnini et al. [5]

Citation: Szychlinska, M.A. Cartilage Repair and Regeneration: Focus on Multi-Disciplinary Strategies—Highlight on Magneto-Responsive Techniques. *Appl. Sci.* **2021**, *11*, 11092. <https://doi.org/10.3390/app112311092>

Received: 3 November 2021

Accepted: 20 November 2021

Published: 23 November 2021

Publisher's Note: MDPI stays neutral with regard to jurisdictional claims in published maps and institutional affiliations.



Copyright: © 2021 by the author. Licensee MDPI, Basel, Switzerland. This article is an open access article distributed under the terms and conditions of the Creative Commons Attribution (CC BY) license (<https://creativecommons.org/licenses/by/4.0/>).

compared the clinical outcomes of mosaicplasty and matrix-assisted autologous chondrocyte transplantation (MACT) at long-term follow-up (12 years post-surgery), concluding that both of these surgical procedures give satisfactory clinical results. Moreover, the authors suggest that MACT is the most suitable approach for the treatment of larger lesions. Indeed, many factors have to be considered when considering different strategies for the osteochondral defect treatment. The studies conducted in the field of histopathological aspects of musculoskeletal diseases, represent a pilot studies for the development of successful regenerative medicine approaches. In the study carried out by Desando et al. [6], which compared the histopathological features of osteochondral units, obtained from patients with both non-traumatic femoral head and with post-traumatic femoral head osteonecrosis. The authors reported substantial differences among them and suggested a multi-disciplinary and multi-targeted approach for osteonecrosis treatment based on its etiology.

Moreover, developing satisfactory strategies for cartilage regeneration requires deeper knowledge on biological systems. When considering the cartilage engineering strategy based on the use of mesenchymal stem cells (MSCs), the environment in which these cells are destined to promote chondrogenesis, has to be well-thought-out. The mechanical stimuli experienced by chondrocytes within the joint play a pivotal role in chondrogenesis and the development of bioreactors able to mimic the biomechanical load on cells in vitro, becomes of fundamental importance in developing new, multi-disciplinary strategies for cartilage regeneration approaches as suggested by Ravalli et al. [7].

3. Magneto-Responsive Techniques for Cartilage Regeneration

With the development of biotechnology, other promising techniques have been developed such as magnetic cell manipulation, achieved by the synergy between magnetic objects and magnetic field [8,9]. In general, there are four techniques based on the magnetic cell manipulation for the tissue engineering approaches. The first one includes the magnetic field-based guiding of the cells to the targeted site, which permits to the relatively small number of cells (i.e., magnetic mesenchymal stem cells) to accumulate at the level of the defect site and promote cartilage regeneration [10,11]. The second one is based on the enhancement of the seeding ability of cells within the scaffold, which permits the cells to migrate symmetrically and to promote the cell condensation, providing a suitable environment for cell proliferation and differentiation [12]. The third technique regards the formation of magnetic scaffolds, where the magnetic force is used to assemble the 3D structure to mimic the native tissue [13,14]. This technique based on magnetic patterning, works across a range of materials (e.g., hydrogels) and diamagnetic objects (e.g., living cells, drug delivering microspheres, etc.), characterized by differential magnetic susceptibility, with the potential to predictably position these objects in 3D materials, in response to brief magnetic field application. It confers several advantages, including remote control ability, sufficient cell density and cell adhesion enhancement, permitting one to achieve a very good grade of engineered tissue biomimicry [8,9]. Zlotnik et al. [15], demonstrated that a naturally diamagnetic objects, comprising living cells, can be predictably positioned throughout the 3D hydrogel. In this study, the magnetic susceptibility of the latter was enhanced by the addition of magnetic contrast agent (gadodiamide). After the cells achieved the required position, by the brief exposure to magnetic field, they were 'locked in' by a photo-crosslinking method. Afterwards, the magnetic contrast agent was washed out of the hydrogel to not interfere with the long-term cell viability. In the study, the authors applied this method to engineer cartilage constructs with a depth-dependent cellularity, mirroring that of the native tissue. The fourth strategy is based on guiding cell assembly into sheet-like structures to stack layer-by-layer, used for the formation of scaffold-free 3D cell culture. In this way, magnetic-labeled cells can be guided to a targeted location and form 3D arrangements in a convenient microenvironment to mimic tissue properties without the use of scaffolds [16,17].

In addition, it has been widely demonstrated that mechanical forces acting as an additional tool to mimic the in vivo environment are also applied to improve cartilage reconstruction as suggested above [7,18]. Magnetic nanoparticles represent the excellent candidates to apply remote magnetic-induced mechanical stimulation. Luciani et al. [19] used magnetic MSCs to enhance their seeding density and condensation into the scaffolds subjected to dynamic bioreactor. The results showed that MSC differentiation was markedly improved. Son et al. [20] exposed magnetic nanoparticle-labeled MSCs to static magnetic field and magnet-derived shear stress, demonstrating higher chondrogenic differentiation efficiency and no hypertrophic effects. Further, Hou et al., [21] demonstrated that the multifunctional hyaluronic acid-graft-amphiphilic gelatin microcapsules, loaded with the superparamagnetic iron oxide nanoparticles and chondrocytes, subjected to static magnetic field and magnet-derived shear stress, were able to stimulate chondrogenesis and fabricate cartilage tissue-mimetic pellets.

4. Conclusions

Several approaches have been evaluated for the cartilage regenerative outcomes including 3D bioprinting, cell-free biphasic scaffolds, mosaicplasty, MACT, and stem cell therapy [3–5,19,22]. Many of them giving encouraging results. However, the innovative multi-functional approaches in this field are still needed to overcome the existing limits. The most promising strategy for the cartilage regeneration seems to be represented by a multi-disciplinary approach based on tissue engineering combining innovative techniques such as formation of magneto-guided zonal cell gradient 3D structures to mimic the native tissue, application of biomechanical stimulation to reproduce the native environment of the joints, and the use of exogenous biomolecules (i.e., drug delivery scaffolds) able to stimulate cell differentiation and counteract the pathologic milieu of the affected joints.

Funding: This research received no external funding.

Acknowledgments: This publication was only possible with the valuable contributions from the authors, reviewers, and the editorial team of *Applied Sciences*.

Conflicts of Interest: The author declares to be a guest editor of the present Special Issue and there are no other conflict of interest.

References

- Ulrich-Vinther, M.; Maloney, M.D.; Schwarz, E.M.; Rosier, R.; O’Keefe, R.J. Articular cartilage biology. *J. Am. Acad. Orthop. Surg.* **2003**, *11*, 421–430. [[CrossRef](#)] [[PubMed](#)]
- Abramoff, B.; Caldera, F.E. Osteoarthritis: Pathology, Diagnosis, and Treatment Options. *Med. Clin. N. Am.* **2020**, *104*, 293–311. [[CrossRef](#)] [[PubMed](#)]
- Dimaraki, A.; Díaz-Payno, P.J.; Minneboo, M.; Nouri-Goushki, M.; Hosseini, M.; Kops, N.; Narcisi, R.; Mirzaali, M.J.; van Osch, G.J.V.M.; Fratila-Apachitei, L.E.; et al. Bioprinting of a Zonal-Specific Cell Density Scaffold: A Biomimetic Approach for Cartilage Tissue Engineering. *Appl. Sci.* **2021**, *11*, 7821. [[CrossRef](#)]
- Berta, A.; Shive, M.S.; Lynn, A.K.; Getgood, A.; Totterman, S.; Busby, G.; Hollenstein, J.; Vasarhelyi, G.; Keki, I.; Hangody, L. Follow-Up Study Evaluating the Long Term Outcome of ChondroMimetic in the Treatment of Osteochondral Defects in the Knee. *Appl. Sci.* **2020**, *10*, 5642. [[CrossRef](#)]
- Zaffagnini, S.; Boffa, A.; Andriolo, L.; Reale, D.; Busacca, M.; Di Martino, A.; Filardo, G. Mosaicplasty versus Matrix-Assisted Autologous Chondrocyte Transplantation for Knee Cartilage Defects: A Long-Term Clinical and Imaging Evaluation. *Appl. Sci.* **2020**, *10*, 4615. [[CrossRef](#)]
- Desando, G.; Roseti, L.; Bartolotti, I.; Dallari, D.; Stagni, C.; Grigolo, B. Histopathological Signatures of the Femoral Head in Patients with Osteonecrosis and Potential Applications in a Multi-Targeted Approach: A Pilot Study. *Appl. Sci.* **2020**, *10*, 3945. [[CrossRef](#)]
- Ravalli, S.; Szychlinska, M.A.; Lauretta, G.; Musumeci, M. New Insights on Mechanical Stimulation of Mesenchymal Stem Cells for Cartilage Regeneration. *Appl. Sci.* **2020**, *10*, 2927. [[CrossRef](#)]
- Delyagina, E.; Li, W.; Ma, N.; Steinhoff, G. Magnetic targeting strategies in gene delivery. *Nanomedicine* **2011**, *6*, 1593–1604. [[CrossRef](#)]
- Xia, Y.; Sun, J.; Zhao, L.; Zhang, F.; Liang, X.J.; Guo, Y.; Weir, M.D.; Reynolds, M.A.; Gu, N.; Xu, H.H.K. Magnetic field and nano-scaffolds with stem cells to enhance bone regeneration. *Biomaterials* **2018**, *183*, 151–170. [[CrossRef](#)]

10. Kamei, G.; Kobayashi, T.; Ohkawa, S.; Kongcharoensombat, W.; Adachi, N.; Takazawa, K.; Shibuya, H.; Deie, M.; Hattori, K.; Goldberg, J.L.; et al. Articular cartilage repair with magnetic mesenchymal stem cells. *Am. J. Sports Med.* **2013**, *41*, 1255–1264. [[CrossRef](#)]
11. Mahmoud, E.E.; Kamei, G.; Harada, Y.; Shimizu, R.; Kamei, N.; Adachi, N.; Misk, N.A.; Ochi, M. Cell Magnetic Targeting System for Repair of Severe Chronic Osteochondral Defect in a Rabbit Model. *Cell Transplant.* **2016**, *25*, 1073–1083. [[CrossRef](#)]
12. Brady, M.A.; Talvard, L.; Vella, A.; Ethier, C.R. Bio-inspired design of a magnetically active trilayered scaffold for cartilage tissue engineering. *J. Tissue Eng. Regen Med.* **2017**, *11*, 1298–1302. [[CrossRef](#)] [[PubMed](#)]
13. Margolis, G.; Polyak, B.; Cohen, S. Magnetic Induction of Multiscale Anisotropy in Macroporous Alginate Scaffolds. *Nano Lett.* **2018**, *18*, 7314–7322. [[CrossRef](#)] [[PubMed](#)]
14. Huang, J.; Liang, Y.; Jia, Z.; Chen, J.; Duan, L.; Liu, W.; Zhu, F.; Liang, Q.; Zhu, W.; You, W.; et al. Development of Magnetic Nanocomposite Hydrogel with Potential Cartilage Tissue Engineering. *ACS Omega* **2018**, *3*, 6182–6189. [[CrossRef](#)] [[PubMed](#)]
15. Zlotnick, H.M.; Clark, A.T.; Gullbrand, S.E.; Carey, J.L.; Cheng, X.M.; Mauck, R.L. Magneto-Driven Gradients of Diamagnetic Objects for Engineering Complex Tissues. *Adv. Mater.* **2020**, *32*, e2005030. [[CrossRef](#)] [[PubMed](#)]
16. Ghosh, S.; Kumar, S.R.; Puri, I.K.; Elankumaran, S. Magnetic assembly of 3D cell clusters: Visualizing the formation of an engineered tissue. *Cell Prolif.* **2016**, *49*, 134–144. [[CrossRef](#)] [[PubMed](#)]
17. Zhang, W.; Yang, G.; Wang, X.; Jiang, L.; Jiang, F.; Li, G.; Zhang, Z.; Jiang, X. Magnetically Controlled Growth-Factor-Immobilized Multilayer Cell Sheets for Complex Tissue Regeneration. *Adv. Mater.* **2017**, *29*, 1703795. [[CrossRef](#)]
18. Szychlińska, M.A.; D'Amora, U.; Ravalli, S.; Ambrosio, L.; Di Rosa, M.; Musumeci, G. Functional Biomolecule Delivery Systems and Bioengineering in Cartilage Regeneration. *Curr. Pharm. Biotechnol.* **2019**, *20*, 32–46. [[CrossRef](#)]
19. Luciani, N.; Du, V.; Gazeau, F.; Richert, A.; Letourneur, D.; Le Visage, C.; Wilhelm, C. Successful chondrogenesis within scaffolds, using magnetic stem cell confinement and bioreactor maturation. *Acta Biomater.* **2016**, *37*, 101–110. [[CrossRef](#)]
20. Son, B.; Kim, H.D.; Kim, M.; Kim, J.A.; Lee, J.; Shin, H.; Hwang, N.S.; Park, T.H. Physical Stimuli-Induced Chondrogenic Differentiation of Mesenchymal Stem Cells Using Magnetic Nanoparticles. *Adv. Healthc. Mater.* **2015**, *4*, 1339–1347. [[CrossRef](#)]
21. Hou, K.T.; Liu, T.Y.; Chiang, M.Y.; Chen, C.Y.; Chang, S.J.; Chen, S.Y. Cartilage Tissue-Mimetic Pellets with Multifunctional Magnetic Hyaluronic Acid-Graft-Amphiphilic Gelatin Microcapsules for Chondrogenic Stimulation. *Polymers* **2020**, *12*, 785. [[CrossRef](#)] [[PubMed](#)]
22. Campos, Y.; Almirall, A.; Fuentes, G.; Bloem, H.L.; Kaijzel, E.L.; Cruz, L.J. Tissue Engineering: An Alternative to Repair Cartilage. *Tissue Eng. Part. B Rev.* **2019**, *25*, 357–373. [[CrossRef](#)] [[PubMed](#)]

Article

Bioprinting of a Zonal-Specific Cell Density Scaffold: A Biomimetic Approach for Cartilage Tissue Engineering

Angeliki Dimaraki ^{1,†}, Pedro J. Díaz-Payno ^{1,2,†}, Michelle Minneboo ¹, Mahdihyeh Nouri-Goushki ¹, Maryam Hosseini ^{1,3}, Nicole Kops ², Roberto Narcisi ², Mohammad J. Mirzaali ¹, Gerjo J. V. M. van Osch ^{1,2,4}, Lidy E. Fratila-Apachitei ¹ and Amir A. Zadpoor ^{1,*}

¹ Department of Biomechanical Engineering, Faculty of Mechanical, Maritime and Materials Engineering, Delft University of Technology, 2628 CD Delft, The Netherlands; a.dimaraki@student.tudelft.nl (A.D.); p.j.diazpayno@tudelft.nl (P.J.D.-P.); M.B.Minneboo@tudelft.nl (M.M.); M.NouriGoushki@tudelft.nl (M.N.-G.); M.Hosseini@tudelft.nl (M.H.); M.J.Mirzaali@tudelft.nl (M.J.M.); G.J.V.M.VanOsch@tudelft.nl (G.J.V.M.v.O.); E.L.Fratila-Apachitei@tudelft.nl (L.E.F.-A.)

² Department of Orthopedics and Sports Medicine, Erasmus MC University Medical Center, 3015 GD Rotterdam, The Netherlands; n.kops@erasmusmc.nl (N.K.); r.narcisi@erasmusmc.nl (R.N.)

³ Department of Chemical Engineering, Faculty of Engineering, Azarbaijan Shahid Madani University, Tabriz 53714-161, Iran

⁴ Department of Otorhinolaryngology, Erasmus MC University Medical Center, 3015 GD Rotterdam, The Netherlands

* Correspondence: A.A.Zadpoor@tudelft.nl

† These authors contributed equally.

Citation: Dimaraki, A.; Díaz-Payno, P.J.; Minneboo, M.; Nouri-Goushki, M.; Hosseini, M.; Kops, N.; Narcisi, R.; Mirzaali, M.J.; van Osch, G.J.V.M.; Fratila-Apachitei, L.E.; et al. Bioprinting of a Zonal-Specific Cell Density Scaffold: A Biomimetic Approach for Cartilage Tissue Engineering. *Appl. Sci.* **2021**, *11*, 7821. <https://doi.org/10.3390/app11177821>

Academic Editor: Rossella Bedini

Received: 20 July 2021

Accepted: 20 August 2021

Published: 25 August 2021

Publisher's Note: MDPI stays neutral with regard to jurisdictional claims in published maps and institutional affiliations.



Copyright: © 2021 by the authors. Licensee MDPI, Basel, Switzerland. This article is an open access article distributed under the terms and conditions of the Creative Commons Attribution (CC BY) license (<https://creativecommons.org/licenses/by/4.0/>).

Abstract: The treatment of articular cartilage defects remains a significant clinical challenge. This is partially due to current tissue engineering strategies failing to recapitulate native organization. Articular cartilage is a graded tissue with three layers exhibiting different cell densities: the superficial zone having the highest density and the deep zone having the lowest density. However, the introduction of cell gradients for cartilage tissue engineering, which could promote a more biomimetic environment, has not been widely explored. Here, we aimed to bioprint a scaffold with different zonal cell densities to mimic the organization of articular cartilage. The scaffold was bioprinted using an alginate-based bioink containing human articular chondrocytes. The scaffold design included three cell densities, one per zone: 20×10^6 (superficial), 10×10^6 (middle), and 5×10^6 (deep) cells/mL. The scaffold was cultured in a chondrogenic medium for 25 days and analyzed by live/dead assay and histology. The live/dead analysis showed the ability to generate a zonal cell density with high viability. Histological analysis revealed a smooth transition between the zones in terms of cell distribution and a higher sulphated glycosaminoglycan deposition in the highest cell density zone. These findings pave the way toward bioprinting complex zonal cartilage scaffolds as single units, thereby advancing the translation of cartilage tissue engineering into clinical practice.

Keywords: bioprinting; biofabrication; tissue engineering; articular cartilage; human chondrocytes; cell density; cell gradient

1. Introduction

Articular cartilage (AC) may be damaged due to aging, disease, or trauma. AC has a limited regenerative capacity that has been attributed to the lack of innervation and the avascular nature of the tissue [1]. AC defects may progress to the subchondral bone to create an osteochondral defect. If left untreated, such defects can potentially lead to the development of osteoarthritis [2,3], a cartilage-degenerating disease affecting over 300 million worldwide and representing a burden on the healthcare systems globally [4,5]. The treatment of AC defects often results in a fibrocartilage tissue with poor long-term outcomes [6], thus presenting a significant clinical challenge. This is partially because the current regenerative and tissue engineering strategies fail to recapitulate the native

organization of the AC tissue. AC is a graded tissue that has three main zones: superficial, middle, and deep. These zones are associated with differences in matrix composition, matrix structural organization, and cell number, which result in gradients with complex physical, mechanical, and biological properties [7]. In adult healthy human articular cartilage, the superficial zone is characterized by thickly packed collagen type II fibers, a high tensile strength, and a high cell density, while the deep zone is characterized by a high sulfated glycosaminoglycan (sGAG) content, high compressive strength, and a low cell density as compared to the other layers [8].

Different biofabrication strategies, such as bioprinting, have been exploited to recapitulate few of the gradients connecting the three zones [9]. Graded scaffolds aim to mimic the highly organized native tissue. Several studies have explored the fabrication of multilayered constructs exhibiting differences in biological [10] or chemical composition [11–14] and physical or mechanical properties [15–17]. Different gradient strategies have also been combined to tailor physical (stiffness) and biochemical (growth factor) gradients that better control stem-cell behavior [18].

To the best of our knowledge, there has been only one study introducing a cell density gradient in a bioprinted construct [19], where swine articular cartilage-derived constructs with different density gradients of rabbit chondrocytes were compared to constructs with equivalent homogeneous cell distribution. In the study, gene expression and sGAG deposition were quantified for the overall constructs. However, limited information was presented regarding the extracellular matrix (ECM) that was deposited by the cells at different densities in each zone. Therefore, further research is warranted to characterize the cell-derived tissue deposition in each of the zones within a graded construct, especially using human material.

The aims of this paper were (i) to design and fabricate scaffolds with three-zone cell density using bioprinting with an alginate-based bioink containing human articular chondrocytes and a poly- ϵ -caprolactone (PCL) support structure, (ii) to characterize the cell viability and cell gradient stability overtime, and (iii) to evaluate the time-dependent deposition of ECM by the cells embedded in the scaffolds. To achieve the cell density gradient, the design of the scaffolds included three zones with three different cell densities. The different zones aimed to mimic both the dimensions and cell density of the superficial, middle, and deep zones as seen in the native structure of articular cartilage.

2. Materials and Methods

2.1. Scaffold Design

Solidworks was used to design a standard tessellation language (.STL) file of scaffold solid form that incorporated both the PCL outer skeleton and the cell-embedded bioink part. The PCL skeleton design was composed of a square base of $8 \times 8 \text{ mm}^2$ with a thickness of two layers (0.4 mm) and four vertical pillars at the corners with a height of 3 mm. The scaffold was designed as a $7.2 \text{ mm} \times 7.2 \text{ mm} \times 3 \text{ mm}$ cube. The designed STL file was then processed in Slic3r [20] to generate the gcode file used by the bioprinter (BIO-X bioprinter, Cellink, Sweden). Briefly, the parameters used in Slic3r were as follows: infill pattern, rectilinear; infill density, 100% for PCL frame design and 10% for scaffold design; infill angle, 90° ; solid infill threshold area, 10; layer height, 0.2 mm; nozzle diameter, 0.2 mm. Two types of scaffolds were designed: a scaffold corresponding to a homogeneous cell density with one zone of 15 layers and a scaffold with three different zones corresponding to the three different cell densities. The dimensions of the zones were chosen to mimic the dimensions of the three different zones in the human articular cartilage. The top zone had a thickness of three layers (0.6 mm), the middle zone had a thickness of seven layers (1.4 mm), and the bottom zone had a thickness of five layers (1 mm), resulting in a total of 15 layers per scaffold.

2.2. Bioink Formulation

An alginate-based biomaterial (IK1020000303, Cellink Bioink, Cellink, Sweden) was mixed with human chondrocytes according to the manufacturer's instructions to create the bioink. Briefly, human articular chondrocytes isolated from hyaline cartilage in the knee and expanded to the second passage were purchased from Lonza (NHAC-kn, Lonza Bioscience, Breda, The Netherlands). The cells were expanded until the third passage in chondrocyte growth medium (CC-3216, Lonza Bioscience, Breda, The Netherlands) according to the manufacturer's instructions, in an incubator at 37 °C, 5% CO₂, and 90% humidity. The cells were trypsinized when confluency was reached, counted, and re-suspended in a growth medium. The hydrogel was taken up from the stock cartridge by a syringe and was mixed gently 10:1 with the cell suspension using a sterile female–female luer lock, and a second syringe was used to homogenize the cells in the bioink. The mixture was transferred to a new cartridge for bioprinting. According to the study by Hunziker et al., the total cell density within the human articular cartilage of a medial femoral condyle is 10×10^3 cell/mm³ [21]. Therefore, the homogeneous scaffold was given a biomimetic total cell density of 10×10^6 cell/mL. Hunziker et al. also described the different cell densities in the different zones of articular cartilage in which it was established that the cell densities corresponding to the superficial, middle, and deep zones are $24 \pm 3 \times 10^3$ cells/mm³, $10 \pm 0.5 \times 10^3$ cells/mm³, and $7 \pm 0.5 \times 10^3$ cells/mm³, respectively [21]. The gradient scaffold was given a similar biomimetic cell density corresponding to each zone of the articular cartilage: superficial (top), middle (middle) and deep (bottom) zones. The top, middle, and bottom zones were designed to respectively have 20×10^6 cells/mL, 10×10^6 cells/mL, and 5×10^6 cells/mL, respectively (Figure 1).

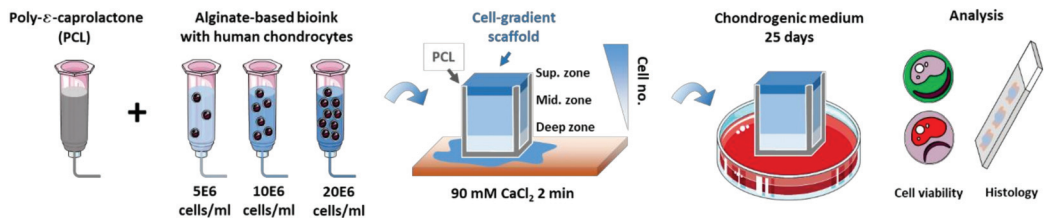


Figure 1. A schematic representation of the fabrication methodology and the in vitro setup of the study. A PCL-reinforced alginate-based scaffold containing human chondrocytes was 3D bioprinted with different cell densities mimicking the cell gradient of the human articular cartilage zones. The scaffold was ionically crosslinked post bioprinting before supplementing with chondrogenic medium for 4 weeks. After in vitro culture, the samples were analyzed for cell viability and for matrix deposition through histological staining.

2.3. Bioprinting

The BIO-X bioprinter (Cellink, Sweden) was UV-sterilized and used inside a cell culture hood to ensure that the bioprinting process would run under sterile conditions. After sterilization, the gcode file was used to print the scaffold. Briefly, the printing surface, nozzle size, temperature, pressure, and speed of each print-head was selected through the bioprinter's interface. The selected parameters for each print-head are presented below (Table 1). Next, the three printheads were manually calibrated to the same spot in the printing surface to ensure a complete match when swapping printheads during the printing process for the different bioinks and biomaterials printed (Video S1). A 10 cm petri dish was used as the printing surface to provide better visibility between the nozzle tip and the printing surface during the calibration phase. The scaffolds were printed on 16 mm coverslips which were placed radially into the 10 cm petri dish. After printing, the scaffolds were treated with 1 mL of crosslinking solution (90 mM CaCl₂, Cellink, Sweden) for 2 min.

Table 1. The parameters used for each printhead during bioprinting. Printheads 1 and 2 were used for the hydrogel layers, while printhead 3 was used to print the outer frame of PCL (RT: room temperature).

Title 1	Material	Nozzle Size	Temperature	Pressure	Speed
Printhead 1	Hydrogel (deep zone)	0.2 mm	RT	14 kPa	12 mm/s
Printhead 2	Hydrogel (superficial and middle zones)	0.2 mm	RT	14 kPa	12 mm/s
Printhead 3	PCL	0.2 mm	210 °C	200 kPa	4 mm/s (base) 0.4 mm/s (struts)

2.4. In Vitro Culture

The bioprinted constructs were cultured in chondrocyte differentiation basal medium (Clonetics™ CDM™ BulletKit™, Lonza, Delft, The Netherlands) containing FBS, insulin, R3-IGF-1, gentamicin/amphotericin B, transforming growth factor- β 1, and transferrin (undisclosed concentrations by Lonza). The differentiation medium was further enriched with 10 ng/mL fresh transforming growth factor- β 3 (SRP3171, Sigma, Delft, The Netherlands) and 70 mM L-ascorbic acid 2-phosphate (A8960, Sigma, The Netherlands) for each medium change, according to the manufacturer's instructions (TS-CC-112-7 02/20, Lonza). The differentiation medium was changed three times a week for 25 days using 2 mL of medium per well (each well contained one scaffold), which was kept in a 24-well plate in an incubator at 37 °C, 90% humidity, and 5% CO₂. The experiment included three scaffolds per condition (graded, homogeneous) per timepoint (day 0 and day 25).

2.5. Mechanical Characterization

The 3D printed scaffolds (cell-free) were mechanically characterized using a uniaxial unconfined compression test using the LLOYD Instruments LR5k compression machine (AMETEK test & calibration instruments). The PCL frame, hydrogel, and the combined scaffolds (PCL and hydrogel) were tested separately using a 100 N load cell with a 0.1 N preload, a 1 mm deflection, and a strain rate of 0.002 s⁻¹ (i.e., a crosshead speed of 0.36 mm/min). From the load–deflection curve generated by the machine on the Nexygen software, 200 data points were exported per test for further analysis. Each of the data points included the recorded time (s), load (N), crosshead travel (mm), and deflection from the preload (mm), which were used for the generation of the stress–strain curves and the calculation of the compressive stiffness of the scaffolds. The stress was calculated by dividing the compression force by the cross-section area, and the strain was defined as the ratio of the crosshead travel to the initial length of the specimens. The stiffness calculations were performed using a moving regression algorithm generated with Gnu R [22] that was used to calculate the linear line with the steepest slope fit of the stress–strain curve. The slope of the linear curve was taken as the value for the compressive stiffness of the scaffolds ($E = \sigma/\epsilon$, MPa).

2.6. Live/Dead Assay

Cell viability was assessed at day 0 (post-printing) and day 25 after culture using live/dead staining (LIVE/DEAD® Viability/Cytotoxicity Kit, ThermoFisher, Delft, The Netherlands). Briefly, the samples were washed twice with 1 × PBS for 5 min before supplementing the scaffolds with 2 mM ethidium homodimer-1 (red, for dead cells) and 5 mM calcein-AM (green, for live cells) in 1 × PBS. The samples were allowed to incubate for 1 h at 37 °C before being washed twice in 1 × PBS and being imaged under a fluorescent microscope (ZOE fluorescent cell imager, Biorad, Delft, The Netherlands).

2.7. Histology Staining

All the specimens were fixed overnight in 4% paraformaldehyde at 4 °C with a tissue–fixative volume ratio of 1:20. Next, the scaffolds were washed twice with PBS, and were placed in a 1:1 solution of 100% EtOH:90 mM Cellink crosslinking agent (final 45 mM CaCl₂) for storage. The samples were paraffin-embedded and were sectioned at a thickness

of 6 μm . The sections were stained with hematoxylin (HHS32, Sigma, The Netherlands) and eosin (HT110232, Sigma, The Netherlands) to examine their cell distribution, with 1% Alcian Blue (TMS-010-C, Sigma, The Netherlands) to analyze their sGAG content, and with Picrosirius Red (365548, Sigma, The Netherlands) for collagen deposition. The stained histological slices were imaged under a DM500 optical Leica microscope.

2.8. Image Analysis

The histological images were analyzed for the cell density in each of the three zones, as well as for the neo-tissue formation (sGAG and collagen deposition) within the hydrogel for all three zones. The analysis of the data was performed using Image J v2.0.0 software. The images were spatially calibrated using their integrated scale bar. For the analysis of H&E staining, the microscopic images were first split into the three-color channels RGB. Then, the green channel was selected as the optimum channel for the identification of the nuclei. Next, the threshold was adjusted before using the “analyze particles” plugin. The minimum size was set between five and 35 pixels depending on the image, while the maximum size was set at 300 pixels. The circularity range was set between 0.45 and 1.00 for all the images. This analysis of the H&E images was performed using the ROI (region of interest) manager to select three regions of interest corresponding to the three different zones and to analyze them separately using a different threshold and size spectrum depending on their specific data. For the samples stained with Alcian Blue and Picrosirius Red, the image analysis was performed with the use of the Trainable Weka Segmentation plugin [23]. This plugin utilizes a segmentation algorithm that combines a collection of machine learning algorithms with a set of selected image features to produce pixel-based segmentations. Three classes were used for the training of the algorithm and the classification of the results: (a) a class for the negative background staining of the alginate, (b) a class for the stained cell nuclei, and (c) a class for the positively stained areas (areas with darker blue or red color for AB and PR, respectively). The training of the algorithm was performed by manually selecting multiple areas belonging to each of the classes using the Image J’s selection tool and categorizing them according to their corresponding class. After that, the features of the input image were extracted and converted to a set of vectors of float values (format for Weka classifiers). Finally, the plugin created and displayed the resulting image. This image was equivalent to the current overlay (8 bit color with each color corresponding to a specific class). The training features used for the training of the algorithm were Gaussian blur, Sobel filter, Hessian matrix, and the difference of the Gaussians. After training, the same classifier was applied to all the images of the same staining. The plugin performed the image segmentation on the basis of the current classifier and the selected features and created a stack of images, each one highlighting one of the selected features. By selecting the desired 8 bit color image from the stack and setting an appropriate threshold, we performed area measurements on the objects within the images to evaluate the sGAG content of the areas positively stained for collagen (for all the zones and timepoints). The ratio between positive area and total area for the samples analyzed is presented as a percentage.

2.9. Statistical Analysis

All quantitative results are presented as the mean \pm standard deviation. Statistical analysis was performed using GraphPad Prism 8 (GraphPad Software, San Diego, CA, USA, Version 8.0.2). For the analysis of the cell density, sGAG content, and collagen content, the experimental groups were analyzed for significant differences using a two-way analysis of variance (ANOVA) and the results were corrected for multiple comparisons using Bonferroni’s post hoc test. For the comparison of the stiffness, as well as for the differences in the cell viability and cell density between the two different scaffold designs, an unpaired *t*-test or one-way ANOVA was performed. Probability *p*-values <0.05 were considered statistically significant.

3. Results

3.1. PCL-Reinforced Alginate Scaffolds with Different Cell Density Zones Can Be Successfully Fabricated as Single Units Using Bioprinting

Firstly, we designed a structure that could combine both an outer frame of stiff PCL and the soft alginate-based bioink with an overall size of 8 mm × 8 mm × 3 mm (Figure 2a–c). For the PCL frame, two different designs were tested: a closed design (Figure S1a) and an open design (Figure 2a and Figure S1b). The open design resulted in a higher viability of the cells in the bioink (Figure S1c–e) and was, therefore, chosen for further experiments. For the bioink, a 10% infill density was selected in order to create channels in the z-direction (Figure 2e) that resulted in visible pores in the scaffold of ~0.230 mm² (Figure 2c) to allow for sufficient nutrient diffusion to all the layers of the cell-laden hydrogel. The different parts of the zonal scaffold showing the PCL frame in yellow and the three different cell density zones in red were sliced into a printing pattern suitable for 3D printing (Figure 2d). The design used for the fabrication of the biomimetic cartilage scaffolds was bioprinted monolithically as a single unit (Figure 2e). The mean compressive stiffness of the scaffolds (PCL + hydrogel) was 8.35 ± 0.43 MPa. This was mostly attributed to the PCL framework, since the mean compressive stiffness of the PCL framework alone was 8.02 ± 0.69 MPa while the hydrogel alone was 0.23 MPa ± 0.01 (Figure 2f).

The next step was to verify that we could 3D print the different zones (top, middle, and bottom) with different cell densities of human chondrocytes (i.e., 20 × 10⁶, 10 × 10⁶, and 5 × 10⁶ cells/mL, respectively), recapitulating some aspects of the cytocomplexity of the human hyaline articular cartilage. Live/dead staining at day 0 post bioprinting demonstrated that it was possible to control such cell distribution, as evidenced by a higher cell density in the top zone and the lowest cell density in the bottom zone (Figure 2g). Overall, a high viability (>90%) of the bioprinted cells was observed throughout the different zones of the scaffolds (Figure 2h).

3.2. Cell Density Can Be Maintained in the Different Zones Overtime In Vitro

To investigate the maintenance of the zonal distribution of the cells over time, we cultured human chondrocytes in the hydrogel for 25 days. We compared the scaffolds with different cell densities, herein called the zonal scaffolds, with the scaffolds in which the cell density (10E6 cells/mL) was constant throughout the entire scaffold. At day 0, right after the bioprinting process took place, a high cell viability was detected for the embedded cells (Figure 3a). In addition, the quantification of the H&E staining at day 0 showed significant differences between the bottom/middle, middle/top, and bottom/top zones of the graded scaffolds (Figure 3b, left), whereas no difference in the cell density was observed throughout the homogeneous scaffolds (Figure 3b, right). After 25 days of culture, cell viability remained high for all the specimens (Figure 3c). In addition, a decrease in the cell density of the middle zone was observed, rendering the cell density between the middle and the bottom zones as not significantly different, while the cell density in the top zone remained significantly higher than the other zones (Figure 3d, left). The cell density of the homogeneous scaffolds remained constant throughout the scaffold thickness for all the timepoints (Figure 3d, right).

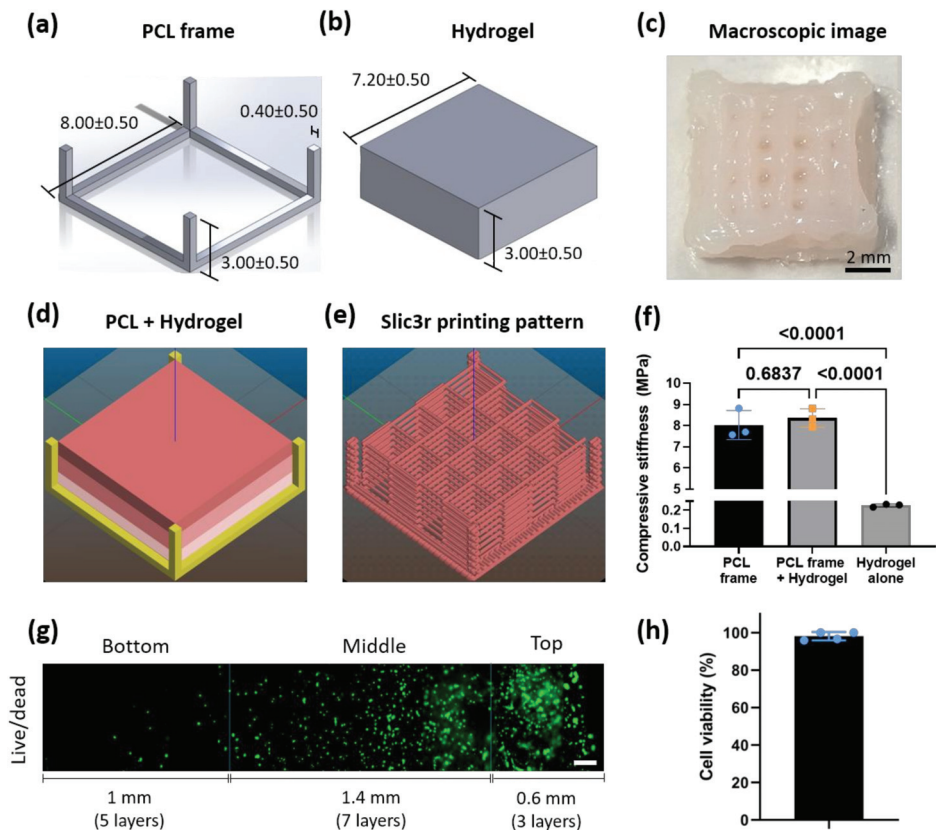


Figure 2. PCL-reinforced alginate scaffolds with different cell density zones can be bioprinted as a single unit. (a) The solid structure created in Solidworks corresponding to the outer PCL frame; (b) the solid structure corresponding to the hydrogel part; (c) a macroscopic image of the top view of a 3D printed scaffold after ionic crosslinking; (d) the different solid structures combined by Slic3r software, showing the PCL in yellow and the hydrogel in different shades of red for the different cell density zones; (e) Slic3r design of the printing pattern showing a 100% infill for the PCL and a 10% infill for the hydrogel; (f) a bar chart showing the mechanical properties (stiffness) of the outer PCL frame, the combined PCL frame + hydrogel, and the hydrogel alone printed scaffolds ($n = 3$); (g) a fluorescent microscopic image of cell viability with live/dead staining (green: live; red: dead) showing the cell distribution in the scaffold bioprinted with three different cell densities for each of the zones: bottom ($5E6$ cell/mL), middle ($10E6$ cells/mL), and top ($20E6$ cells/mL) at day 0. Lines are drawn on the image to illustrate the approximate division of the zones. Scale bar = $200 \mu\text{m}$; (h) the corresponding quantification of the overall live and dead cells ($n = 4$).

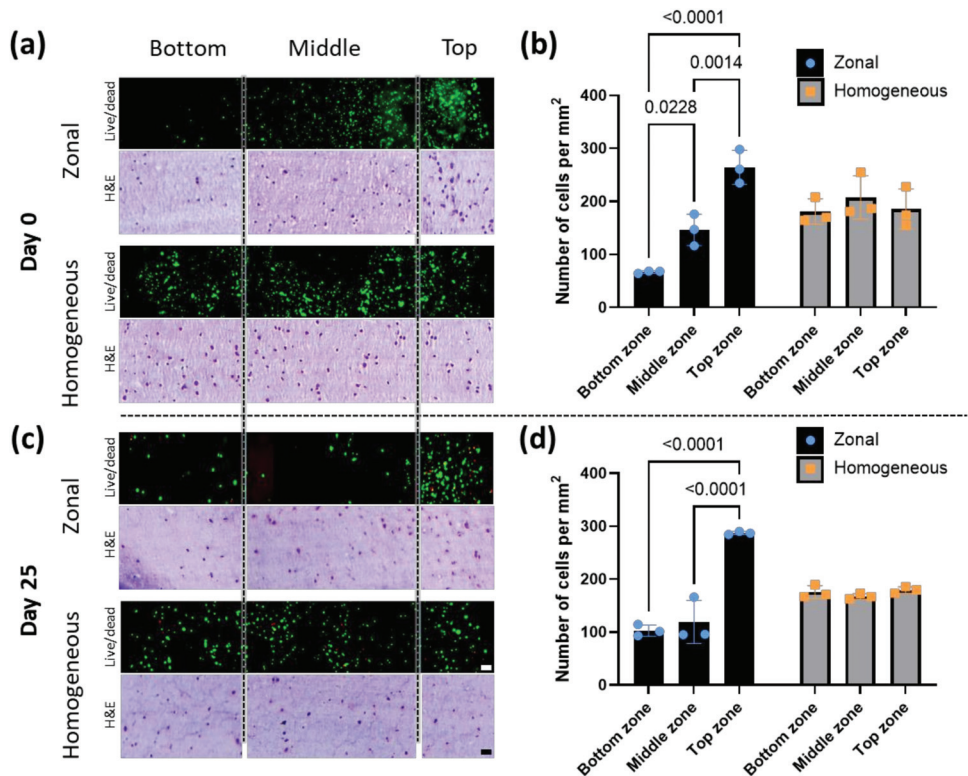


Figure 3. Gradient cell density can be maintained in the zonal scaffold over time in vitro culture; (a) fluorescent microscopic images indicate cell viability based on live/ dead staining (green: alive; red: dead) and bright-field microscopy images of the H&E staining (matrix: violet; nuclei: dark purple) showing the cell distribution for the three different zones, bottom, middle, and top, of the zonal and homogeneous bioprinted scaffolds at day 0; (b) the quantification of the number of the cells from the H&E staining at day 0; (c) the live/ dead and H&E images of the zonal and homogeneous scaffold at day 25; (d) the quantification of the number of cells from the H&E staining at day 28 ($n = 3$; p -values < 0.05 are shown). Scale bar: 100 μm .

3.3. Bioprinted Zonal Scaffold with Different Cell Densities Leads to a Gradient Cell-Derived ECM Deposition

The evaluation of the sGAG and collagen deposition in the bioprinted scaffolds was performed on the basis of the analysis of Alcian Blue and Picrosirius Red histological staining of the scaffold cross-sections. At day 0, the histological analysis showed the background staining for the basal bioink material (alginate and methylcellulose) with a weak staining for Alcian Blue (Figure 4a) and a strong pink (negative for collagen) staining for Picrosirius Red (Figure 4c). A semiquantitative analysis of the stained samples was performed using an optimized threshold to subtract the background staining from positively stained areas (Figure 4b,d).

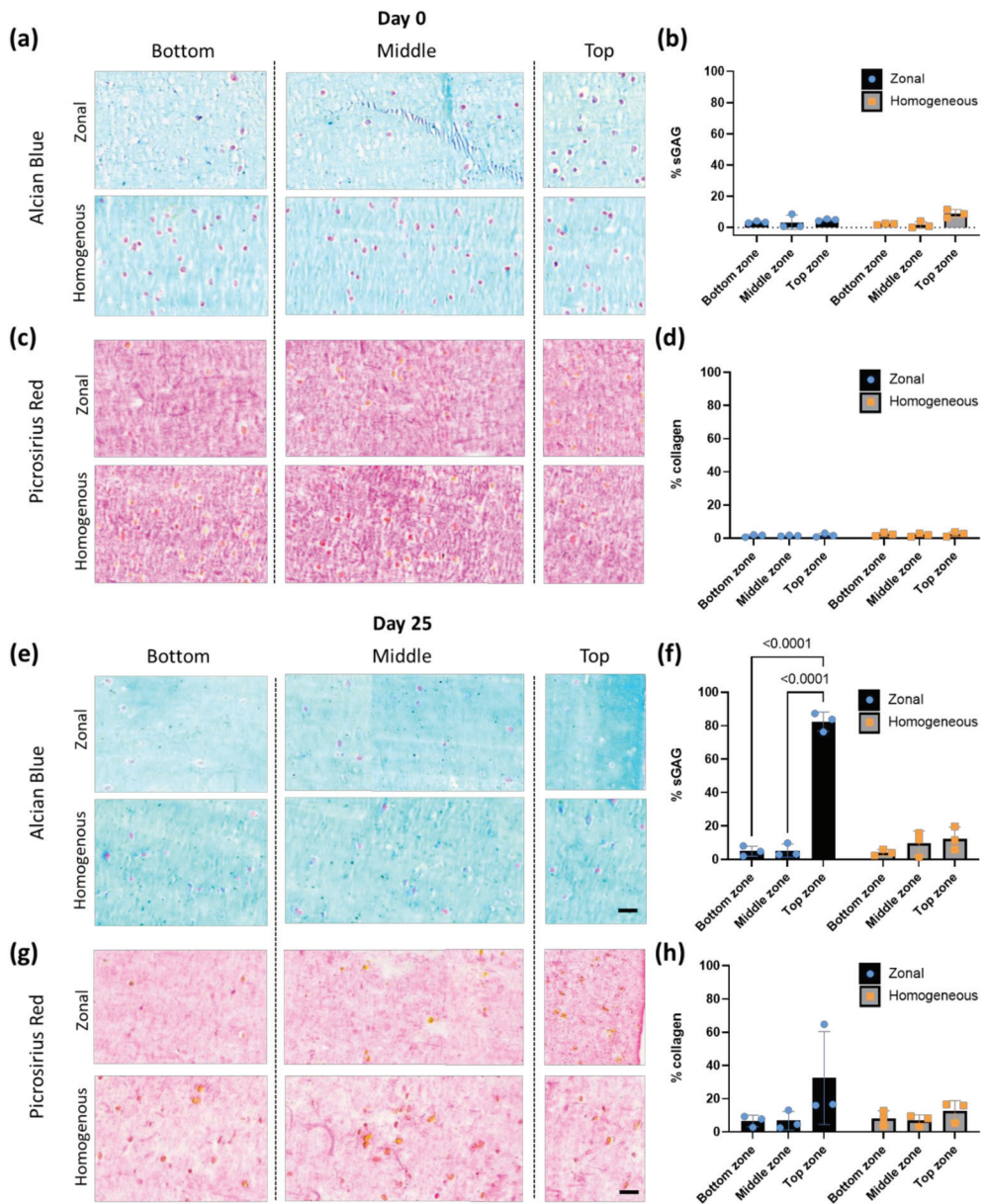


Figure 4. Bioprinted zonal scaffolds with cell density gradients result in differential cartilage-like tissue deposition; (a) histological images of zonal or homogeneous scaffold bioprinted with human chondrocytes and evaluated for sGAG with Alcian Blue staining (AB) at day 0; (b) the corresponding semiquantitative zonal analysis of the AB staining; (c) histological images evaluated for collagen deposition with Picrosirius Red staining (PSR) at day 0; (d) the corresponding semiquantitative zonal analysis of the PSR staining; (e) the histological images evaluated for sGAG with AB after 25 days in culture; (f) the corresponding semiquantitative zonal analysis of the AB staining; (g) histological images evaluated for collagen with PSR; (h) the corresponding semiquantitative zonal analysis of the PSR staining ($n = 3$; p -values < 0.05 are shown). Scale bar: 100 μ m.

At day 25 of culture, both types of staining demonstrated that the scaffolds supported the deposition of cartilage-like tissue components. In the zonal scaffold, Alcian Blue staining revealed an increased deposition of sGAG in the top zone of the scaffold at day 25, as indicated by a strong Alcian Blue signal (Figure 4e, zonal, AB, top). The semiquantification of the staining revealed the zonal manner in which sGAG was deposited within the scaffolds over time, displaying a significantly increase from the bottom to the top zone (Figure 4f, left), which was in accordance with the cell density distribution within the scaffolds. The homogeneous scaffolds deposited a similar amount of sGAG in all the different zones at day 25 (Figure 4e, homogeneous, AB and Figure 3f, right). For the collagen deposition, it was observed that chondrocytes appeared to mainly secrete small amounts of pericellular collagen according to the intense orange-red staining observed (which is positive for collagen staining) after 25 days of culture (Figure 4g). Similar to the result of Alcian Blue staining, some samples exhibited a trend toward stronger staining in the top zone of the specimens. By comparison, the homogeneous scaffolds revealed no differences in their staining throughout the section. The statistical analysis of the semiquantitative values corresponding to Picrosirius Red revealed a trend of increasing collagen deposition in the top zone of some of the zonal scaffolds. However, no significant differences were found between the groups after 25 days of culture (Figure 4h).

4. Discussion

In this study, we aimed to generate a cartilage scaffold of a clinically relevant size that mimics the gradient distribution of cells that is observed across the three distinct zones of the native tissue in hyaline articular cartilage of the human condyle and to analyze the cell viability and cell-derived matrix deposition. Over time in culture, the generated zonal scaffolds led to a gradient in cartilage-like matrix deposition. For printing each zonal scaffold, four different inks (one ink and three bioinks) were used to print different parts of the scaffold. Every printing part used its own printhead except for the middle and top zones where the bioink-containing cartridge had to be interchanged for every printed scaffold. This allowed us to simultaneously 3D print a PCL frame and the different chondrocyte-embedded zones with clinically relevant thicknesses and zone-specific cell densities. Few papers have investigated the 3D printing of more than one bioink for a single construct [10,19,24–26], probably due to the lack of several printheads or impracticality due to the constant changing of the printing cartridges that results in a time-consuming process. Recent studies suggest the use of coaxial needles [27] or continuous chaotic printing [28] as alternatives to generate multicellular heterogeneous systems. Several studies have combined PCL with bioinks to enhance the compressive stiffness of hydrogels [29–31]. In our study, the PCL frame helped the maintenance of the structural integrity of the scaffolds during bioprinting and subsequent *in vitro* culture. In addition, a PCL frame can be useful for future *in vivo* implantation [32,33]. Previous studies have shown that different cell densities can lead to different mechanical properties which are correlated with the amount of sGAG produced. In this study, we did not perform mechanical characterization of the hydrogel overtime. Therefore, future studies should also focus on the effect of different cell densities on the mechanical properties of the scaffold overtime. Regarding the PCL reinforcement, in most studies, this reinforcement is done by printing a mesh of PCL fibers in between hydrogel fibers, where the fiber orientation alternates orthogonally after every layer. In this study, however, it was determined that passing the hot (210 °C) thermoplastic nozzle right next to the cell-embedded hydrogel fibers negatively affects the chondrocyte viability, which has been also noted in other studies [34]. Therefore, another design approach was chosen in which the PCL would act as an outer skeleton for the hydrogel, concentrating the cell-embedded volume of the bioink at the center and maintaining its shape throughout its thickness. This approach was able to significantly increase the bulk mechanical properties compared to the bioink alone, as others have demonstrated [29–31]. Other studies also explored the pre-printing of PCL structures and then either cast or z-printed the bioink in the channels of the PCL mesh [35]. Despite

this option giving more freedom, as it decouples the fabrication process of the outer frame and the bioprinting of the bioink, z-print is not yet an option available in all 3D printing systems. After fabrication of such complex structures, live/dead and histological analysis demonstrated that human chondrocytes still retained high viability and zone-specific cell densities. In addition, this cell density gradient was shown to be maintained during *in vitro* culture for 25 days, resulting in a gradient in tissue deposition as compared to homogeneous scaffolds. Previous studies aiming to fabricate similar constructs with different cell density layers through bioprinting have not shown such clear cell distribution or its maintenance over time [19]. For example, it has been reported that cell gradient in scaffolds of 3 mm thickness fail due to the fusion of the zones during bioprinting. Moreover, the analysis of that study was focused on the overall scaffold rather than on the individual zones [19]. It is noteworthy that the difference in cell number between the middle and the bottom zones in the gradient scaffold is less apparent after culture in differentiation medium. Although cells do not tend to migrate in alginate, this particular bioink formulation containing methylcellulose may allow for some cellular migration [36] from the middle to the bottom layer, perhaps in the search for available nutrients and oxygen. This potential migration may have been caused by the cell gradient itself, as no changes in cell number were observed in the homogeneous scaffold. Further research is needed to verify this hypothesis. Despite the presence of the tissue deposition gradients, low amounts of glycosaminoglycan and collagen were seen in all the groups. This may be due to the alginate-based bioinks that offer good printability [25,30,35,37–41] but do not offer enzymatic-derived tissue remodeling [42], which have been suggested to potentially act as a physical barrier for tissue secretion *in vitro*, as also observed by others [43–45]. On the other hand, alginate-based biomaterials have been shown to be capable of generating cartilage when implanted *in vivo* [46,47], suggesting that other factors may also be playing a role in this regard. For instance, chondrocytes from only one donor were used in our study, and it is known that there can be some variability between donors or even between chondrocytes from different zones [45]. Regarding tissue deposition, it is interesting to point out that the superficial zone of native mature articular cartilage is characterized by a lower sGAG presence than the other zones. Our scaffold demonstrated that having a higher cell density in the superficial zone will result in higher sGAG. However, the tissue formed in our scaffold is still in development and yet far from what is seen in articular cartilage tissue. It will be necessary to evaluate how applications of these different zones would influence eventual tissue that is formed using *in vivo* models. Our study is in agreement with the previous studies showing that constructs with a higher cell density result in higher cartilage-like matrix deposition [48,49] and enhanced gene expression of cartilage markers [19]. This study focused on the recapitulation of the cell gradient observed in native hyaline articular cartilage. However, there are other gradients that could be interesting to investigate or even to combine. For instance, AC has been shown to have a gradient in stiffness [50–53]. Previous research has aimed to combine a stiffness gradient achieved by photo-crosslinking with a growth factor gradient achieved by mixing both TGF- β 1 and BMP-2 in the hydrogel (before crosslinking). These gradients proved capable of regulating the number of embedded hMSCs and their differentiation toward bone- or cartilage-like matrix-producing cells [18]. In addition, from a developmental biology perspective, cartilage starts as a soft template. Therefore, it may be interesting to explore the generation of the stiffness gradients that occur in time. This points to the need for the development of new 4D bioprinting approaches that investigate the use of stimulus-responsive biomaterials to answer such complex questions [54].

5. Conclusions

In this study, zonal cartilage scaffolds with clinically relevant sizes and cell densities were successfully bioprinted as single units. The different zonal cell densities were partially maintained *in vitro* for 25 days. In addition, the scaffolds led to a gradient in the extracellular matrix components produced by the embedded human chondrocytes. These findings

shed some light on the effects of zonal cell gradients on the formation of new tissue matrix and help in addressing the remaining obstacles in order to accelerate the translation of cartilage tissue engineering into clinical practice.

Supplementary Materials: The following are available online at <https://www.mdpi.com/article/10.3390/app11177821/s1>: Figure S1. PCL design can affect cell viability; Video S1. A clip of the bioprinting process.

Author Contributions: Conceptualization, A.D., R.N., L.E.F.-A. and A.A.Z.; methodology, P.J.D.-P., A.D., M.M., M.H. and N.K.; software, P.J.D.-P. and A.D.; formal analysis, P.J.D.-P. and A.D.; investigation, P.J.D.-P. and A.D.; writing—original draft preparation, P.J.D.-P. and A.D.; writing—review and editing, P.J.D.-P., G.J.V.M.v.O., L.E.F.-A. and A.A.Z.; supervision, P.J.D.-P., M.N.-G., M.J.M. and L.E.F.-A.; project administration, L.E.F.-A. and A.A.Z.; funding acquisition, G.J.V.M.v.O. and A.A.Z. All authors have read and agreed to the published version of the manuscript.

Funding: This research was funded by the Dutch Medical Delta project: RegMed4D.

Data Availability Statement: The data that support the findings of this study are available from the corresponding author, [A.A.Z.], upon reasonable request.

Conflicts of Interest: The authors declare no conflict of interest.

References

- Myers, K.R.; Sgaglione, N.A.; Grande, D.A. Trends in biological joint resurfacing. *Bone Jt. Res.* **2013**, *2*, 193–199. [[CrossRef](#)] [[PubMed](#)]
- Brittberg, M.; Lindahl, A.; Nilsson, A.; Ohlsson, C.; Isaksson, O.; Peterson, L. Treatment of deep cartilage defects in the knee with autologous chondrocyte transplantation. *N. Engl. J. Med.* **1994**, *331*, 889–895. [[CrossRef](#)]
- Ahern, B.; Parvizi, J.; Boston, R.; Schaefer, T. Preclinical animal models in single site cartilage defect testing: A systematic review. *Osteoarthr. Cartil.* **2009**, *17*, 705–713. [[CrossRef](#)] [[PubMed](#)]
- James, S.L.; Abate, D.; Abate, K.H.; Abay, S.M.; Abbafati, C.; Abbasi, N.; Abbastabar, H.; Abd-Allah, F.; Abdela, J.; Abdelalim, A.; et al. Global, regional, and national incidence, prevalence, and years lived with disability for 354 diseases and injuries for 195 countries and territories, 1990–2017: A systematic analysis for the global burden of disease study 2017. *Lancet* **2018**, *392*, 1789–1858. [[CrossRef](#)]
- Roseti, L.; Grigolo, B. Host environment: Scaffolds and signaling (tissue engineering) articular cartilage regeneration: Cells, scaffolds, and growth factors. In *Bio-Orthopaedics: A New Approach*; Springer: Berlin/Heidelberg, Germany, 2017; pp. 87–103. ISBN 9783662541814.
- Kreuz, P.; Steinwachs, M.; Erggelet, C.; Krause, S.; Konrad, G.; Uhl, M.; Südkamp, N. Results after microfracture of full-thickness chondral defects in different compartments in the knee. *Osteoarthr. Cartil.* **2006**, *14*, 1119–1125. [[CrossRef](#)]
- Ansari, S.; Khorshidi, S.; Karkhaneh, A. Engineering of gradient osteochondral tissue: From nature to lab. *Acta Biomater.* **2019**, *87*, 41–54. [[CrossRef](#)] [[PubMed](#)]
- Huber, M.; Trattig, S.; Lintner, F. Anatomy, biochemistry, and physiology of articular cartilage. *Investig. Radiol.* **2000**, *35*, 573–580. [[CrossRef](#)]
- Bracaglia, L.G.; Smith, B.T.; Watson, E.; Arumugasaamy, N.; Mikos, A.G.; Fisher, J.P. 3D printing for the design and fabrication of polymer-based gradient scaffolds. *Acta Biomater.* **2017**, *56*, 3–13. [[CrossRef](#)] [[PubMed](#)]
- Levato, R.; Webb, W.; Otto, I.A.; Mensinga, A.; Zhang, Y.; van Rijen, M.; Khan, I.; Malda, J. The bio in the ink: Cartilage regeneration with bioprintable hydrogels and articular cartilage-derived progenitor cells. *Acta Biomater.* **2017**, *61*, 41–53. [[CrossRef](#)]
- Parisi, C.; Salvatore, L.; Veschini, L.; Serra, M.P.; Hobbs, C.; Madaghiele, M.; Sannino, A.; Di Silvio, L. Biomimetic gradient scaffold of collagen-hydroxyapatite for osteochondral regeneration. *J. Tissue Eng.* **2020**, *11*, 11. [[CrossRef](#)]
- Liu, E.; Zhu, D.; Diaz, E.C.G.; Tong, X.; Yang, F. Gradient hydrogels for optimizing niche cues to enhance cell-based cartilage regeneration. *Tissue Eng. Part A* **2020**, *27*, 929–939. [[CrossRef](#)] [[PubMed](#)]
- Gao, F.; Xu, Z.; Liang, Q.; Liu, B.; Li, H.; Wu, Y.; Zhang, Y.; Lin, Z.; Wu, M.; Ruan, C.; et al. Direct 3D printing of high strength biohybrid gradient hydrogel scaffolds for efficient repair of osteochondral defect. *Adv. Funct. Mater.* **2018**, *28*, 1706644. [[CrossRef](#)]
- Chen, H.; Deng, C.; Li, J.; Yao, Q.; Chang, J.; Wang, L.; Wu, C. 3D printing of a lithium-calcium-silicate crystal bioscaffold with dual bioactivities for osteochondral interface reconstruction. *Biomaterials* **2019**, *196*, 138–150. [[CrossRef](#)] [[PubMed](#)]
- Zhu, D.; Tong, X.; Trinh, P.; Yang, F. Mimicking cartilage tissue zonal organization by engineering tissue-scale gradient hydrogels as 3D cell niche. *Tissue Eng. Part A* **2018**, *24*, 1–10. [[CrossRef](#)]
- Sun, Y.; You, Y.; Jiang, W.; Wang, B.; Wu, Q.; Dai, K. 3D bioprinting dual-factor releasing and gradient-structured constructs ready to implant for anisotropic cartilage regeneration. *Sci. Adv.* **2020**, *6*, eaay1422. [[CrossRef](#)]
- Nowicki, M.A.; Castro, N.J.; Plesniak, M.W.; Zhang, L.G. 3D printing of novel osteochondral scaffolds with graded microstructure. *Nanotechnology* **2016**, *27*, 414001. [[CrossRef](#)]

18. Jeon, O.; Alt, D.S.; Linderman, S.; Alsberg, E. Biochemical and physical signal gradients in hydrogels to control stem cell behavior. *Adv. Mater.* **2013**, *25*, 6366–6372. [CrossRef]
19. Ren, X.; Wang, F.; Chen, C.; Gong, X.; Yin, L.; Yang, L. Engineering zonal cartilage through bioprinting collagen type II hydrogel constructs with biomimetic chondrocyte density gradient. *BMC Musculoskelet. Disord.* **2016**, *17*, 1–10. [CrossRef] [PubMed]
20. Slic3r. Slic3r-Open Source 3D Printing Toolbox. Available online: <https://slic3r.org/> (accessed on 6 July 2021).
21. Hunziker, E.; Quinn, T.; Häuselmann, H.-J. Quantitative structural organization of normal adult human articular cartilage. *Osteoarthr. Cartil.* **2002**, *10*, 564–572. [CrossRef]
22. R Core Team. *R: A Language and Environment for Statistical Computing*; R Foundation for Statistical Computing: Vienna, Austria, 2018. Available online: <https://www.R-project.org> (accessed on 20 August 2019).
23. Arganda-Carreras, I.; Kaynig, V.; Rueden, C.; Eliceiri, K.; Schindelin, J.E.; Cardona, A.; Seung, H.S. Trainable weka segmentation: A machine learning tool for microscopy pixel classification. *Bioinformatics* **2017**, *33*, 2424–2426. [CrossRef] [PubMed]
24. Li, C.; Faulkner-Jones, A.; Dun, A.R.; Jin, J.; Chen, P.; Xing, Y.; Yang, Z.; Li, Z.; Shu, W.; Liu, D.; et al. Rapid formation of a supramolecular polypeptide-DNA hydrogel for in situ three-dimensional multilayer bioprinting. *Angew. Chem. Int. Ed.* **2015**, *54*, 3957–3961. [CrossRef] [PubMed]
25. Li, H.; Tan, Y.J.; Leong, K.F.; Li, L. 3D bioprinting of highly thixotropic alginate/methylcellulose hydrogel with strong interface bonding. *ACS Appl. Mater. Interfaces* **2017**, *9*, 20086–20097. [CrossRef]
26. Kolesky, D.B.; Homan, K.A.; Skylar-Scott, M.A.; Lewis, J.A. Three-dimensional bioprinting of thick vascularized tissues. *Proc. Natl. Acad. Sci. USA* **2016**, *113*, 3179–3184. [CrossRef] [PubMed]
27. Dai, X.; Liu, L.; Ouyang, J.; Xingliang, D.; Zhang, X.; Lan, Q.; Xu, T. Coaxial 3D bioprinting of self-assembled multicellular heterogeneous tumor fibers. *Sci. Rep.* **2017**, *7*, 1–11. [CrossRef] [PubMed]
28. Chávez-Madero, C.; De León-Derby, M.D.; Samandari, M.; Ceballos-González, C.F.; Bolívar, E.; Mendoza-Buenrostro, C.C.; Holmberg, S.; Garza-Flores, N.A.; Almajhadi, M.A.; González-Gamboa, I.; et al. Using chaotic advection for facile high-throughput fabrication of ordered multilayer micro- and nanostructures: Continuous chaotic printing. *Biofabrication* **2020**, *12*, 035023. [CrossRef]
29. Lee, J.-S.; Hong, J.M.; Jung, J.W.; Shim, J.-H.; Oh, J.-H.; Cho, D.-W. 3D printing of composite tissue with complex shape applied to ear regeneration. *Biofabrication* **2014**, *6*, 024103. [CrossRef] [PubMed]
30. Daly, A.; Critchley, S.E.; Rencsok, E.M.; Kelly, D.J. A comparison of different bioinks for 3D bioprinting of fibrocartilage and hyaline cartilage. *Biofabrication* **2016**, *8*, 045002. [CrossRef] [PubMed]
31. Castilho, M.; Hochleitner, G.; Wilson, W.; Van Rietbergen, B.; Dalton, P.D.; Groll, J.; Malda, J.; Ito, K. Mechanical behavior of a soft hydrogel reinforced with three-dimensional printed microfibre scaffolds. *Sci. Rep.* **2018**, *8*, 1–10. [CrossRef] [PubMed]
32. Freeman, F.; Browe, D.; Nulty, J.; Von Eeuw, S.; Grayson, W.L.; Kelly, D.J. Biofabrication of multiscale bone extracellular matrix scaffolds for bone tissue engineering. *Eur. Cells Mater.* **2019**, *38*, 168–187. [CrossRef]
33. Critchley, S.; Sheehy, E.; Cunniffe, G.; Diaz-Payno, P.; Carroll, S.F.; Jeon, O.; Alsberg, E.; Brama, P.A.; Kelly, D.J. 3D printing of fibre-reinforced cartilaginous templates for the regeneration of osteochondral defects. *Acta Biomater.* **2020**, *113*, 130–143. [CrossRef]
34. Schuurman, W.; Khristov, V.; Pot, M.W.; van Weeren, P.R.; Dhert, W.J.A.; Malda, J. Bioprinting of hybrid tissue constructs with tailorable mechanical properties. *Biofabrication* **2011**, *3*, 021001. [CrossRef]
35. Schipani, R.; Scheurer, S.; Florentin, R.; Critchley, S.E.; Kelly, D.J. Reinforcing interpenetrating network hydrogels with 3D printed polymer networks to engineer cartilage mimetic composites. *Biofabrication* **2020**, *12*, 035011. [CrossRef]
36. Garrett, Q.; Simmons, P.A.; Xu, S.; Vehige, J.; Zhao, Z.; Ehrmann, K.; Willcox, M. Carboxymethylcellulose binds to human corneal epithelial cells and is a modulator of corneal epithelial wound healing. *Investig. Ophthalmol. Vis. Sci.* **2007**, *48*, 1559–1567. [CrossRef]
37. Yang, X.; Lu, Z.; Wu, H.; Li, W.; Zheng, L.; Zhao, J. Collagen-alginate as bioink for three-dimensional (3D) cell printing based cartilage tissue engineering. *Mater. Sci. Eng. C* **2018**, *83*, 195–201. [CrossRef]
38. Ávila, H.M.; Schwarz, S.; Rotter, N.; Gatenholm, P. 3D bioprinting of human chondrocyte-laden nanocellulose hydrogels for patient-specific auricular cartilage regeneration. *Bioprinting* **2016**, *1–2*, 22–35. [CrossRef]
39. Bendtsen, S.T.; Quinnell, S.P.; Wei, M. Development of a novel alginate-polyvinyl alcohol-hydroxyapatite hydrogel for 3D bioprinting bone tissue engineered scaffolds. *J. Biomed. Mater. Res. Part A* **2017**, *105*, 1457–1468. [CrossRef] [PubMed]
40. Markstedt, K.; Mantas, A.; Tournier, L.; Ávila, H.M.; Hägg, D.; Gatenholm, P. 3D bioprinting human chondrocytes with Nanocellulose-Alginate bioink for cartilage tissue engineering applications. *Biomacromolecules* **2015**, *16*, 1489–1496. [CrossRef] [PubMed]
41. de Melo, B.A.G.; Jodat, Y.A.; Mehrotra, S.; Calabrese, M.; Kamperman, T.; Mandal, B.B.; Santana, M.H.A.; Alsberg, E.; Leijten, J.; Shin, S.R. 3D printed cartilage-like tissue constructs with spatially controlled mechanical properties. *Adv. Funct. Mater.* **2019**, *29*, 1906330. [CrossRef]
42. Lee, K.Y.; Mooney, D.J. Alginate: Properties and biomedical applications. *Prog. Polym. Sci.* **2012**, *37*, 106–126. [CrossRef]
43. Van Susante, J.L.C.; Buma, P.; Van Osch, G.J.; Versleyen, D.; Van Der Kraan, P.M.; Van Der Berg, W.B.; Homminga, G.N. Culture of chondrocytes in alginate and collagen carrier gels. *Acta Orthop. Scand.* **1995**, *66*, 549–556. [CrossRef]

44. van Osch, G.J.; Berg, W.B.V.D.; Hunziker, E.B.; Häusselmann, H.J. Differential effects of IGF-1 and TGF β -2 on the assembly of proteoglycans in pericellular and territorial matrix by cultured bovine articular chondrocytes. *Osteoarthr. Cartil.* **1998**, *6*, 187–195. [[CrossRef](#)] [[PubMed](#)]
45. Malda, J.; Hoop, W.T.; Schuurman, W.; Van Osch, G.J.; Van Weeren, P.R.; Dhert, W.J. Localization of the potential zonal marker clusterin in native cartilage and in tissue-engineered constructs. *Tissue Eng. Part A* **2010**, *16*, 897–904. [[CrossRef](#)] [[PubMed](#)]
46. Pleumeekers, M.M.; Nimeskern, L.; Koevoet, W.L.M.; Kops, N.; Poulblon, R.M.L.; Stok, K.S.; Van Osch, G.J.V.M. The in vitro and in vivo capacity of culture-expanded human cells from several sources encapsulated in alginate to form cartilage. *Eur. Cells Mater.* **2014**, *27*, 264–280. [[CrossRef](#)]
47. Marijnissen, W.J.; van Osch, G.J.; Aigner, J.; van der Veen, S.W.; Hollander, A.P.; Verwoerd-Verhoef, H.L.; Verhaar, J. Alginate as a chondrocyte-delivery substance in combination with a non-woven scaffold for cartilage tissue engineering. *Biomaterials* **2002**, *23*, 1511–1517. [[CrossRef](#)]
48. Talukdar, S.; Nguyen, Q.T.; Chen, A.C.; Sah, R.L.; Kundu, S.C. Effect of initial cell seeding density on 3D-engineered silk fibroin scaffolds for articular cartilage tissue engineering. *Biomaterials* **2011**, *32*, 8927–8937. [[CrossRef](#)]
49. Mauck, R.; Wang, C.-B.; Oswald, E.; Ateshian, G.; Hung, C. The role of cell seeding density and nutrient supply for articular cartilage tissue engineering with deformational loading. *Osteoarthr. Cartil.* **2003**, *11*, 879–890. [[CrossRef](#)]
50. Moshtagh, P.R.; Pouran, B.; Korthagen, N.M.; Zadpoor, A.A.; Weinans, H. Guidelines for an optimized indentation protocol for measurement of cartilage stiffness: The effects of spatial variation and indentation parameters. *J. Biomech.* **2016**, *49*, 3602–3607. [[CrossRef](#)] [[PubMed](#)]
51. Ebenstein, D.; Kuo, A.; Rodrigo, J.J.; Reddi, A.H.; Ries, M.; Pruitt, L. A nanoindentation technique for functional evaluation of cartilage repair tissue. *J. Mater. Res.* **2004**, *19*, 273–281. [[CrossRef](#)]
52. Bae, W.C.; Lewis, C.W.; Levenston, M.; Sah, R.L. Indentation testing of human articular cartilage: Effects of probe tip geometry and indentation depth on intra-tissue strain. *J. Biomech.* **2006**, *39*, 1039–1047. [[CrossRef](#)] [[PubMed](#)]
53. Antons, J.; Marascio, M.G.M.; Nohava, J.; Martin, R.; Applegate, L.A.; Bourban, P.E.; Pioletti, D.P. Zone-dependent mechanical properties of human articular cartilage obtained by indentation measurements. *J. Mater. Sci. Mater. Med.* **2018**, *29*, 1–8. [[CrossRef](#)] [[PubMed](#)]
54. Wan, Z.; Zhang, P.; Liu, Y.; Lv, L.; Zhou, Y. Four-dimensional bioprinting: Current developments and applications in bone tissue engineering. *Acta Biomater.* **2020**, *101*, 26–42. [[CrossRef](#)] [[PubMed](#)]

Article

Follow-Up Study Evaluating the Long Term Outcome of ChondroMimetic in the Treatment of Osteochondral Defects in the Knee

Agnes Berta ^{1,†}, Matthew S. Shive ^{2,*†}, Andrew K. Lynn ³, Alan Getgood ⁴, Saara Totterman ⁵, Grahame Busby ⁶, Jerome Hollenstein ⁶, Gábor Vásárhelyi ¹, Imre Kéki ⁷ and László Hangody ^{1,8}

¹ Department of Orthopaedics and Traumatology, Uzsoki Hospital, 1145 Budapest, Hungary; berta.agnes@uzsoki.hu (A.B.); vasarhelyigabor@uzsoki.hu (G.V.); hangody@uzsoki.hu (L.H.)

² MS² INSIGHT Consulting, LLC, Denver, CO 80220, USA

³ Fluid Analytics Cambridge, Cambridge CB1 8DH, UK; andrew.lynn@fluidic.com

⁴ Fowler Kennedy Sport Medicine Clinic, University of Western Ontario, London, ON N6A 3K7, Canada; agetgoo@uwo.ca

⁵ Qmetrics Technologies Pittsford, New York, NY 14534, USA; saara.totterman@qmetricstech.com

⁶ Collagen Solutions Plc Eden Prairie, Eden Prairie, MN 55344, USA; g.busby@terumoaoartic.com (G.B.); jerome.hollenstein@collagensolutions.com (J.H.)

⁷ Nuclear Medicine Uzsoki Hospital, 1145 Budapest, Hungary; keki@uzsoki.hu

⁸ Department of Traumatology, Semmelweis University, 1085 Budapest, Hungary

* Correspondence: matthew.shive@aic.com

† Co-First Authors.

Received: 7 June 2020; Accepted: 11 August 2020; Published: 14 August 2020

Abstract: Scaffolds are thought to be a key element needed for successful cartilage repair treatments, and this prospective extension study aimed to evaluate long-term structural and clinical outcomes following osteochondral defect treatment with a cell-free biphasic scaffold. Structural outcomes were assessed using quantitative 3-D magnetic resonance imaging (MRI) and morphological segmentation to determine the percentage of defect filling and repair cartilage T2 relaxation times, and clinical outcomes were determined with the modified Cincinnati Rating System, and the Knee Injury and Osteoarthritis Outcome Score (KOOS). Seventeen subjects with osteochondral defects in the knee were treated with ChondroMimetic scaffolds, from which 15 returned for long-term evaluation at a mean follow-up of 7.9 ± 0.3 years. The defects treated were trochlear donor sites for mosaicplasty in 13 subjects, and medial femoral condyle defects in 2 subjects. MRI analysis of scaffold-treated defects found a mean total defect filling of $95.2 \pm 3.6\%$, and a tissue mean T2 relaxation time of 52.5 ± 4.8 ms, which was identical to the T2 of ipsilateral control cartilage (52.3 ± 9.2 ms). The overall modified Cincinnati Rating System score was statistically significant from baseline ($p = 0.0065$), and KOOS subscales were equivalent to other cartilage repair techniques. ChondroMimetic treatment resulted in a consistently high degree of osteochondral defect filling with durable, cartilage-like repair tissue at 7.9 years, potentially associated with clinical improvement.

Keywords: biphasic scaffold; osteochondral defect; cartilage repair; quantitative MRI; calcium phosphate

1. Introduction

Articular cartilage damage continues to present a therapeutic challenge, and despite multiple and differing approaches ranging from bone marrow stimulation [1], autologous chondrocyte implantation (ACI) [2], and various grafting procedures incorporating allografts and autografts [3,4], none are recognized as sufficient. Recent reviews demonstrate that clinical research has failed to substantiate the

superiority of one technique or product, in large part because of heterogeneous patient demographics, the differing etiologies of defects, and the varying study designs and outcome measures [5–7]. The lack of longer term (5–10 years) clinical evidence in cartilage repair further limits evidence-based treatment algorithms. Nonetheless, the fundamental goal of any cartilage repair treatment should be to avoid the progression to secondary osteoarthritis [8,9], by achieving structural repair that is comparable to native hyaline cartilage, and thereby assuring long-term durability, joint function, and pain relief.

ChondroMimetic (Collagen Solutions, Plc) was developed to be a cell-free, osteochondral scaffold for use in cartilage repair. The biphasic implant comprises a 2 mm, unmineralized, type I bovine collagen and chondroitin-6-sulphate glycosaminoglycan (collagen/GAG) chondral layer, coupled to a 6mm, mineralized, subchondral bone layer, containing collagen/GAG and calcium phosphate brushite. These two distinct layers are separated by a continuous or ‘soft’ interface that closely mimics the compositional transition between mineralized bone and unmineralized cartilage at the tide mark [10]. As an open-cell foam, the ChondroMimetic scaffold which allows compression during surgical handling for press-fit implantation, followed by auto-expansion to fit the defect shape, bridging any gaps or irregularities [11]. In a defect with stable margins, ChondroMimetic offers structural and mechanical protection for the marrow-derived blood clot, similarly to mechanisms claimed for other techniques (e.g., autologous matrix-induced chondrogenesis (AMIC) [12], BST-CarGel [13]). Large animal preclinical studies with ChondroMimetic demonstrated a consistency in osteochondral repair characterized by a high degree of cartilage defect filling with a hyaline-like repair tissue in both medial femoral condyle and trochlear defect sites [14–16].

Since long term data (>5 years post treatment) is fast becoming a required component for clinical decision-making in cartilage repair, the aim of this prospective extension study was to determine the long-term effectiveness of ChondroMimetic treatment of osteochondral defects in subjects enrolled in a previous short-term study. Using 3D quantitative magnetic resonance imaging (MRI) techniques, a consistently high degree of osteochondral defect filling with durable, cartilage-like repair tissue was found at 7.9 years and potential clinical benefit.

2. Methods

2.1. Study Design and Participants

This study was an extension of a prospective, interventional study which enrolled 17 subjects between February 2009 and March 2010 at a single clinical site (formerly unpublished). The 17 eligible subjects (8 males, 9 females) were between 18 and 50 years of age with at least one osteochondral defect measuring <12 mm in the knee. Subjects with a body mass index >40 kg/m² or a previous cartilage repair treatment in the index knee were excluded. All subjects who participated in the original interventional study were eligible to be enrolled in the extension study, which was designed to provide long-term follow up at a single time point which included a clinic visit and a single MRI scan. All subjects were asked to provide written informed consent prior to extension study activities, which were approved by national and local ethics review boards. Both studies were performed in accordance with guidelines for Good Clinical Practice. This extension study was registered with [ClinicalTrials.gov](https://clinicaltrials.gov) (NCT03385642).

2.2. Interventional Details

During the original interventional study, following osteochondral defect preparation, the pre-loaded implant was hydrated with saline through the hydration portal in the delivery device, which was then positioned perpendicular to the defect with the tip inserted to the full defect depth. Simultaneous advancement of the implant and withdrawal of the device tip left the implant to expand into the defect volume. ChondroMimetic scaffolds were used to treat mosaicplasty donor sites in the trochlea in 15/17 subjects concurrent with mosaicplasty treatment of 12 femoral condyle defects and 3 ankle defects. ChondroMimetic scaffolds were also used to treat primary femoral condyle defects

in 2/17 subjects. Ultimately, scaffolds chosen for use ranged from 6.5–8.5 mm in diameter. None of the subjects included in the study had tibial articular defects.

2.3. Outcome Measures

Neither the subjects nor the investigator were blinded to treatment in this study, but the administration of identical validated questionnaires, standardized acquisition of MRI scans, and subsequent semi-automated, quantitative MRI analysis of repair tissue structure by an independent 3rd party minimized method and analysis bias.

2.3.1. Structural Repair

Repair tissue structure, defined as the quantity (i.e., degree of defect filling (%)) and quality (T2 relaxation time) of new cartilage tissue, was assessed by three-dimensional (3D) quantitative MRI conducted at an imaging core lab (Qmetrics Technologies, Rochester, NY, USA) using, validated segmentation and 3D reconstruction techniques [17,18] which have been applied in Phase 3 clinical trials of cartilage repair and multiple osteoarthritis studies [19–21]. Standardized MRI scans were acquired for each subject upon enrolment into the extension study with a Siemens 3T MAGNETOM® Verio, A Tim+Dot System and dedicated Tx-Rx CP extremity coil at a single, prequalified and trained MRI clinic. Technician training and scanner magnet qualification were conducted prior to trial activities. A uniformity and linearity phantom scan was performed for quality control. Imaging phantoms within the field of view served as internal controls.

The imaging protocol was designed to provide very high spatial resolution with high in-plane resolution and thin slices for all sequences. The study images were acquired using a fat-suppressed 3D spoiled gradient-echo (FS SPGR) sequence in sagittal and axial planes (slice thickness: 2 mm), and a 2D dual-echo fat-suppressed fast spin-echo (FS dual echo) sequence in the sagittal plane (slice thickness 1.2 mm). For morphological analyses of cartilage, cartilage defects, bone and bone defects, sagittal and axial FS SPGR series were used. Sagittal FS dual-echo series were used for T2 analyses. All scans were sent to an imaging core lab for centralized scan quality review, storage, and quantitative analysis. The sagittal 3D FS SPGR series and the sagittal FS dual echo series were segmented for bone and cartilage using a semi-automated atlas-based segmentation method [17]. The segmentations were reviewed and edited, if needed, by a musculoskeletal radiologist with expertise in cartilage repair. Original cartilage and bone defect boundaries for each subject were manually established on FS SPGR and FS dual echo segmentations using edited segmentation of MRI scans (sagittal dual echo) obtained 10 days post-operatively in the original interventional ChondroMimetic study.

The segmented 3D volume of new repair tissue at follow-up was then used to quantitatively determine the degree of defect filling (%) and the mean T2 relaxation time of cartilage repair tissue. Filling was calculated as a ratio of new repair tissue (bone and cartilage) to the original osteochondral defect volume. In cases where multiple donor sites in the same knee were treated, confluence of defects was observed in the trabecular bone resulting in a single defect volume and a single fill ratio. A radiologist-selected region of interest (ROI) of cartilage on an untouched area of the trochlea in the same knee was segmented and analyzed for each subject as a native T2 control.

2.3.2. Clinical Benefit

Clinical outcomes at the extension study timepoint were evaluated using two subject self-reported questionnaires. The modified Cincinnati Rating System has 8 components in the score, assessing pain, swelling, giving way, overall activity levels and walking, stairs, running activity, and jumping/twisting. With this instrument, a higher score is a better result and a lower score implies greater disability. Grading of the scores followed that proposed by Bentley et al. [22], where a score of <30 as “poor”, 30–54 as “fair”, 55–79 as “good” and >80 as “excellent”.

The Knee injury and Osteoarthritis Outcome Score (KOOS) [23] in the Likert format has 5 subscales: Pain, other Symptoms, Function in daily living, Function in Sport and Recreation and knee-related

Quality of Life. Scores are attributed by dimension, ranging from 0 to 100 (high score better outcome). The KOOS score was not administered in the original interventional study, and therefore baseline scores were not available.

2.4. Statistical Considerations

All statistical analyses were conducted using SAS 9.4 or above (SAS Institute Inc., Cary, NC, USA). All graphs were produced in Microsoft Excel 2016 (Microsoft Inc., Redmond, WA, USA). For statistical analysis purposes, baseline was defined for clinical outcome data as data collected pre-operatively, and for MRI analyses, 10 day post-operatively. Quantitative structural repair outcomes underwent univariate and descriptive analyses, investigating the scores at the single study time point for the degree of defect filling (total volume), and for repair tissue quality (T2). Clinical outcome data underwent univariate and descriptive analyses, for both modified Cincinnati Rating System and KOOS subscales. Statistical comparisons used Student's *t*-tests.

3. Results

3.1. Enrolment and Subject Characteristics

Enrolment into the extension study targeted 8-year follow-up for the 17 subjects in the original clinical study. Ultimately, 15 of the original 17 subjects completed the single extension study visit, and their demographic characteristics are shown in Table 1. The study population was balanced by gender, and subjects received from 1 to 5 ChondroMimetic scaffolds, per knee, to treat trochlear donor sites for mosaicplasty in 13 subjects, and medial femoral condyle defects in 2 subjects. A total of 14 additional procedures since enrolment into the original interventional study were recorded by 12 individual subjects. The majority of these interventions involved either arthroscopy of knees or ankles or intra-articular injections. No interventions were specifically attributed to the ChondroMimetic treatment by the Investigator.

Table 1. Follow-up Characteristics of Trial Subjects †.

Characteristic	Chondromimetic (n = 15)
Consented subjects from original study, n (%)	15 (88)
Follow-up, years	7.9 ± 0.3
Age, years	32.7 ± 9.3
Gender, n (%)	
Male	7 (46.7)
Female	8 (53.3)
Body Mass Index, kg/m ²	25.3 ± 4.2
Smokers, n (%)	2 (13.3)
Index defects and implants	
Mosaicplasty donor site(s), n (%)	13 (86.7)
Medial femoral condyle defect, n (%)	2 (13.3)
Defect volume including missing bone, mm ³ ‡	1573 ± 1233
ChondroMimetic Implants/knee, median (range)	2 (1–5)
Follow-up Pain, n (%) *	
No knee pain	11 (73.3)
Mild knee pain	2 (13.3)
Moderate knee pain	2 (13.3)
Follow-up Activity Level, n (%) *	
Unlimited	8 (53)
Slightly limited	4 (27)
Moderately limited	3 (20)
Additional interventions since treatment	
Index knee related procedures ^	12
Non-knee related procedures	2

† Plus-minus values are means ± standard deviation unless otherwise indicated. ‡ Determined using quantitative 3D magnetic resonance imaging (MRI) of 10 days postoperative scans. ^ Hyaluronic acid injection (4); microfracture of new primary lesion (3); second-look arthroscopy (5). * From physical examination and standardized interview during the 8-year study visit.

There were no withdrawals from the extension study. The only missing data in the study was MRI analysis from 1 subject who did not yield usable scans due to movement.

3.2. Repair Outcomes

3.2.1. Structural Repair

The quantity and quality of ChondroMimetic repair tissues was determined for 14 subjects (the MRI from the fifteenth subject was unusable due to movement; see Table 2). ChondroMimetic-treated osteochondral defects at 7.9 years post-treatment demonstrated a substantial degree of defect filling of $95.2 \pm 3.6\%$. Figure 1 shows the Total Defect Fill (%) of individual subjects and illustrates a low variability and consistently high degree of defect filling following ChondroMimetic treatment. In addition, subjects treated with ChondroMimetic had a mean T2 relaxation time of 52.5 ± 4.8 ms for the cartilage repair tissue ROI, which was nearly equal to the T2 relaxation time of the ipsilateral native control cartilage regions (52.3 ± 9.2 ms ($p = 0.94$)), and suggestive of a very similar tissue biochemical make-up and structure. The T2 standard deviations calculated for each repair tissue volume were comparable to native cartilage (17.3 ± 3.3 vs. 13.1 ± 5.3 ms), with a variance that was statistically equal to that of native cartilage ($p = 0.11$ by F-test).

Table 2. Structural repair outcomes by 3 dimensional MRI at 7.9 years follow-up (n = 14).

Variable	Outcome
Total defect fill (%)	95.2 ± 3.6 (89.8, 99.9)
T2 relaxation time (ms)	
Cartilage repair tissue	52.5 ± 4.8 (44.4, 58.5) ⁺
Ipsilateral native cartilage	52.3 ± 9.2 (39.9, 78.5)

Values are presented as means \pm standard deviation (min, max). T2 = transverse relaxation time; MRI = magnetic resonance imaging. ⁺ $p = 0.94$ by Student's *t*-test compared to native cartilage.

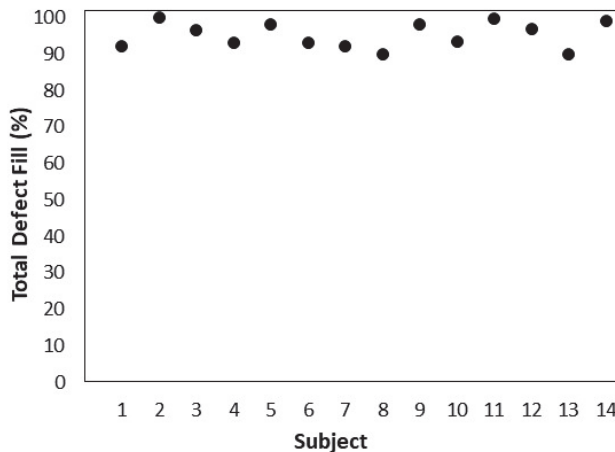


Figure 1. Total Defect Fill (%) by quantitative MRI for individual subjects at a mean followup of 7.9 years after ChondroMimetic treatment. Total Defect Fill (%) was determined using 3D quantitative magnetic resonance imaging by calculating the ratio of the new repair tissue (bone and cartilage) volume at followup, to original defect (bone and cartilage) volume acquired from 10 days post-operative scans (baseline). (n = 14).

Using each scan series, full 3D reconstructions were generated of treated knees at the 10-day post-operative baseline, and at follow-up, to assist in visualizing the morphological impact of

ChondroMimetic repair. Figure 2 illustrates a representative reconstruction conducted for a 29-year-old female subject who received 5 ChondroMimetic scaffolds in the trochlea, which are clearly visible filling the newly treated osteochondral defects in Figure 2A by 2D MRI, and are similarly visible in the 3D rendering (Figure 2B). At the follow-up after 8 years and 3 months, both the subchondral bone and cartilage aspects of the original defects appear as near-normal in both Figure 2C,D, compared with ipsilateral control regions in Figure 2E.

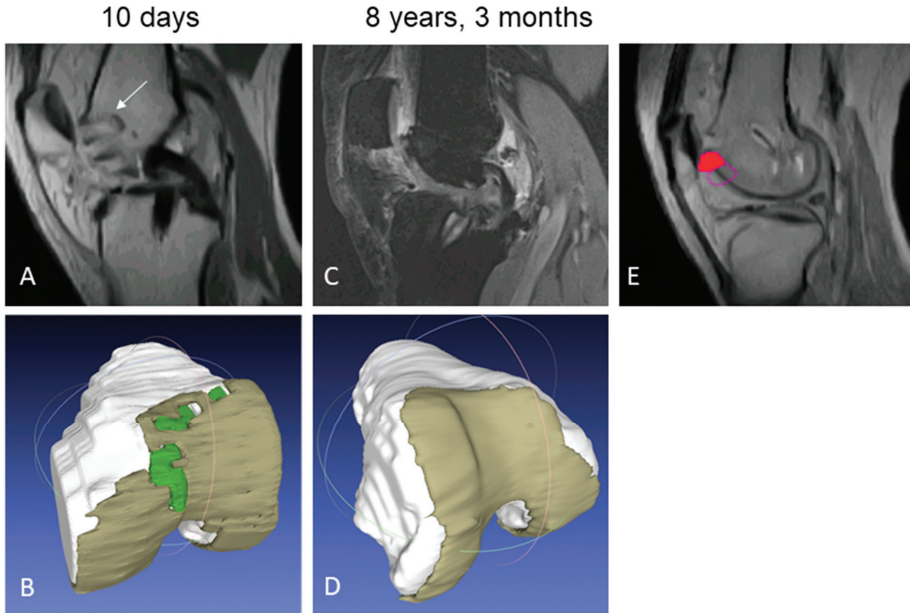


Figure 2. Longitudinal MRI reconstruction of a ChondroMimetic-treated subject knee at 10 days (A,B) and 8 years, 3 months (C,D). (A) By 2D MRI, 5 ChondroMimetic implants can be observed with hyper-intense peri-implant boundaries, and lack of cartilage-like signal (white arrow). (B) 3D rendering of knee yields ChondroMimetic implants (green) surrounded by cartilage (brown) by automated software based on MRI signal. (C) At the follow-up after 8 years and 3 months, treated bone defects are filled with bony repair tissue and the treated cartilage defect is filled with cartilaginous repair tissue. (D) Automated rendering demonstrates cartilaginous tissue in repaired defects congruous with surrounding cartilage. (E) The trochlear control region of interest (filled red circle) of native cartilage used for T2 relaxation time comparison. The open purple circle shows an unused, alternate control region of interest.

3.2.2. Clinical Benefit

The modified Cincinnati Rating System overall score at the study timepoint was 80.9 ± 15.5 , which was statistically significant from baseline ($p = 0.0065$) and represents a grading of ‘excellent’.

The KOOS subscale data are presented in Figure 3. The mean pain score was 90.0 ± 11.4 . The mean symptom score was 80.0 ± 15.8 . The mean function in daily living (ADL) score was 93.4 ± 9.1 . The mean function in sports and recreational activities (Sports/Rec) score was 68.7 ± 24.7 . The knee related quality of life (QOL) mean score was 66.7 ± 22.2 .

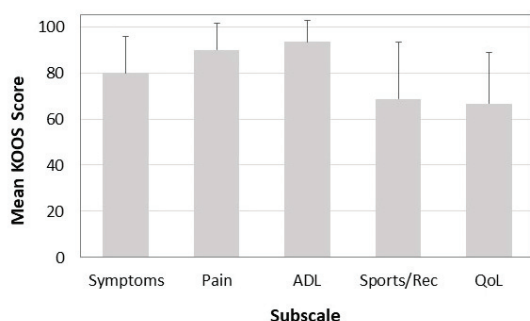


Figure 3. Knee Injury and Osteoarthritis Outcome Scores (KOOS) for ChondroMimetic subjects at a mean follow-up of 7.9 years. Data represents mean + standard deviation (n = 15).

4. Discussion

The main finding of the current study is that voluminous, high quality repair cartilage results from ChondroMimetic treatment of osteochondral defects after 7.9 years, supporting the hypothesis that ChondroMimetic brings consistent and durable long-term structural repair with an appropriate safety profile. Improvements in clinical outcomes were highly significant over the baseline ($p < 0.0065$) for the 7.9-year follow-up, which suggests a benefit of ChondroMimetic treatment when used as backfill for mosaicplasty donor sites. The use of validated, three-dimensional quantitative MRI [17,18], which assessed the repair tissue quantity and quality, is a particularly valuable aspect of this study, with a high level of standardization and precision and conducted under Good Clinical Practice guidelines.

The high degree of defect filling by new bone and repair cartilage seen in ChondroMimetic defects at 7.9 years (95.2%) is a critical outcome, as any joint resurfacing should aim to reestablish mechanical homeostasis and anatomical shape with an integrated surface, particularly since chondrocyte-mediated biosynthesis, remodeling, and either tissue repair or degradation over time is dependent on the mechanical loading conditions of cartilage [24]. Normal surface morphology and joint articulation would be expected to improve biomechanical conditions and inhibit the degeneration of defect and peri-defect tissues and slow the progression of secondary osteoarthritis [8,9]. This particular outcome was not fully unexpected, since critical size osteochondral defects in goat knees treated with ChondroMimetic scaffolds yielded similarly striking filling [14]. Furthermore, this level of defect filling is greater than that resulting from another off-the-shelf biological scaffold, BST-CarGel, at 5 year post-treatment, which produced %Fill of 93.79%, as determined by very similar quantitative MRI methods [13].

Quantitative MRI also identified durable, high quality cartilage repair tissue by T2 relaxation time for ChondroMimetic-treated defects. T2 relaxation time is well known to be sensitive to, and highly dependent on, the extracellular cartilage matrix and particularly the collagen network structure, orientation, as well as macromolecular concentration, and tissue hydration [25–29]. When acquired under standardized conditions coupled with three-dimensional segmentation of regions of interest, T2 relaxation time has been an effective, quantitative method for comparing repair tissue to native articular cartilage, and/or to repair tissue resulting from another treatment [13,30,31]. Here, the determination of the quality of repair is evidenced by the closeness of measured T2 values to that found from the ipsilateral normal articular cartilage (52.3 vs. 52.5 ms, $p = 0.94$), indicating a near-normal level of tissue quality after 7.9 years. The overall level of repair tissue organization achieved is further evidenced by the T2 standard deviations calculated for each repair tissue volume, which were comparable to native cartilage with a variance that was statistically equal to that of native cartilage. In contrast, a tissue with regions of differing organization, or of mixed hyaline-fibrocartilage tissue, would be expected to have a more widespread variance than normal cartilage. When comparing to T2 outcomes resulting from MRI studies with other scaffolds, ChondroMimetic repair tissue demonstrated

a similar closeness to native control cartilage as a study with Hyalograft C [32] in the knee, but was improved compared to the MaioRegen scaffold in the ankle [30], and BST-CarGel in the knee [13], neither of which resulted in T2 relaxation times similarly close to control cartilage. This finding also confirms consistency of repair in improved collagen-based organization and content, which are necessary components for long-term durability of cartilage since collagen breakdown is considered to be a critical step in the progression of osteoarthritis [33,34].

It may be considered a limitation of the study that ChondroMimetic was used as back-fill treatment for the majority of osteochondral defects (13/15) in the study, particularly since it is generally believed that mosaicplasty donor sites are: (1) not exposed to weight bearing forces; and (2) ultimately filled with a fibrocartilage through self-repair processes and are asymptomatic [35]. To the contrary, donor sites experience high loads with daily activities, depending on their size and location, from 1.3 times up to 7.8 times body weight [36]. Furthermore, Andrade et al. [37] reviewed 21 original mosaicplasty studies comprising 1726 patients and found that donor site morbidity reportedly occurs in 5.9–16.9% of cases and manifests through crepitation and knee stiffness, instability during activities of daily living, and persistent pain. The fact that in this study no adverse events or symptoms were reported to be related to donor sites or ChondroMimetic implants over the 7.9 year follow-up, and modified Cincinnati and KOOS scores demonstrated a high level of satisfaction, demonstrates that ChondroMimetic treatment was safe and may suggest some clinical benefit, further supported by the MRI-assessed high quality cartilage repair. Furthermore, the regeneration of bone and cartilage to near-native levels of fill and biochemical structure suggest that Chondromimetic may fit into an algorithm for treatment of full-thickness, primary cartilage lesions. Indeed, two full weight bearing primary defects on the medial femoral condyles were treated in this study with ChondroMimetic and demonstrated similarly high degrees of total defect fill (mean: 95.85%) and high quality repair tissue with T2 relaxation times comparable to native cartilage (means: 46.7 ms vs. 47.7 ms, respectively), in addition to satisfactory clinical benefit.

A true study limitation was the lack of an active control group, such as microfracture, which has been suggested by current regulatory guidance [38]. But use of an ipsilateral native cartilage control ROI for quantitative structural outcomes provided an appropriate internal control for making a determination of quality and durability of cartilage repair. Also, the small sample size of the study could limit the interpretation of the results. However, the low variance in both clinical and structural quantitative MRI outcomes nonetheless supports a consistency in repair that would likely be maintained with a larger sample size. Long-term follow-up studies can also present challenges that limit interpretation of study outcomes. For example, here, 14 procedures were conducted in the index knee of 12 subjects over the 8-year follow-up period. However, it can be concluded that it is highly unlikely that these procedures had any effect on the assessments conducted for this study. In 2 cases, the procedures were not knee related (e.g., lung biopsy). The other 12 included: (1) hyaluronic acid injections in 4 subjects performed at least 12 months prior to the extension study visit, and therefore would be expected to have lost any therapeutic effect; (2) microfracture of new primary lesions in 3 subjects, although this would represent a worst case scenario since the procedure could worsen the pain at the time of the extension study visit, or simply decrease the new pain associated with the new lesion back to baseline levels; and (3) second-look arthroscopy in 5 subjects, conducted 1–2 years post-operative by the investigator and unrelated to the study (e.g., to remove bone material from an HTO; to remove malleolar screws from ankles).

The ChondroMimetic scaffold was designed to provide a cell-free cartilage repair alternative, with biological components and architecture, conducive to the re-establishment of the subchondral bone whilst supporting regeneration of articular cartilage. With time and experience, it has been generally recognized that scaffolds are essential in supporting the processes of cartilage repair and indeed, almost all current approaches have incorporated some type of scaffold. So-called “augmented bone marrow stimulation” involves concurrent implantation of an exogenous scaffold (e.g., AMIC [12], BST-CarGel [13], Biocartilage [39]), 3rd generation ACI techniques incorporate membranes to support

cell delivery and residency (Hyalograft C [40], MACI [41]), and grafting techniques, by their nature, involve implantation of natural osteochondral scaffolds [42]. The need to have cells, at all, is being questioned when scaffolds alone, with their low cost and simplicity, bring equivalent results in a more cost-effective manner [43].

5. Conclusions

Treatment of osteochondral defects in the knee with the ChondroMimetic scaffold was associated with a consistently high degree of filling with a cartilage-like repair tissue over a long-term (7.9 year) follow-up period, improved clinical scores, and noted lack of donor site morbidity, underscoring potential benefits of a cell-free, single step scaffold from both a clinical and a health economic standpoint.

Author Contributions: Conceptualization, A.B., M.S.S., G.B. and J.H.; Formal analysis, M.S.S. and S.T.; Funding acquisition, G.B. and J.H.; Investigation, A.B., G.V., I.K. and L.H.; Methodology, A.B. and M.S.S.; Project administration, A.B. and G.B.; Supervision, M.S.S. and L.H.; Visualization, M.S.S.; Writing—original draft, M.S.S.; Writing—review & editing, A.B., M.S.S., A.K.L., A.G., S.T., G.B., J.H. and L.H. All authors read and approved the final manuscript.

Funding: Collagen Solutions (study sponsor) was the sole funding source and was responsible for study design, data interpretation, and manuscript publication.

Conflicts of Interest: G.B. and J.H. were employees of the study sponsor at the time of the study. M.S.S., A.K.L. and A.G. receive consultancy fees from the study sponsor. A.K.L. holds equity in the study sponsor. A.G. receives consultancy fees and research support from Smith & Nephew and Ossur. A.B., S.T., G.V., I.K. and L.H. have no potential conflict of interest to declare.

Ethical Approval: Ethics approval was obtained from the National Scientific and Ethical Committee of the Medical Research Council of Hungary (ETT TUKEB) (Reference: 58813-/2016/EKU) and the local Research Ethics Committee of Uzsoki Hospital (Uzsoki IKEB) (Reference: 223-IK/2016).

List of Abbreviations

2D	two dimensional
3D	three dimensional
ACI	Autologous chondrocyte implantation
AMIC	autologous matrix-induced chondrogenesis
CCI	characterized chondrocyte implantation
FS SPGR	fat-suppressed 3D spoiled gradient-echo
GAG	glycosaminoglycan
kg	kilogram
KOOS	Knee Injury and Osteoarthritis Outcome Score
m	meter
mm	millimeter
ms	millisecond
MRI	Magnetic Resonance Imaging
PRP	Platelet rich plasma
QoL	Quality of life
ROI	region-of-interest
T2	Transverse relaxation time

References

1. Steadman, J.R.; Rodkey, W.G.; Briggs, K.K. Microfracture: Its History and Experience of the Developing Surgeon. *Cartilage* **2010**, *1*, 78–86. [[CrossRef](#)] [[PubMed](#)]
2. Peterson, L.; Vasiladis, H.S.; Brittberg, M.; Lindahl, A. Autologous chondrocyte implantation: A long-term follow-up. *Am. J. Sports Med.* **2010**, *38*, 1117–1124. [[CrossRef](#)] [[PubMed](#)]
3. Bugbee, W.D.; Pallante-Kichura, A.L.; Gortz, S.; Amiel, D.; Sah, R. Osteochondral allograft transplantation in cartilage repair: Graft storage paradigm, translational models, and clinical applications. *J. Orthop. Res. Off. Publ. Orthop. Res. Soc.* **2016**, *34*, 31–38. [[CrossRef](#)] [[PubMed](#)]

4. Hangody, L.; Duska, Z.; Karpati, Z. Autologous Osteochondral Mosaicplasty. *Tech. Knee Surg.* **2002**, *1*, 13–22. [[CrossRef](#)]
5. Riboh, J.C.; Cvetanovich, G.L.; Cole, B.J.; Yanke, A.B. Comparative efficacy of cartilage repair procedures in the knee: A network meta-analysis. *Knee Surg. sports Traumatol. Arthrosc. Off. J. ESSKA* **2017**, *25*, 3786–3799. [[CrossRef](#)]
6. Mundi, R.; Bedi, A.; Chow, L.; Crouch, S.; Simunovic, N.; Sibilsky Enselman, E.; Ayeni, O.R. Cartilage Restoration of the Knee: A Systematic Review and Meta-analysis of Level 1 Studies. *Am. J. Sports Med.* **2016**, *44*, 1888–1895. [[CrossRef](#)]
7. Richter, D.L.; Schenck, R.C., Jr.; Wascher, D.C.; Treme, G. Knee Articular Cartilage Repair and Restoration Techniques: A Review of the Literature. *Sports Health* **2016**, *8*, 153–160. [[CrossRef](#)]
8. Buckwalter, J.A.; Mankin, H.J. Articular Cartilage Part II: Degeneration and osteoarthritis, repair, regeneration and transplantation. *J. Bone Jt. Surg.* **1997**, *79*, 612–632. [[CrossRef](#)]
9. Davies-Tuck, M.L.; Wluka, A.E.; Wang, Y.; Teichtahl, A.J.; Jones, G.; Ding, C.; Cicuttini, F.M. The natural history of cartilage defects in people with knee osteoarthritis. *OARS* **2008**, *16*, 337–342. [[CrossRef](#)]
10. Harley, B.A.; Lynn, A.K.; Wissner-Gross, Z.; Bonfield, W.; Yannas, I.V.; Gibson, L.J. Design of a multiphase osteochondral scaffold III: Fabrication of layered scaffolds with continuous interfaces. *J. Biomed. Mater. Res.* **2010**, *92*, 1078–1093. [[CrossRef](#)]
11. Harley, B.A.; Lynn, A.K.; Wissner-Gross, Z.; Bonfield, W.; Yannas, I.V.; Gibson, L.J. Design of a multiphase osteochondral scaffold. II. Fabrication of a mineralized collagen-glycosaminoglycan scaffold. *J. Biomed. Mater. Res.* **2010**, *92*, 1066–1077. [[CrossRef](#)] [[PubMed](#)]
12. Gille, J.; Behrens, P.; Volpi, P.; de Girolamo, L.; Reiss, E.; Zoch, W.; Anders, S. Outcome of Autologous Matrix Induced Chondrogenesis (AMIC) in cartilage knee surgery: Data of the AMIC Registry. *Arch. Orthop. Trauma Surg.* **2013**, *133*, 87–93. [[CrossRef](#)] [[PubMed](#)]
13. Shive, M.S.; Stanish, W.D.; McCormack, R.; Forriol, F.; Mohtadi, N.; Pelet, S.; Desnoyers, J.; Methot, S.; Vehik, K.; Restrepo, A. BST-CarGel(R) Treatment Maintains Cartilage Repair Superiority over Microfracture at 5 Years in a Multicenter Randomized Controlled Trial. *Cartilage* **2015**, *6*, 62–72. [[CrossRef](#)] [[PubMed](#)]
14. Getgood, A.M.; Kew, S.J.; Brooks, R.; Aberman, H.; Simon, T.; Lynn, A.K.; Rushton, N. Evaluation of early-stage osteochondral defect repair using a biphasic scaffold based on a collagen-glycosaminoglycan biopolymer in a caprine model. *Knee* **2012**, *19*, 422–430. [[CrossRef](#)] [[PubMed](#)]
15. Getgood, A.; Henson, F.; Skelton, C.; Herrera, E.; Brooks, R.; Fortier, L.A.; Rushton, N. The Augmentation of a Collagen/Glycosaminoglycan Biphasic Osteochondral Scaffold with Platelet-Rich Plasma and Concentrated Bone Marrow Aspirate for Osteochondral Defect Repair in Sheep: A Pilot Study. *Cartilage* **2012**, *3*, 351–363. [[CrossRef](#)] [[PubMed](#)]
16. Getgood, A.; Henson, F.; Skelton, C.; Brooks, R.; Guehring, H.; Fortier, L.A.; Rushton, N. Osteochondral tissue engineering using a biphasic collagen/GAG scaffold containing rhFGF18 or BMP-7 in an ovine model. *J. Exp. Orthop.* **2014**, *1*, 13. [[CrossRef](#)]
17. Tamez-Pena, J.G.; Farber, J.; Gonzalez, P.C.; Schreyer, E.; Schneider, E.; Totterman, S. Unsupervised segmentation and quantification of anatomical knee features: Data from the Osteoarthritis Initiative. *IEEE Trans. Biomed. Eng.* **2012**, *59*, 1177–1186. [[CrossRef](#)]
18. Tamez-Peña, J.; Shive, M.; Restrepo, A.; Gonzalez, P.; Schreyer, E.; Totterman, S. Validation of an Objective, Analyst-Independent, Non-Invasive Method for Assessing Effectiveness of Cartilage Repair Therapies in Multicenter RCTs. In Proceedings of the 6th International Workshop on Osteoarthritis Imaging, Hilton Head, SC, USA, 12–14 July 2012.
19. Stanish, W.D.; McCormack, R.; Forriol, F.; Mohtadi, N.; Pelet, S.; Desnoyers, J.; Restrepo, A.; Shive, M.S. Novel scaffold-based BST-CarGel treatment results in superior cartilage repair compared with microfracture in a randomized controlled trial. *J. Bone Jt. Surg. Am. Vol.* **2013**, *95*, 1640–1650. [[CrossRef](#)]
20. Gatti, A.A.; Noseworthy, M.D.; Stratford, P.W.; Brennehan, E.C.; Totterman, S.; Tamez-Pena, J.; Maly, M.R. Acute changes in knee cartilage transverse relaxation time after running and bicycling. *J. Biomech.* **2017**, *53*, 171–177. [[CrossRef](#)]
21. Farber, J.M.; Totterman, S.M.; Martinez-Torteya, A.; Tamez-Pena, J.G. Scan-rescan precision of subchondral bone curvature maps from routine 3D DESS water excitation sequences: Data from the Osteoarthritis Initiative. *Comput. Biol. Med.* **2016**, *69*, 83–91. [[CrossRef](#)]

22. Bentley, G.; Biant, L.C.; Carrington, R.W.; Akmal, M.; Goldberg, A.; Williams, A.M.; Skinner, J.A.; Pringle, J. A prospective, randomised comparison of autologous chondrocyte implantation versus mosaicplasty for osteochondral defects in the knee. *J. Bone Jt. Surg. Br. Vol.* **2003**, *85*, 223–230. [[CrossRef](#)] [[PubMed](#)]
23. Bekkers, J.E.; de Windt, T.S.; Raijmakers, N.J.; Dhert, W.J.; Saris, D.B. Validation of the Knee Injury and Osteoarthritis Outcome Score (KOOS) for the treatment of focal cartilage lesions. *OARS* **2009**, *17*, 1434–1439. [[CrossRef](#)] [[PubMed](#)]
24. Grodzinsky, A.J.; Levenston, M.E.; Jin, M.; Frank, E.H. Cartilage tissue remodeling in response to mechanical forces. *Annu. Rev. Biomed. Eng.* **2000**, *2*, 691–713. [[CrossRef](#)] [[PubMed](#)]
25. Mosher, T.J.; Dardzinski, B.J. Cartilage MRI T2 relaxation time mapping: Overview and applications. *Semin. Musculoskelet. Radiol.* **2004**, *8*, 355–368. [[CrossRef](#)] [[PubMed](#)]
26. Nieminen, M.T.; Rieppo, J.; Toyras, J.; Hakumaki, J.M.; Silvennoinen, J.; Hyttinen, M.M.; Helminen, H.J.; Jurvelin, J.S. T2 relaxation reveals spatial collagen architecture in articular cartilage: A comparative quantitative MRI and polarized light microscopic study. *Magn. Reson. Med. Off. J. Soc. Magn. Reson. Med.* **2001**, *46*, 487–493. [[CrossRef](#)]
27. Trattnig, S.; Mamisch, T.C.; Welsch, G.; Glaser, C. Quantitative T2 Mapping of Matrix-Associated Autologous Chondrocyte Transplantation at 3 Tesla: An In Vivo Cross-Sectional Study. *Investig. Radiol.* **2007**, *42*, 442–448. [[CrossRef](#)]
28. Xia, Y.; Moody, J.B.; Alhadlaq, H. Orientational dependence of T2 relaxation in articular cartilage: A microscopic MRI (microMRI) study. *Soc. Magn. Reson. Med.* **2002**, *48*, 460–469. [[CrossRef](#)]
29. White, L.M.; Sussman, M.S.; Hurtig, M.; Probyn, L.; Tomlinson, G.; Kandel, R. Cartilage T2 assessment: Differentiation of normal hyaline cartilage and reparative tissue after arthroscopic cartilage repair in equine subjects. *Radiology* **2006**, *241*, 407–414. [[CrossRef](#)]
30. Kaipel, M.; Schreiner, M.; Kellner, R.; Klikovits, J.; Apprich, S.; Brix, M.; Boszotta, H.; Domayer, S.; Trattnig, S. Beneficial clinical effects but limited tissue quality following osteochondral repair with a cell-free multilayered nano-composite scaffold in the talus. *Foot Ankle Surg.* **2017**, *23*, 302–306. [[CrossRef](#)]
31. Lansdown, D.A.; Wang, K.; Cotter, E.; Davey, A.; Cole, B.J. Relationship Between Quantitative MRI Biomarkers and Patient-Reported Outcome Measures After Cartilage Repair Surgery: A Systematic Review. *Orthop. J. Sports Med.* **2018**, *6*, 2325967118765448. [[CrossRef](#)]
32. Welsch, G.H.; Mamisch, T.C.; Domayer, S.E.; Dorotka, R.; Kutscha-Lissberg, F. Cartilage T2 Assessment at 3-T MR Imaging: In Vivo Differentiation of Normal Hyaline Cartilage from Reparative Tissue after Two Cartilage Repair Procedures—Initial Experience¹. *Radiology* **2008**, *247*, 154–161. [[CrossRef](#)]
33. Eyre, D. Collagen of articular cartilage. *Arthritis Res.* **2002**, *4*, 30–35. [[CrossRef](#)] [[PubMed](#)]
34. Wu, J.P.; Kirk, T.B.; Zheng, M.H. Study of the collagen structure in the superficial zone and physiological state of articular cartilage using a 3D confocal imaging technique. *J. Orthop. Surg. Res.* **2008**, *3*, 29. [[CrossRef](#)] [[PubMed](#)]
35. Hangody, L.; Feczko, P.; Bartha, L.; Bodo, G.; Kish, G. Mosaicplasty for the treatment of articular defects of the knee and ankle. *Clin. Orthop. Relat. Res.* **2001**, *391*, 328–336. [[CrossRef](#)] [[PubMed](#)]
36. Flynn, T.W.; Soutas-Little, R.W. Patellofemoral joint compressive forces in forward and backward running. *J. Orthop. Sports Phys. Ther.* **1995**, *21*, 277–282. [[CrossRef](#)]
37. Andrade, R.; Vasta, S.; Pereira, R.; Pereira, H.; Papalia, R.; Karahan, M.; Oliveira, J.M.; Reis, R.L.; Espregueira-Mendes, J. Knee donor-site morbidity after mosaicplasty—A systematic review. *J. Exp. Orthop.* **2016**, *3*, 31. [[CrossRef](#)]
38. US Food and Drug Administration. *Guidance for Industry: Preparation of IDEs and INDs for Products Intended to Repair or Replace Knee Cartilage*; US Food and Drug Administration: Washington, DC, USA, 2011.
39. Abrams, G.; Mall, N.A.; Fortier, L.; Roller, B.L.; Cole, B.J. BioCartilage: Background and Operative Technique. *Oper. Tech. Sports Med.* **2013**, *21*, 116–124. [[CrossRef](#)]
40. Brix, M.O.; Stelzeneder, D.; Chiari, C.; Koller, U.; Nehrer, S.; Dorotka, R.; Windhager, R.; Domayer, S.E. Treatment of Full-Thickness Chondral Defects With Hyalograf C in the Knee: Long-term Results. *Am. J. Sports Med.* **2014**, *42*, 1426–1432. [[CrossRef](#)]
41. Brittberg, M.; Recker, D.; Ilgenfritz, J.; Saris, D.B.F.; Group, S.E.S. Matrix-Applied Characterized Autologous Cultured Chondrocytes Versus Microfracture: Five-Year Follow-up of a Prospective Randomized Trial. *Am. J. Sports Med.* **2018**, *46*, 1343–1351. [[CrossRef](#)]

42. Frenkel, S.R.; Di Cesare, P.E. Scaffolds for articular cartilage repair. *Ann. Biomed. Eng.* **2004**, *32*, 26–34. [[CrossRef](#)]
43. Kon, E.; Roffi, A.; Filardo, G.; Tesei, G.; Marcacci, M. Scaffold-based cartilage treatments: With or without cells? A systematic review of preclinical and clinical evidence. *Arthrosc. J. Arthrosc. Relat. Surg.* **2015**, *31*, 767–775. [[CrossRef](#)] [[PubMed](#)]



© 2020 by the authors. Licensee MDPI, Basel, Switzerland. This article is an open access article distributed under the terms and conditions of the Creative Commons Attribution (CC BY) license (<http://creativecommons.org/licenses/by/4.0/>).

Article

Mosaicplasty versus Matrix-Assisted Autologous Chondrocyte Transplantation for Knee Cartilage Defects: A Long-Term Clinical and Imaging Evaluation

Stefano Zaffagnini ¹, Angelo Boffa ^{1,*}, Luca Andriolo ¹, Davide Reale ¹, Maurizio Busacca ², Alessandro Di Martino ¹ and Giuseppe Filardo ^{3,4}

¹ 2nd Orthopaedic and Traumatologic Clinic, IRCCS Istituto Ortopedico Rizzoli, 40136 Bologna, Italy; stefano.zaffagnini@unibo.it (S.Z.); lucas.andriolo@gmail.com (L.A.); dawidh.reale@gmail.com (D.R.); aledimartino75@gmail.com (A.D.M.)

² Reference Center of Radiology in Research; IRCCS Istituto Ortopedico Rizzoli, 40136 Bologna, Italy; maurizio.busacca@ior.it

³ Applied and Translational Research (ATR) Center, IRCCS Istituto Ortopedico Rizzoli, 40136 Bologna, Italy; ortho@gfilardo.com

⁴ Orthopaedic and Traumatology Unit, Ospedale Regionale di Lugano, EOC, 6900 Lugano, Switzerland

* Correspondence: angeloboffa@libero.it; Tel.: +39-051-636-6567

Received: 26 May 2020; Accepted: 1 July 2020; Published: 3 July 2020

Abstract: Different surgical procedures have been proposed over the past few years to treat cartilage lesions. The aim of this study was to compare mosaicplasty and matrix-assisted autologous chondrocyte transplantation (MACT) at long-term follow-up. Forty-three patients were included: 20 mosaicplasty and 23 MACT. Patients were evaluated before and 12 years after surgery with the International Knee Documentation Committee (IKDC) subjective and objective scores for symptoms and function, and with the Tegner score for activity level. Magnetic Resonance Imaging (MRI) was used to evaluate repair tissue with the MOCART 2.0 score. Mosaicplasty and MACT showed good clinical and MRI results (IKDC subjective score 75.3 ± 21.8 and 81.8 ± 13.0 , both $p < 0.0005$). Mosaicplasty presented a 10% reoperation rate and a 25% overall failure rate, while no failures were documented in MACT ($p = 0.016$). While size did not influence the results in the MACT group, mosaicplasty presented lower IKDC objective and Tegner scores in lesions bigger than 2 cm^2 ($p = 0.031$ and $p = 0.014$, respectively). Mosaicplasty and MACT presented both satisfactory clinical and MRI results at long-term follow-up. However, for larger lesions, MACT presented better subjective and objective outcomes, as well as less failures, which should be considered when choosing the most suitable treatment for patients affected by knee cartilage lesions.

Keywords: mosaicplasty; MACT; ACI; scaffold; osteochondral autologous transplantation; OAT; cartilage; knee

1. Introduction

Articular cartilage lesions of the knee are a common issue, often affecting a young population and causing pain and functional impairment, with consequent high social impact [1,2]. Due to the limited cartilage healing potential and the difficulty to restore complex biomechanical features, chondral defects remain a challenging problem [3]. Thus, to avoid their deleterious consequences, such as the risk of further cartilage loss and osteoarthritis (OA) development, numerous surgical procedures have been proposed over the years to restore the articular surface with hyaline-like, durable repair tissue, from reconstructive techniques to the more ambitious regenerative strategies [4–7]. For these surgical

approaches, the first procedures described were osteochondral autologous transplantation (OAT) and autologous chondrocyte implantation (ACI), respectively [8,9]. These techniques demonstrated promising results up to long-term follow-up, but they also showed several drawbacks, such as significant donor site morbidity for OAT [10], and the risk of graft hypertrophy for ACI [11]. Moreover, both procedures were doomed by the complexity and morbidity of the surgical procedure, requiring an arthrotomy, and thus producing a higher risk of joint stiffness and arthrofibrosis [12,13].

Therefore, these approaches have been further developed to overcome the aforementioned limitations. On the one hand, the introduction of the mosaicplasty technique involved the use of multiple autologous osteochondral plugs of smaller diameter compared to OAT, thus causing lower morbidity, transferred from lower weight-bearing areas to the cartilage defect [14]. On the other hand, matrix-assisted autologous chondrocyte transplantation (MACT) was introduced to overcome ACI drawbacks thanks to the use of different types of scaffolds for chondrocyte culture and the direct transplantation of a bioengineered tissue, a more manageable and stronger implant for an easier and more stable positioning of the cell-scaffold construct [15]. Moreover, both options can be performed through an arthroscopic approach, allowing to reduce patient's morbidity, surgical time, recovery, and complications related to open surgery [14,16]. Both techniques showed promising short-term results, later confirmed by studies at long-term follow-up [17,18]. Mosaicplasty was suggested to provide better clinical results compared to MACT at short-term [19], but data on long-term comparison between these two techniques are still lacking.

The aim of this study was to compare the clinical outcomes and the quality of repair tissue provided by mosaicplasty and MACT for the treatment of knee cartilage defects at long-term follow-up.

2. Materials and Methods

2.1. Patient Selection

All patients undergoing a cartilage repair procedure were prospectively followed, and clinical outcomes were collected in an institutional database, approved by the Hospital Ethics Committee and Internal Review Board of the Rizzoli Orthopedic Institute, Bologna, Italy (prot. gen. n. 39667). Informed consent of all patients was obtained. Surgical indications for these procedures were as follows: focal cartilage knee defects graded III–IV according to International Cartilage Regeneration & Joint Preservation Society (ICRS) classification in patients complaining of clinical symptoms (pain, swelling, locking, and giving way) after failure of conservative treatments. Contra-indications for surgery were untreated limb misalignment or knee instability, diffuse arthritis or bipolar (“kissing”) lesions, and other general medical conditions such as infectious, tumor, metabolic, rheumatic, and inflammatory diseases. A definitive diagnosis of chondral lesion and sizing was performed during the arthroscopic procedure. Patients who presented with an anterior cruciate (ACL) lesion at the time of surgery underwent the combined ACL reconstruction in the same surgical session with cartilage harvesting.

A statistician, blinded to the treatment outcome, extracted two homogeneous groups of patients from the general database treated with mosaicplasty or MACT. These groups were comparable both in terms of patient demographics and cartilage lesion features. In detail, male or female patients were included, aged between 18 and 40 years, with body mass index (BMI) between 18.5 and 30, treated for lesions involving only femoral condyles (excluding trochlea and tibial plateau), with defect size between 1.0 and 3.0 cm², traumatic or degenerative etiology (excluding osteochondritis dissecans lesions), and evaluated up to a minimum 10-year follow-up. According to these criteria, 43 patients were included in the study: 20 mosaicplasty and 23 MACT. The specific characteristics of the two groups are reported in Table 1. Statistical analysis confirmed that the two treatment groups were homogeneous with regard to gender, age, BMI, activity level, defect size and location, etiology, combined and previous surgery.

Table 1. Comparison of patient and lesion characteristics in the two groups.

Baseline Characteristics	Mosaicplasty	MACT	Comparison
Patients, n (Men/Women)	20 (15/5)	23 (18/5)	NS
Age, y mean (SD)	28.7 (7.3)	29.1 (5.9)	NS
BMI, mean (SD)	23.4 (2.6)	24.0 (2.4)	NS
Sport activity, n (%)			
Non-competitive level	11 (55.0%)	12 (52.2%)	NS
Competitive level	9 (45.0%)	11 (47.8%)	
Etiology, n (%)			
Traumatic	5 (25.0%)	12 (52.2%)	NS
Degenerative	15 (75.0%)	11 (47.8%)	
Combined surgery, n (%)	15 (75.0%)	15 (65.2%)	
ACL reconstruction, n	9 (45.0%)	12 (52.2%)	NS
Meniscal treatment, n	11 (55.0%)	10 (43.5%)	
Previous surgery, %	8 (40.0%)	11 (47.8%)	
ACL reconstruction, n	4 (20.0%)	3 (13.0%)	NS
Meniscal treatment, n	3 (15.0%)	4 (17.4%)	
Cartilage treatment, n	1 (5.0%)	4 (17.4%)	
Defect size, cm ² (SD)	2.0 (0.6)	2.0 (0.6)	NS
Location, n (%)			
Medial Femoral Condyle	12 (60.0%)	12 (52.2%)	NS
Lateral Femoral Condyle	8 (40.0%)	11 (47.8%)	

Statistical analysis showed no significant differences between the two groups. ACL, anterior cruciate ligament; BMI, body mass index; MACT, matrix-assisted autologous chondrocyte transplantation; NS, not significant; SD, standard deviation; y, years.

2.2. Surgical Techniques and Rehabilitation Protocols

Arthroscopic mosaicplasty was performed in one step using the Autogenous Osteochondral Grafting System (Smith & Nephew, London, UK) surgical instrumentation, as previously described [20]. In brief, damaged cartilaginous and fibrous tissue was excised, and the lesion was then measured for size and location. Recipient 15 mm deep holes were made perpendicular to the cartilage surface. After preparing the defect area, osteochondral grafts were harvested. The donor site was preferentially the superolateral ridge of the femoral condyle, whereas the superomedial ridge was used only when four grafts were necessary. Tubular chisels were used to harvest the graft and then, with a smooth cannula, the grafts were delivered into the defect. One plug was used in 4 patients, 2 plugs in 9 patients, 3 plugs in 5 patients, and 4 plugs in 2 patients. The stability of the plugs was tested by cyclic bending of the knee while grafts were visualized.

Arthroscopic MACT was performed in two steps as previously described [21]. In brief, the first procedure consisted of an arthroscopic biopsy of healthy cartilage, sent for chondrocyte cell culture and subsequent seeding onto a hyaluronic acid-based scaffold (Hyaff 11, Fidia Advanced Biopolymers Laboratories, Padova, Italy) to obtain the bioengineered tissue Hyalograft C (Fidia Advanced Biopolymers Laboratories, Padova, Italy). After 6 weeks, the second step was performed, and the bioengineered tissue was arthroscopically implanted through cannulated devices. Because of the physical adhesive characteristics of the graft, no fibrin glue or sutures were used to fix the implant. Under arthroscopic control, the stability of implanted patches was evaluated during cyclic bending of the knee.

Postoperative rehabilitation protocols were comparable for both treatments. Postoperative management focused on early mobilization to facilitate faster resolution of swelling, promote healing and joint nutrition, and prevent adhesions. Passive knee range of motion (ROM) exercises on a continuous passive motion (CPM) machine (0°–30°) and static quadriceps exercises were started few days after surgery. Usually, 90° of knee flexion was reached within 4 weeks and full ROM within 8 weeks after surgery. Toe-touch ambulation with crutches and braces in full extension was allowed the third or fourth week and was usually completed within 6 to 8 weeks after surgery. Progressive

recovery of functional daily activities and muscle strength were performed, with particular care during exercises in open kinetic chain, which were allowed only after 12 weeks. In the mosaicplasty group, full athletic activity was permitted after 4 months and contact and traumatic sports were allowed after 6 months. In the MACT group, high-impact activities were discouraged until 10 to 12 months after implantation.

2.3. Clinical and Radiological Evaluation

Patients were evaluated before surgery and prospectively for a mean of 12 years of follow-up (140.2 ± 15.1 months, range 120–168 months) with the International Knee Documentation Committee (IKDC) subjective and objective scores for the evaluation of knee symptoms and function, and with the Tegner score for activity level. Effusion and passive motion deficit were used to determine the final functional grade of the knee (A—normal, B—nearly normal, C—abnormal, or D—severely abnormal). Failures were also recorded: the procedures were considered to have failed if the patient needed a reoperation because of symptoms related to the primary defect. For these patients, the scores of the latest follow-up available before reoperation were carried forward at the final follow-up. Besides surgical failures, patients without a clinically significant improvement (10 IKDC subjective points compared with the baseline evaluation, as previously described [22]) were considered to be a clinical failure.

Magnetic Resonance Imaging (MRI) was used to evaluate the repair tissue in 30 knees (15 of the mosaicplasty group and 15 of the MACT group) at long-term follow-up. MRI evaluation was performed using a 1.5-T superconducting magnet (General Electric Co, Fairfield, Connecticut) with a dedicated phased array (8 channels) HD knee coil. The following sequences were used for graft evaluation: sagittal fast spin echo proton density weighted with fat saturation (TR 3500, TE 22, FOV 16, slice thickness 3 mm, Matr 320×256); sagittal T2 MAP (TR 1000, echoes 8 FOV 16, Th. 3 mm Matr 320×224); sagittal 3D “Cube” proton density weighted (TR 2500, TE 30, FOV 20, slice thickness 0.8 mm Matr 288×288); coronal fast spin echo proton density weighted with fat saturation (TR 2600, TE 40, FOV 16, slice thickness 4 mm, Matr 320×224); axial fast spin echo proton density weighted with fat saturation (TR 2600, TE 40, FOV 16, slice thickness 4 mm, Matr 320×224). The magnetic resonance observation of cartilage repair tissue (MOCART) 2.0 scoring system was applied for graft evaluation, which considers seven variables to describe morphology and signal intensity of the repair tissue [23]. All imaging evaluations were performed by an orthopedic surgeon and a musculoskeletal radiologist experienced in cartilage regeneration procedures in consensus.

2.4. Statistical Methods

All continuous data were expressed in terms of mean \pm SD, categorical variables were expressed as proportions or percentages. The Shapiro-Wilk test was performed to test normality of continuous variables. The Levene test was used to assess the homoscedasticity of the data. Repeated measures ANOVA was performed to compare the scores at different follow-up times. The one way ANOVA test was performed to assess the between group differences of continuous and normally distributed and homoscedastic data; the Mann-Whitney test was used otherwise. The Spearman rank correlation was used to assess correlations between numerical scores and continuous data, the Kendall’s tau correlation was used to assess correlations between ordinal scores and continuous data. Pearson’s chi square exact test was performed to investigate relationships between grouping variables. For all tests $p < 0.05$ was considered significant. All statistical analysis was performed using SPSS v.19.0 (IBM Corp., Armonk, NY, USA).

3. Results

Both groups showed a marked improvement of all clinical scores from baseline to the last follow-up. The IKDC subjective score improved significantly in the mosaicplasty group from the basal level of 38.1 ± 11.8 to 75.3 ± 21.8 ($p < 0.0005$) at the final follow-up. Similarly, in the MACT group there was

a significant improvement from the basal level of 37.6 ± 14.9 to the final follow-up of 81.8 ± 13.0 ($p < 0.0005$). No significant differences in the IKDC subjective scores were found between mosaicplasty and MACT groups (Figure 1).

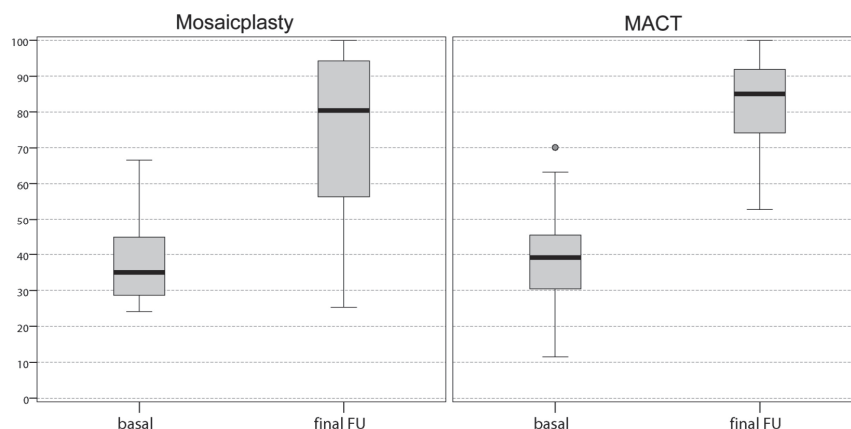


Figure 1. Comparison of the International Knee Documentation Committee (IKDC) subjective score achieved at a final follow-up of 12 years by both groups of patients. The values are expressed in median and 25th and 75th percentiles. No significant differences were found between the two groups. FU, follow-up.

The IKDC objective score in the mosaicplasty group improved from baseline, where no knees were evaluated as normal or nearly normal (13 C, 7 D), to 16 normal or nearly normal knees at 12 years of follow-up (7 A, 9 B, 3 C, 1 D). In the MACT group, this score improved from 7 normal or nearly normal knees at baseline (1 A, 6 B, 9 C, 7 D) to 23 at the final follow-up (16 A, 7 B). The IKDC objective score improvement was significantly higher in the MACT group compared with the mosaicplasty group at 12 years of follow-up ($p = 0.029$). The Tegner score in the mosaicplasty group showed a significant improvement from 2.9 ± 1.4 at the pre-operative evaluation to 5.0 ± 2.4 at the final follow-up ($p = 0.043$); however, the mean activity level remained lower vs. pre-injury (7.1 ± 2.0 , $p = 0.081$). Similarly, the Tegner score of the MACT group showed a statistically significant improvement ($p = 0.001$) from the pre-operative level (1.6 ± 1.5) to the final follow-up (5.3 ± 2.1), although also in this case without reaching the pre-injury level (7.0 ± 1.6 , $p = 0.081$). No significant differences were found in the Tegner scores between mosaicplasty and MACT at the final follow-up, with only eight patients for each group achieving the pre-injury activity level 12 years after surgery (Figure 2).

Two patients of the mosaicplasty group failed (one with four plugs and one with three plugs) and were treated with MACT 2 years after the treatment, fixing a 10% reoperation rate. At the final mean follow-up of 12 years, three more patients in the mosaicplasty group (one patient with one plug, one with two plugs, and one with four plugs) were considered clinical failures, for an overall failure rate of 25%, significantly higher compared to the MACT group, where no surgical or clinical failures occurred ($p = 0.016$).

The MRI findings of 30 knees (15 mosaicplasty and 15 MACT), analyzed with the MOCART 2.0 scoring system, showed a high rate of cartilage defect filling in both groups, and a complete integration into the adjacent cartilage in half of the patients in both groups. However, the surface of the repair tissue was damaged in the majority of cases. The structure of the repair tissue was homogeneous in most cases, and the signal intensity was normal (isointense) in half of the patients in both groups. At subchondral bone level, a bony defect or bony overgrowth was reported in the majority of patients, while an edema-like marrow signal was reported in almost half of the patients in both groups (Figures 3

and 4). No significant differences were reported between the two groups in the overall MOCART 2.0 scores and in all the seven subscales (Table 2).

Further analysis was performed to determine the parameters that influenced the clinical outcome at the final follow-up in the two treatment groups. Defect size was found to significantly influence the final IKDC scores between the two groups, with MACT producing significantly higher objective results ($p = 0.031$) and a tendency for higher subjective results compared to mosaicplasty (81.8 ± 18.3 vs 58.8 ± 25.0 , $p = 0.092$) for lesions $> 2 \text{ cm}^2$. Moreover, while size did not influence results in the MACT group, patients with lesions bigger than 2 cm^2 had a lower improvement in their activity level as measured by Tegner ($p = 0.014$) (Figure 5). Conversely, age, sex, BMI, site, etiology, number of plugs (for the mosaicplasty group), and previous or associated surgery did not significantly influence the final clinical outcome. No correlations were also found between MOCART 2.0 total scores or subscales and basal parameters, including age, BMI, and defect size. Moreover, no correlations were found between clinical scores (IKDC subjective and objective, and Tegner score) and MOCART 2.0 total scores or subscales at final follow-up.

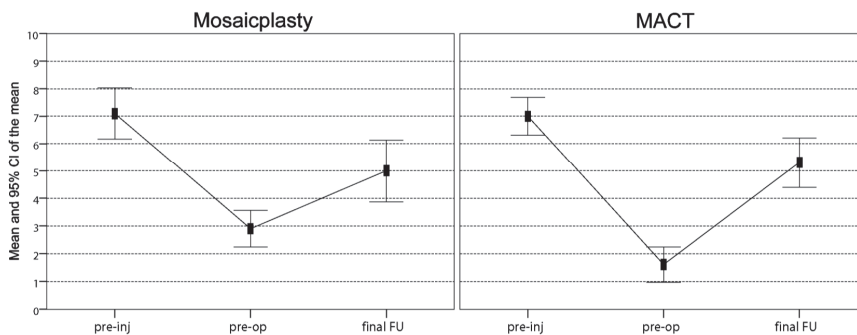


Figure 2. Comparison of the Tegner scores achieved at a final follow-up of 12 years. In both groups, scores improved significantly from the pre-operative level to the final follow-up, even though the mean activity level remained significantly lower vs. pre-injury. No differences were found in sports activity levels between the two groups. FU, follow-up; Pre-inj, pre-injury; Pre-op, pre-operative.

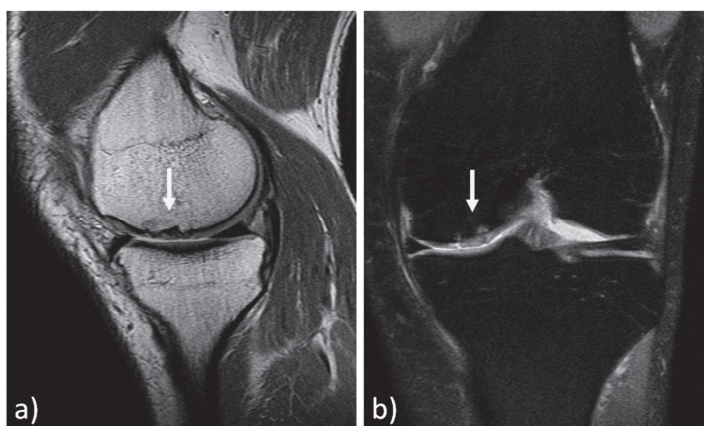


Figure 3. MRI evaluation at 11 years' follow-up of a medial femoral condyle lesion treated with mosaicplasty in a 37-year-old man. Sagittal 3D "Cube" PD (a) and coronal PD FAT SAT (b) demonstrate a good filling of the defect (arrows) and a complete integration into adjacent cartilage. However, there is an inhomogeneous structure of the repair tissue with adjacent bony overgrowth.

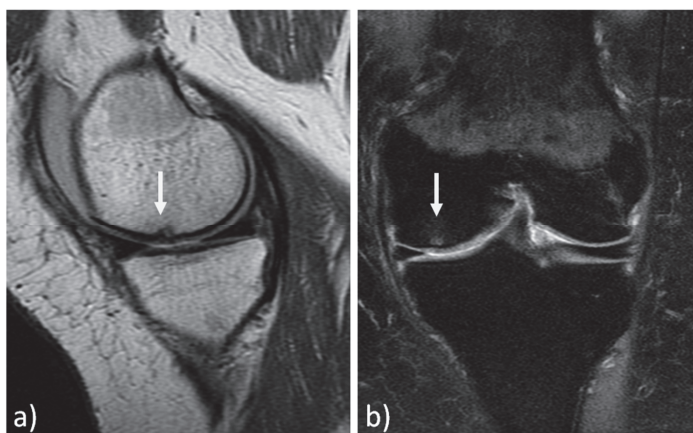


Figure 4. MRI evaluation at 9 years' follow-up of a medial femoral condyle lesion treated with matrix-assisted autologous chondrocyte transplantation in a 39-year-old woman. Sagittal 3D “Cube” PD (a) and coronal PD FAT SAT (b) demonstrate a good filling of the defect (arrows) and integration into adjacent cartilage, a homogeneous structure and a normal signal intensity of the repair tissue. Moreover, no significant bony defect, bony overgrowth, or major subchondral changes were detected.

Table 2. Magnetic resonance Observation of Cartilage Repair Tissue (MOCART) 2.0 evaluation.

MOCART 2.0 Knee Score: Cartilage Repair Tissue Assessment		Mosaicplasty Group	MACT Group	Comparison	
1	Volume fill of cartilage defect	Complete filling or minor hypertrophy	4 (26.7%)	4 (26.7%)	NS
		Major hypertrophy (≥ 150%) or 75% to 99% filling	6 (40.0%)	8 (53.3%)	
		50% to 74% filling	4 (26.7%)	3 (20.0%)	
		25% to 49% filling	1 (6.6%)	0	
< 25% filling or complete delamination in situ		0	0		
2	Integration into adjacent cartilage	Complete	8 (53.3%)	8 (53.3%)	NS
		Split-like defect ≤ 2 mm	3 (20.0%)	6 (40.0%)	
		Defect > 2 mm but < 50% of repair tissue length	4 (26.7%)	1 (6.7%)	
Defect ≥ 50% of repair tissue length		0	0		
3	Surface of the repair tissue	Intact	5 (33.3%)	3 (20.0%)	NS
		Damaged: < 50% of the repair tissue diameter	8 (53.3%)	10 (66.6%)	
		Damaged: ≥ 50% of the repair tissue diameter	2 (13.4%)	2 (13.4%)	
4	Structure of the repair tissue	Homogeneous	11 (73.3%)	10 (66.7%)	NS
		Inhomogeneous	4 (26.7%)	5 (33.3%)	
5	Signal intensity of the repair tissue	Normal	7 (46.7%)	9 (60.0%)	NS
		Minor abnormal: minor hyperintense or minor hypointense	7 (46.7%)	6 (40.0%)	
		Severely abnormal	1 (6.6%)	0	
6	Bony defect or bony overgrowth	No bony defect or bony overgrowth	7 (46.6%)	5 (33.3%)	NS
		Bony defect: depth < thickness of adjacent cartilage or overgrowth < 50% of adjacent cartilage	4 (26.7%)	9 (60.0%)	
		Bony defect: depth ≥ thickness of adjacent cartilage or overgrowth ≥ 50% of adjacent cartilage	4 (26.7%)	1 (6.7%)	
7	Subchondral changes	No major subchondral changes	8 (53.3%)	8 (53.3%)	NS
		Minor edema-like marrow signal: maximum diameter < 50% of the repair tissue diameter	7 (46.7%)	4 (26.7%)	
		Severe edema-like marrow signal: maximum diameter ≥ 50% of the repair tissue diameter	0	3 (20.0%)	
		Subchondral cysts ≥ 5 mm or osteonecrosis-like signal	0	0	
Total score, mean ± SD		-	74.0 ± 17.1	75.7 ± 13.6	NS

MACT, matrix-assisted autologous chondrocyte transplantation; MOCART, magnetic resonance observation of cartilage repair tissue; NS, not significant; SD, standard deviation.

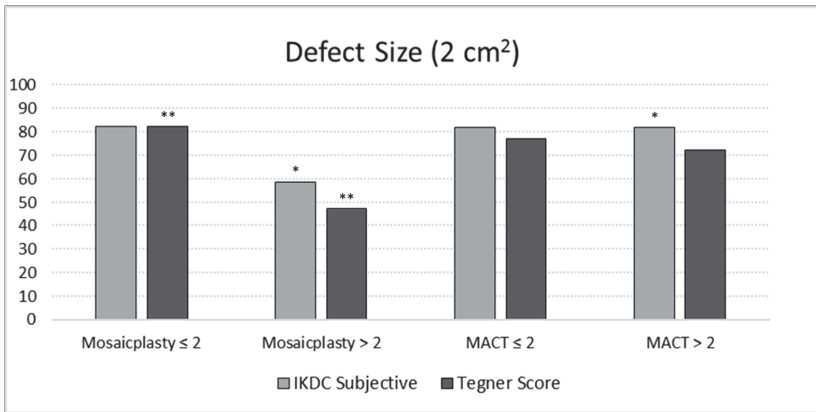


Figure 5. Evaluation of the defect size effect on the International Knee Documentation Committee (IKDC) subjective score and the percentage Tegner Score improvement at a final follow-up of 12 years in both groups of patients. The asterisk (*) indicates for the MACT group a tendency for higher subjective results compared to the mosaicplasty group for the defect area > 2 cm² (p = 0.092). The double asterisk (**) indicates a lower improvement in terms of Tegner Score for the defect area > 2 cm² in the mosaicplasty group (p = 0.014).

4. Discussion

The main finding of this study is that both mosaicplasty and MACT techniques provided satisfactory clinical results at long-term follow-up in two homogeneous groups of patients affected by knee cartilage defects. Additionally, the MRI evaluation suggested a good and durable quality of repair tissue, although without correlations with the clinical outcomes. The comparative analysis of the two procedures suggested that while similar results were obtained for small lesions, MACT should be preferred versus mosaicplasty when addressing larger knee cartilage defects.

The overall clinical results reported in this study are in line with other recently published long-term studies, showing that both mosaicplasty and MACT may offer satisfactory and durable results when applied for the treatment of relatively small chondral lesions of knee femoral condyles [17,24–26]. In the largest available study of mosaicplasty that included 831 patients evaluated at 10 years of follow-up, Hangody et al. reported 92% good-to-excellent results with a low complication rate [26]. Similarly, Andriolo et al. performed a long-term evaluation at 15 years of follow-up in 113 patients treated with MACT, reporting a significant and stable clinical scores improvement. Even the failure rates reported in this study reflect the literature findings, with higher failure rates documented in patients treated with mosaicplasty technique compared to MACT. Pareek et al. [13] found that, at an average follow-up of 10 years, patients who underwent mosaicplasty had an overall failure rate of 28% and a reoperation rate of 19%, thus reflecting the results obtained in the current study (overall failure rate of 25% and a reoperation rate of 10%). The survival of MACT of the present study appears to be actually higher than previous findings. A systematic review reported a failure rate of 10.4% at mid-long term follow-up in patients treated with MACT [27]. However, these differences may be due to the different populations of patients considered; other studies demonstrated a higher failure rate in some patients categories, such as knee osteoarthritis and patellar defects [25,28], and these types of patients were excluded in the current study, where no failures were documented in the MACT group.

Long-term results of both mosaicplasty and MACT have also been evaluated in comparison with other cartilage repair techniques. Compared to microfractures, mosaicplasty resulted in significantly better outcomes in several studies at long-term follow-up [29–31]. In particular, even though both mosaicplasty and microfractures presented a worsening of results at 10 years, Gudas et al. [32] reported significantly better results in patients treated with mosaicplasty, which presented a higher

activity level, a lower failure rate, and a lower radiographic evidence of osteoarthritic degenerative progression. These results may be explained by the better quality of repair tissue provided by the use of autologous graft compared to fibrocartilage obtained with bone marrow stimulation techniques [32]. Similarly, MACT also presented better patient-reported outcome scores and lower failures compared to microfractures [33,34]. Additionally in this case, the excellent durability of MACT results could be explainable by the hyaline-like tissue restored [35], compared to the fibrocartilaginous repair tissue provided by microfractures as demonstrated by MRI studies [36,37].

The role of MRI in assessing cartilage repair tissue has been widely reported [38], and the imaging results of this study confirmed the literature findings in both treatment groups, with high MOCART 2.0 scores. However, several suboptimal imaging findings were also documented, both in terms of surface integrity and subchondral bone alterations, although these findings did not correlate with clinical results. To this regard, previous studies were controversial in regard the clinical significance of MRI findings. Tetta et al. [39] showed that mosaicplasty implants with a better imaging appearance also presented better objective and subjective scores, and Kon et al. [40] confirmed this correlation in patients treated with MACT. Conversely, Adrian et al. [41], while demonstrating a good-quality repair tissue at 10 years after MACT, found no correlation between clinical outcome and MRI results. These controversial findings have to be interpreted in light of a meta-analysis investigating the correlation between MRI and clinical outcomes after cartilage repair [42]. In fact, only 28% of the included studies found such correlation, leaving unanswered the question of whether MRI is reliable in predicting clinical outcomes after cartilage repair. Therefore, caution should be recommended when interpreting MRI findings and greater importance should be placed on the patient clinical evaluation. This is especially true in a comparative study such as the current one, aiming at determining the most suitable treatment in patients affected by cartilage lesions.

The present study compared both clinical and imaging outcomes of mosaicplasty and MACT at long-term follow-up. The results of these techniques in the literature, evaluated singularly, were confirmed, with good and long-lasting results and a low surgical failure rate. Mosaicplasty and MACT also showed similar overall clinical outcomes and comparable tissue repair quality at MRI evaluation. However, this comparative analysis underlined some interesting aspects. MACT presented better clinical results in relatively larger cartilage lesions, better objective findings, and a lower failure rate compared to mosaicplasty. These findings are inconsistent with the only available comparative analysis of these two techniques at short-term follow-up [19]. In detail, Clavé et al. reported a significantly greater symptom improvement 2 years after treatment for mosaicplasty compared to MACT in defects larger than 3.5 cm², while no significant difference was found for smaller lesions [19]. On the other hand, in contrast to these results, Bentley et al. [43] reported a higher rate of failure in patients with large cartilage lesions treated with mosaicplasty compared to first-generation ACI at long-term follow-up, thus underlining that mosaicplasty is not a suitable option for the treatment of large lesions. This result was confirmed by other authors that investigated the significance of the lesion size for mosaicplasty technique, showing better clinical improvement in patients affected by small lesions [44,45]. An important aspect related to the lesion size is the number of plugs used to cover the defect being correlated with the clinical outcomes and the failure rate [45]. A limited number of plugs could correlate with better results probably because of the cylindrical shape of the grafts that does not allow optimal coverage of the lesion site by multiple grafts, leaving residual small uncovered areas that might impair or diminish the healing process [46,47].

Another important aspect that needs to be taken into account when evaluating cartilage procedures is the clinical profiling, aimed at determining the patient and lesion characteristics which may play a prognostic role on the final outcome [48]. Many studies evaluated several factors that can influence the failure rate of both these techniques. Among them, age, sex, etiology and size of the defect seem to modify the failure rate, with female patients, older patients and those affected by degenerative or larger lesions, complex cases, and patients undergoing salvage treatment being more at risk of failures [13,24,25,49,50]. Such profiling of patient characteristics which may influence the outcome

were not possible in this series due to the low number of patients, although interesting findings could be underlined for the most suitable treatment indication based on the lesion size.

The current study has limitations that should be considered in the interpretation of the results. First of all, the retrospective design, with consequent lack of randomization, may entail an inclusion bias, with different patients treated with different procedures. Nevertheless, data were collected prospectively, and the strict patient selection by a statistician blinded to the study outcome allowed us to obtain two homogeneous groups to compare, thus allowing us to draw conclusions about the selected population. The absence of an intermediate evaluation is another limitation. Unfortunately, some patients of the two treatment groups were not evaluated at the intermediate follow-ups, hindering the possibility to better understand possible oscillations of the outcomes over time between the two techniques. Nevertheless, short and mid-term follow-ups of both procedures have already been reported in the literature. Secondly, the relatively small number of patients evaluated hindered the possibility to confirm some correlations between outcome and influencing factors. Moreover, a slight (although not significant) heterogeneity was present between the two groups in terms of etiology, with some more degenerative cases in the mosaicplasty group. Nevertheless, the current survey represents the largest population evaluated in a comparative long-term analysis, and allowed meaningful clinical and MRI results, showing overall good results over time for both techniques, but lower results for mosaicplasty in lesions larger than 2 cm². Other limitations are the absence of arthroscopic and histologic examinations, and of a radiologic follow-up, often considered the ideal technique for evaluating cartilage quality and OA evolution. Moreover, the imaging evaluation was not available for all patients, because some patients declined to undergo MRI exam. Nevertheless, the high rate of MRI evaluations at long-term follow-up and the use of the recent MOCART 2.0 tool offered important information regarding the state of the repair tissue and of the whole joint, leaving the analysis of the degenerative progression to future studies with longer follow-up times.

Alternative solutions have been explored to restore the articular surface while overcoming the drawbacks of mosaicplasty and MACT, aiming at lowering costs, simplifying the procedure, and improving long-term results [51,52]. The most recent developments involve the use of cell sources for one-step solutions or the application of biomaterials, such as a cell-free approach [53–56]. Nevertheless, while research is moving forward, it is fundamental to keep documenting the results of the most established procedures like mosaicplasty and MACT, to better understand how much and how long can patients benefit from these cartilage procedures, to detect the ideal candidates through a patient profiling, and to set a reference point to measure the potential of the other emerging solutions.

Author Contributions: Conceptualization, S.Z. and G.F.; methodology, M.B. and A.D.M.; data curation, D.R.; writing—original draft preparation, A.B. and L.A.; writing—review and editing, G.F.; supervision, A.D.M., M.B., G.F., and S.Z. All authors have read and agreed to the published version of the manuscript.

Funding: This research received no external funding.

Conflicts of Interest: S.Z. has received institutional support from Fidia Farmaceutici, Cartiheal, IGEA Clinical Biophysics, Biomet, and Kensey Nash; grant support from I+; and royalties from Springer. The funders had no role in the design of the study; in the collection, analyses, or interpretation of data; in the writing of the manuscript, or in the decision to publish the results. The other authors declare no conflict of interest.

References

1. Everhart, J.S.; Campbell, A.B.; Abouljoud, M.M.; Kirven, J.C.; Flanigan, D.C. Cost-efficacy of knee cartilage defect treatments in the United States. *Am. J. Sports Med.* **2020**, *48*, 242–251. [[CrossRef](#)] [[PubMed](#)]
2. Chubinskaya, S.; Haudenschild, D.; Gasser, S.; Stannard, J.; Krettek, C.; Borrelli, J., Jr. Articular cartilage injury and potential remedies. *J. Orthop. Trauma* **2015**, *29*, 47–52. [[CrossRef](#)] [[PubMed](#)]
3. Filardo, G.; Kon, E.; Roffi, A.; Di Martino, A.; Marcacci, M. Scaffold-based repair for cartilage healing: A systematic review and technical note. *Arthroscopy* **2013**, *29*, 174–186. [[CrossRef](#)] [[PubMed](#)]
4. Ambra, L.F.; de Girolamo, L.; Mosier, B.; Gomoll, A.H. Review: Interventions for Cartilage Disease: Current State-of-the-Art and Emerging Technologies. *Arthritis Rheumatol.* **2017**, *69*, 1363–1373. [[CrossRef](#)]

5. Heijink, A.; Gomoll, A.H.; Madry, H.; Drobic, M.; Filardo, G.; Espregueira-Mendes, J.; Van Dijk, C.N. Biomechanical considerations in the pathogenesis of osteoarthritis of the knee. *Knee Surg. Sports Traumatol. Arthrosc.* **2012**, *20*, 423–435. [\[CrossRef\]](#)
6. Davies-Tuck, M.L.; Wluka, A.E.; Wang, Y.; Teichtahl, A.J.; Jones, G.; Ding, C.; Cicuttini, F.M. The natural history of cartilage defects in people with knee osteoarthritis. *Osteoarthr. Cartil.* **2008**, *16*, 337–342. [\[CrossRef\]](#) [\[PubMed\]](#)
7. Richter, D.L.; Schenck, R.C., Jr.; Wascher, D.C.; Treme, G. Knee articular cartilage repair and restoration techniques: A review of the literature. *Sports Health* **2016**, *8*, 153–160. [\[CrossRef\]](#)
8. Yamashita, F.; Sakakida, K.; Suzu, F.; Takai, S. The transplantation of an autogeneic osteochondral fragment for osteochondritis dissecans of the knee. *Clin. Orthop. Relat. Res.* **1985**, *201*, 43–50. [\[CrossRef\]](#)
9. Brittberg, M.; Lindahl, A.; Nilsson, A.; Ohlsson, C.; Isaksson, O.; Peterson, L. Treatment of deep cartilage defects in the knee with autologous chondrocyte transplantation. *N. Engl. J. Med.* **1994**, *331*, 889–895. [\[CrossRef\]](#)
10. Andrade, R.; Vasta, S.; Pereira, R.; Pereira, H.; Papalia, R.; Karahan, M.; Oliveira, J.M.; Reis, R.L.; Espregueira-Mendes, J. Knee donor-site morbidity after mosaicplasty—A systematic review. *J. Exp. Orthop.* **2016**, *3*, 31. [\[CrossRef\]](#)
11. Minas, T. Autologous chondrocyte implantation for focal chondral defects of the knee. *Clin. Orthop. Relat. Res.* **2001**, *391*, 349–361. [\[CrossRef\]](#)
12. Kon, E.; Verdonk, P.; Condello, V.; Delcogliano, M.; Dhollander, A.; Filardo, G.; Pignotti, E.; Marcacci, M. Matrix-assisted autologous chondrocyte transplantation for the repair of cartilage defects of the knee: systematic clinical data review and study quality analysis. *Am. J. Sports Med.* **2009**, *37*, 156–166. [\[CrossRef\]](#) [\[PubMed\]](#)
13. Pareek, A.; Reardon, P.J.; Maak, T.G.; Levy, B.A.; Stuart, M.J.; Krych, A.J. Long-term outcomes after osteochondral autograft transfer: A systematic review at mean follow-up of 10.2 years. *Arthroscopy* **2016**, *32*, 1174–1184. [\[CrossRef\]](#) [\[PubMed\]](#)
14. Hangody, L.; Kish, G.; Karpati, Z.; Szerb, I.; Udvarhelyi, I. Arthroscopic autogenous osteochondral mosaicplasty for the treatment of femoral condylar articular defects A preliminary report. *Knee Surg. Sports Traumatol. Arthrosc.* **1997**, *5*, 262–267. [\[CrossRef\]](#) [\[PubMed\]](#)
15. Kon, E.; Delcogliano, M.; Filardo, G.; Montaperto, C.; Marcacci, M. Second generation issues in cartilage repair. *Sports Med. Arthrosc. Rev.* **2008**, *16*, 221–229. [\[CrossRef\]](#)
16. Cortese, F.; McNicholas, M.; Janes, G.; Gillogly, S.; Abelow, S.P.; Gigante, A.; Coletti, N. Arthroscopic Delivery of Matrix-Induced Autologous Chondrocyte Implant: International Experience and Technique Recommendations. *Cartilage* **2012**, *3*, 156–164. [\[CrossRef\]](#)
17. Solheim, E.; Hegna, J.; Oyen, J.; Harlem, T.; Strand, T. Results at 10 to 14 years after osteochondral autografting (mosaicplasty) in articular cartilage defects in the knee. *Knee* **2013**, *20*, 287–290. [\[CrossRef\]](#)
18. Zaffagnini, S.; Vannini, F.; Di Martino, A.; Andriolo, L.; Sessa, A.; Perdisa, F.; Balboni, F.; Filardo, G. Low rate of return to pre-injury sport level in athletes after cartilage surgery: A 10-year follow-up study. *Knee Surg. Sports Traumatol. Arthrosc.* **2019**, *27*, 2502–2510. [\[CrossRef\]](#)
19. Clave, A.; Potel, J.F.; Servien, E.; Neyret, P.; Dubrana, F.; Stindel, E. Third-generation autologous chondrocyte implantation versus mosaicplasty for knee cartilage injury: 2-year randomized trial. *J. Orthop. Res.* **2016**, *34*, 658–665. [\[CrossRef\]](#)
20. Filardo, G.; Kon, E.; Perdisa, F.; Tetta, C.; Di Martino, A.; Marcacci, M. Arthroscopic mosaicplasty: Long-term outcome and joint degeneration progression. *Knee* **2015**, *22*, 36–40. [\[CrossRef\]](#)
21. Filardo, G.; Kon, E.; Di Martino, A.; Patella, S.; Altadonna, G.; Balboni, F.; Bragonzoni, L.; Visani, A.; Marcacci, M. Second-generation arthroscopic autologous chondrocyte implantation for the treatment of degenerative cartilage lesions. *Knee Surg. Sports Traumatol. Arthrosc.* **2012**, *20*, 1704–1713. [\[CrossRef\]](#) [\[PubMed\]](#)
22. Filardo, G.; Andriolo, L.; Balboni, F.; Marcacci, M.; Kon, E. Cartilage failures. Systematic literature review, critical survey analysis, and definition. *Knee Surg. Sports Traumatol. Arthrosc.* **2015**, *23*, 3660–3669. [\[CrossRef\]](#)
23. Schreiner, M.M.; Raudner, M.; Marlovits, S.; Bohndorf, K.; Weber, M.; Zalaudek, M.; Rohrich, S.; Szomolanyi, P.; Filardo, G.; Windhager, R.; et al. The MOCART (Magnetic Resonance Observation of Cartilage Repair Tissue) 2.0 Knee Score and Atlas. *Cartilage* **2019**. [\[CrossRef\]](#) [\[PubMed\]](#)

24. Brix, M.O.; Stelzeneder, D.; Chiari, C.; Koller, U.; Nehrer, S.; Dorotka, R.; Windhager, R.; Domayer, S.E. Treatment of Full-Thickness Chondral Defects with Hyalograft C in the Knee: Long-term Results. *Am. J. Sports Med.* **2014**, *42*, 1426–1432. [[CrossRef](#)] [[PubMed](#)]
25. Andriolo, L.; Reale, D.; Di Martino, A.; Zaffagnini, S.; Vannini, F.; Ferruzzi, A.; Filardo, G. High rate of failure after matrix-assisted autologous chondrocyte transplantation in osteoarthritic knees at 15 years of follow-up. *Am. J. Sports Med.* **2019**, *47*, 2116–2122. [[CrossRef](#)]
26. Hangody, L.; Fules, P. Autologous osteochondral mosaicplasty for the treatment of full-thickness defects of weight-bearing joints: Ten years of experimental and clinical experience. *J. Bone Jt. Surg. Am.* **2003**, *85*, 25–32. [[CrossRef](#)]
27. Andriolo, L.; Merli, G.; Filardo, G.; Marcacci, M.; Kon, E. Failure of autologous chondrocyte implantation. *Sports Med. Arthrosc. Rev.* **2017**, *25*, 10–18. [[CrossRef](#)]
28. Kon, E.; Filardo, G.; Gobbi, A.; Berruto, M.; Andriolo, L.; Ferrua, P.; Crespiatico, I.; Marcacci, M. Long-term results after hyaluronan-based MACT for the treatment of cartilage lesions of the patellofemoral joint. *Am. J. Sports Med.* **2016**, *44*, 602–608. [[CrossRef](#)]
29. Solheim, E.; Hegna, J.; Inderhaug, E. Long-term clinical follow-up of microfracture versus mosaicplasty in articular cartilage defects of medial femoral condyle. *Knee* **2017**, *24*, 1402–1407. [[CrossRef](#)]
30. Solheim, E.; Hegna, J.; Inderhaug, E. Long-term survival after microfracture and mosaicplasty for knee articular cartilage repair: A comparative study between two treatments cohorts. *Cartilage* **2020**, *11*, 71–76. [[CrossRef](#)]
31. Solheim, E.; Hegna, J.; Strand, T.; Harlem, T.; Inderhaug, E. Randomized study of long-term (15–17 years) outcome after microfracture versus mosaicplasty in knee articular cartilage defects. *Am. J. Sports Med.* **2018**, *46*, 826–831. [[CrossRef](#)] [[PubMed](#)]
32. Gudas, R.; Gudaite, A.; Pocius, A.; Gudiene, A.; Cekanauskas, E.; Monastyreckiene, E.; Basevicius, A. Ten-year follow-up of a prospective, randomized clinical study of mosaic osteochondral autologous transplantation versus microfracture for the treatment of osteochondral defects in the knee joint of athletes. *Am. J. Sports Med.* **2012**, *40*, 2499–2508. [[CrossRef](#)]
33. Kon, E.; Gobbi, A.; Filardo, G.; Delcogliano, M.; Zaffagnini, S.; Marcacci, M. Arthroscopic second-generation autologous chondrocyte implantation compared with microfracture for chondral lesions of the knee: Prospective nonrandomized study at 5 years. *Am. J. Sports Med.* **2009**, *37*, 33–41. [[CrossRef](#)] [[PubMed](#)]
34. Everhart, J.S.; Jiang, E.X.; Poland, S.G.; Du, A.; Flanigan, D.C. Failures, reoperations, and improvement in knee symptoms following matrix-assisted autologous chondrocyte transplantation: A meta-analysis of prospective comparative trials. *Cartilage* **2019**. [[CrossRef](#)] [[PubMed](#)]
35. Brittberg, M.; Peterson, L.; Sjogren-Jansson, E.; Tallheden, T.; Lindahl, A. Articular cartilage engineering with autologous chondrocyte transplantation. A review of recent developments. *J. Bone Jt. Surg. Am.* **2003**, *85*, 109–115. [[CrossRef](#)] [[PubMed](#)]
36. Mithoefer, K.; McAdams, T.; Williams, R.J.; Kreuz, P.C.; Mandelbaum, B.R. Clinical efficacy of the microfracture technique for articular cartilage repair in the knee: An evidence-based systematic analysis. *Am. J. Sports Med.* **2009**, *37*, 2053–2063. [[CrossRef](#)]
37. Domayer, S.E.; Kutscha-Lissberg, F.; Welsch, G.; Dorotka, R.; Nehrer, S.; Gabler, C.; Mamisch, T.C.; Trattnig, S. T2 mapping in the knee after microfracture at 3.0 T: Correlation of global T2 values and clinical outcome-preliminary results. *Osteoarthr. Cartil.* **2008**, *16*, 903–908. [[CrossRef](#)]
38. Liu, Y.W.; Tran, M.D.; Skalski, M.R.; Patel, D.B.; White, E.A.; Tomasian, A.; Gross, J.S.; Vangsness, C.T.; Matcuk, G.R., Jr. MR imaging of cartilage repair surgery of the knee. *Clin. Imaging* **2019**, *58*, 129–139. [[CrossRef](#)]
39. Tetta, C.; Busacca, M.; Moio, A.; Rinaldi, R.; Delcogliano, M.; Kon, E.; Filardo, G.; Marcacci, M.; Albisinni, U. Knee osteochondral autologous transplantation: Long-term MR findings and clinical correlations. *Eur. J. Radiol.* **2010**, *76*, 117–123. [[CrossRef](#)]
40. Kon, E.; Di Martino, A.; Filardo, G.; Tetta, C.; Busacca, M.; Iacono, F.; Delcogliano, M.; Albisinni, U.; Marcacci, M. Second-generation autologous chondrocyte transplantation: MRI findings and clinical correlations at a minimum 5-year follow-up. *Eur. J. Radiol.* **2011**, *79*, 382–388. [[CrossRef](#)]
41. Aldrian, S.; Zak, L.; Wondrasch, B.; Albrecht, C.; Stelzeneder, B.; Binder, H.; Kovar, F.; Trattnig, S.; Marlovits, S. Clinical and radiological long-term outcomes after matrix-induced autologous chondrocyte transplantation: A prospective follow-up at a minimum of 10 years. *Am. J. Sports Med.* **2014**, *42*, 2680–2688. [[CrossRef](#)]

42. Windt, d.T.S.; Welsch, G.H.; Brittberg, M.; Vonk, L.A.; Marlovits, S.; Trattinig, S.; Saris, D.B. Is magnetic resonance imaging reliable in predicting clinical outcome after articular cartilage repair of the knee? A systematic review and meta-analysis. *Am. J. Sports Med.* **2013**, *41*, 1695–1702. [[CrossRef](#)] [[PubMed](#)]
43. Bentley, G.; Biant, L.C.; Vijayan, S.; Macmull, S.; Skinner, J.A.; Carrington, R.W. Minimum ten-year results of a prospective randomised study of autologous chondrocyte implantation versus mosaicplasty for symptomatic articular cartilage lesions of the knee. *J. Bone Jt. Surg. Br.* **2012**, *94*, 504–509. [[CrossRef](#)] [[PubMed](#)]
44. Marcacci, M.; Kon, E.; Delcogliano, M.; Filardo, G.; Busacca, M.; Zaffagnini, S. Arthroscopic autologous osteochondral grafting for cartilage defects of the knee: Prospective study results at a minimum 7-year follow-up. *Am. J. Sports Med.* **2007**, *35*, 2014–2021. [[CrossRef](#)]
45. Ollat, D.; Lebel, B.; Thaunat, M.; Jones, D.; Mainard, L.; Dubrana, F.; Versier, G. Mosaic osteochondral transplantations in the knee joint, midterm results of the SFA multicenter study. *Orthop. Traumatol. Surg. Res.* **2011**, *97*, 160–166. [[CrossRef](#)]
46. Hangody, L.; Kish, G.; Karpati, Z.; Udvarhelyi, I.; Szigeti, I.; Bely, M. Mosaicplasty for the treatment of articular cartilage defects: Application in clinical practice. *Orthopedics* **1998**, *21*, 751–756. [[CrossRef](#)] [[PubMed](#)]
47. Filardo, G.; Kon, E.; Di Matteo, B.; Di Martino, A.; Marcacci, M. Single-plug autologous osteochondral transplantation: Results at minimum 16 years' follow-up. *Orthopedics* **2014**, *37*, e761–e767. [[CrossRef](#)]
48. Filardo, G.; Kon, E.; Andriolo, L.; Di Matteo, B.; Balboni, F.; Marcacci, M. Clinical profiling in cartilage regeneration: Prognostic factors for midterm results of matrix-assisted autologous chondrocyte transplantation. *Am. J. Sports Med.* **2014**, *42*, 898–905. [[CrossRef](#)]
49. Filardo, G.; Kon, E.; Andriolo, L.; Vannini, F.; Buda, R.; Ferruzzi, A.; Giannini, S.; Marcacci, M. Does patient sex influence cartilage surgery outcome? Analysis of results at 5-year follow-up in a large cohort of patients treated with Matrix-assisted autologous chondrocyte transplantation. *Am. J. Sports Med.* **2013**, *41*, 1827–1834. [[CrossRef](#)]
50. Pareek, A.; Carey, J.L.; Reardon, P.J.; Peterson, L.; Stuart, M.J.; Krych, A.J. Long-term outcomes after autologous chondrocyte implantation: A systematic review at mean follow-up of 11.4 years. *Cartilage* **2016**, *7*, 298–308. [[CrossRef](#)]
51. Dholander, A.A.; Guevara Sanchez, V.R.; Almqvist, K.F.; Verdonk, R.; Verbruggen, G.; Verdonk, P.C. The use of scaffolds in the treatment of osteochondral lesions in the knee: Current concepts and future trends. *J. Knee Surg.* **2012**, *25*, 179–186. [[CrossRef](#)]
52. Filardo, G.; Andriolo, L.; Angele, P.; Berruto, M.; Brittberg, M.; Condello, V.; Chubinskaya, S.; Girolamo, d.L.; Di Martino, A.; Di Matteo, B.; et al. Scaffolds for Knee Chondral and Osteochondral Defects: Indications for Different Clinical Scenarios. A Consensus Statement. *Cartilage* **2020**. [[CrossRef](#)] [[PubMed](#)]
53. Gobbi, A.; Whyte, G.P. Long-term clinical outcomes of one-stage cartilage repair in the knee with hyaluronic acid-based scaffold embedded with mesenchymal stem cells sourced from bone marrow aspirate concentrate. *Am. J. Sports Med.* **2019**, *47*, 1621–1628. [[CrossRef](#)] [[PubMed](#)]
54. Yamagata, K.; Nakayamada, S.; Tanaka, Y. Use of mesenchymal stem cells seeded on the scaffold in articular cartilage repair. *Inflamm. Regen.* **2018**, *38*, 4. [[CrossRef](#)] [[PubMed](#)]
55. Boffa, A.; Previtali, D.; Altamura, S.A.; Zaffagnini, S.; Candrian, C.; Filardo, G. Platelet-Rich Plasma Augmentation to Microfracture Provides a Limited Benefit for the Treatment of Cartilage Lesions: A Meta-analysis. *Orthop. J. Sports Med.* **2020**, *8*, 2325967120910504. [[CrossRef](#)] [[PubMed](#)]
56. Andriolo, L.; Reale, D.; Di Martino, A.; Boffa, A.; Zaffagnini, S.; Filardo, G. Cell-free scaffolds in cartilage knee surgery: A systematic review and meta-analysis of clinical evidence. *Cartilage* **2019**. [[CrossRef](#)] [[PubMed](#)]



Article

Histopathological Signatures of the Femoral Head in Patients with Osteonecrosis and Potential Applications in a Multi-Targeted Approach: A Pilot Study

Giovanna Desando ^{1,*†}, Livia Roseti ^{1,†}, Isabella Bartolotti ^{1,*}, Dante Dallari ², Cesare Stagni ² and Brunella Grigolo ¹

¹ SSD Laboratorio RAMSES, IRCCS Istituto Ortopedico Rizzoli, 40136 Bologna, Italy; livia.roseti@ior.it (L.R.); brunella.grigolo@ior.it (B.G.)

² Chirurgia Ortopedica Ricostruttiva Tecniche Innovative-Banca del Tessuto Muscoloscheletrico (BTM), IRCCS Istituto Ortopedico Rizzoli, 40136 Bologna, Italy; dante.dallari@ior.it (D.D.); cesare.stagni@ior.it (C.S.)

* Correspondence: giovanna.desando@ior.it (G.D.); isabella.bartolotti@ior.it (I.B.);
Tel.: +39-051-6366803 (G.D.); +39-051-4689945 (I.B.)

† Giovanna Desando and Livia Roseti equally contributed to the work.

Received: 7 May 2020; Accepted: 4 June 2020; Published: 6 June 2020

Abstract: (1) Background: Osteonecrosis (ON) of the femoral head is a disabling disease for which limited treatment options exist. Identifying therapeutic targets of its evolution could provide crucial insights into multi-targeted approaches. The aim of this pilot study was to assess the histopathological features of patients with non-traumatic femoral head (NTFH) and post-traumatic femoral head (PTFH) ON to produce a fresh vision for clinical use. (2) Methods: We got biopsies from patients with different ON stages, according to the ARCO system. Samples from multi-organ donors were used as controls. Histological and immunohistochemical evaluations were performed on the osteochondral unit. (3) Results: The PTFH group displayed several fibrotic reactions, a small stem cell pool and a lower international cartilage repair society (ICRS)-I score than NTFH, which instead presented intact cartilage similar to the controls. Immunostaining for collagen I and autotaxin confirmed these features in the PTFH group, which displayed top levels of MMP-13 involved in cartilage loss and reduced CB-2 in the underlying bone. Both groups manifested a similar pattern of apoptotic and pain mediators. (4) Conclusions: The different histopathological features suggest a multi-disciplinary and multi-targeted approach for ON. Further studies are necessary to measure the effect size to gain clinical evidence.

Keywords: osteonecrosis; osteochondral unit; tissue remodelling and repair; multi-targeted approach

1. Introduction

Osteonecrosis (ON) of the femoral head is a progressive and disabling disease, affecting active patients between the third and fifth decade of life with a high burden on the healthcare system [1–3]. The pathogenesis of ON involves the interplay of genetic, local and metabolic aspects with a different incidence rate among men and women (ratio male/female: 4:1) [4–7]. It is possible to identify two major types of ON aetiologies. The aetiology in ON patients with post-traumatic femoral head (PTFH) ON includes previous traumatic events; non-traumatic femoral head (NTFH) ON aetiology includes corticosteroid use, alcohol abuse, obesity, autoimmune diseases, and immunosuppressive therapies [7–9]. The pathology reflects a dynamic course leading to femoral head collapse because of subchondral bone fractures and inadequate bone repair [10–12]. Skeletal complications and pain in ON patients occurs because of abnormal osteoblastic and osteolytic activities [13,14]. In particular,

ON patients showed impaired action of the OPG/RANKL/RANK signalling pathway [9,14]. Wang X. and his group observed a similar behaviour whereby ON patients displayed increased levels of osteoprotegerin (OPG), receptor activator of nuclear factor- κ B (RANK), and its ligand (RANKL) genes in ON necrotic areas [15]. Beyond such classical signalling pathways, scientists have even started testing the role of cannabinoids (CN) in bone repair, as bone-marrow-derived osteoclasts and osteoblasts [16], MC3T3 E1 osteoblast-like cells [17] and osteocytes express CN receptors [18]. Beyond the critical role of bone in the ON setting, scientists have pointed great attention towards the articular cartilage, because of its close anatomic continuity and communication with the underlying subchondral bone [19,20]. In particular, several authors stressed the clinical significance of considering structural cartilage changes following the mechanical stress induced by the collapse of the subchondral bone in ON [21–23]. However, these changes contribute to altering the biomechanics of the joint leading to OA progression and finally to joint destruction.

There is no gold-standard treatment for ON because of the controversial results [24,25]. Selecting treatment options for ON depends on many factors, including the pathology stage, patients' age and health conditions, and lesion size and location [26,27]. In particular, treatments for ON management in the pre-collapse stage include non-surgical (weight control), pharmacological or biophysical techniques, and mesenchymal stromal cell (MSC)-based therapy [27–31]. Total hip arthroplasty is among the best therapeutic alternatives after the collapse of the femoral head. However, it has its disadvantages (e.g., infection, revision, and dislocation) [24,25]. Therefore, many scientists focused on femoral head regeneration. In 2002, Hernigou P. and his group reported promising results following MSC therapy in ON patients in the pre-collapse stage at 5 to 10 years of clinical follow-up [29]. A recent review summarised that MSCs could regenerate the necrotic area of the femoral head by injecting the suspension into the lateral artery of the circumflex or loading on carriers via core decompression and implantation [32]. Testing the crosstalk between cartilage and the underlying subchondral bone is essential to achieve global comprehension of physiological responses in ON disease. Differences between ON patients with various aetiologies could give first perspectives for tailored-based therapies. In this light, we conducted a small-scale preliminary (pilot) study aimed at evaluating histopathological features in two ON patient groups with NTFH and PTFH. Study design foresaw investigating several mediators modulating the osteochondral unit to get more knowledge of potential therapeutic targets for ON. In particular, we selected collagen I and autotaxin (ATX) to test the fibrotic reactions commonly causing poor mechanical properties and the limited capacity of MSCs to differentiate towards collagen type II in cartilage [33,34]. The axis ATX/lysophosphatidic acid (LPA) regulates collagen type I biosynthesis and plays essential functions in bone metabolism, thus resulting in an attractive molecular target [34,35]. We tested tissue destruction by selecting matrix metalloproteinases (MMP-13) and aggrecanases (ADAMTS-5), causing the proteolytic cleavage of collagens and the aggrecan protein [36]. As for apoptosis reactions, we tested active caspase 3, which is a well-known biochemical marker of both early- and late-stage apoptosis [37]. We tested the endocannabinoid receptor-2 (CB-2), as it is present in distinct cell types of the joint, like chondrocytes, bone cells, progenitor cells during osteoarthritis and rheumatoid arthritis with potential therapeutic implications [38]. We chose the neurotrophin nerve growth factor (NGF) and the nociceptive peptide substance P (SP) to test the pain response [39,40].

2. Materials and Methods

2.1. Patient Data and Surgical Procedure

This study obtained approval from the Ethics Committee of IRCCS Istituto Ortopedico Rizzoli (Prot. gen. n. 26146 del. 31.10.2006). Eleven male patients with clinical and radiological signs of ON of the femoral head gave their informed written consent to this study. We selected patients according to specific inclusion and exclusion criteria. Inclusion criteria foresaw the enrolment of male patients with a mean age between 18–50 years and clear signs of hip osteonecrosis by MRI.

Exclusion criteria foresaw the exclusion of patients showing metabolic diseases, rheumatoid arthritis, autoimmune and neurological disorders. In this study, five ON patients showed NTFH (mean age 37 ± 4 ; range: 30–43), whereas six ON patients had PTFH (mean age/SD: 30 ± 3 ; range: 25–37). The aetiology of the NTFH group included glucocorticoid treatment. ON patients included in the NTFH group did not report aetiology for alcohol abuse and autoimmune diseases; only one patient had a chronic bowel disorder. NTFH and PTFH patients underwent preoperative MRI and X-ray using the Association Research Circulation Osseous (ARCO) evaluation system [41]. This system considers the size of the necrotic lesion, its femoral head extent, and the joint involvement (Stage I: normal on X-ray and CT; Stage IV: the destruction of joint with secondary arthritic changes; A, B and C describe the extent of ON involvement: A: non-articular, B: medial; C: central). We reported a scientific diagram of the weight-bearing area of the femoral epiphysis where we harvested biopsies (see Supplementary Figure S1). Patients' femoral heads underwent surgical repair with a synthetic resorbable osteochondral scaffold plug. During the procedure, surgeons collected osteochondral biopsies of the lesions from the weight-bearing area of the femoral head with a 10-mm diameter through a 12–14-mm deep trocar. All samples were processed for histological and immunohistochemical analyses. We used the femoral head from three male multi-organ donors (mean age/SD: 35 ± 5 ; range: 30–40) as healthy controls. Multi-organ donors did not suffer from any musculoskeletal disease. We selected the donors through the bone bank program for tissue donation after the family's donor consent. Femur harvesting was performed within six hours from asystole, and involved its excision and placement in Dulbecco-modified Eagle medium with L-glutamine, NaHCO_3 , and antibiotics, and storage at 4°C .

2.2. Histological Assessment

Osteochondral samples were fixed with 10% buffered formalin and decalcified in 4% hydrochloric acid and 5% formic acid [42]. After processing with a graded alcohol series, specimens were embedded in paraffin. We tested proteoglycan and collagen content by staining tissue sections with 0.1% Safranin-O/0.02% Fast Green (Sigma Aldrich, St Louis, MO, USA). International Cartilage Repair Society (ICRS)-I score was used for evaluating the histological features [43]. This score considers six parameters: surface, matrix organization, cell distribution, cell viability, subchondral bone and cartilage mineralization. It has a range from 0 (presence of fibrous tissue) up to 18 (presence of healthy osteochondral tissue). We assessed necrotic bone lesions with the Ficat and Arlet classification system [44]. This system considers four types of bone necrosis. Its score ranges from 0 (slight disease) to 4 (severe disease). Six microscopic fields, spaced 20 sections, were assessed for each sample by two blinded investigators (GD, IB) with an Eclipse 90i microscope (Nikon, Melville, NY, USA).

2.3. Immunohistochemical Analyses

Analyses for collagen type I, caspase-3, MMP-13, ADAMTS-5, autotaxin, NGF, SP, and CB-2 were performed. After antigen retrieval with 0.1% proteinase (Sigma) at 37°C for 20 min, the sections were blocked with 2% bovine serum albumin (Sigma) in phosphate-buffered saline for 30 min. Then, an incubation with human collagen type I (2 $\mu\text{g}/\text{mL}$; Chemicon International, Temecula, CA, USA), caspase-3 (5 $\mu\text{g}/\text{mL}$; R&D Systems), ADAMTS-5 (1 $\mu\text{g}/\text{mL}$, Abcam), MMP-13 (5 $\mu\text{g}/\text{mL}$, R&D Systems, Minneapolis, MN, USA), autotaxin (2 $\mu\text{g}/\text{mL}$; R&D Systems), NGF (1 $\mu\text{g}/\text{mL}$, Chemicon), and CB-2 (5 $\mu\text{g}/\text{mL}$; Novus Biologicals) was carried out. Specific negative controls were performed by omitting the primary antibodies or using an isotype-matched control while we stained nuclei with CAT hematoxylin (Biocare Medical). Six microscopic fields (100 \times magnification) were assessed for each sample by a blinded investigator with a semi-quantitative method. We firstly segmented cartilage and the subchondral bone for each marker by selecting zones apart from the tidemark, especially for the PTFH group where the tidemark was fragmented. Image acquisition and processing with an Eclipse 90i microscope (Nikon) and NIS-Elements Software were used for the image analysis of stained sections with the Hue/Saturation/Intensity (HSI) system. Hue (H) was assessed by setting the threshold for

positive pixels at 220 to 255. Ranges from 0 to 150 were threshold values for S and I. The measurement of positive cells and area for each marker was done on the entire osteochondral sample (10× objective lens) and expressed as a percentage of positive cells and area on a scale from 0 (no protein expression) to 100 (the highest protein expression).

2.4. Statistical Analysis

Graph Pad Prism software was adopted for statistical analysis. The Kolmogorov–Smirnov test was used to test the data distribution. We used the Mann–Whitney U test for unpaired data to assess differences in NTFH and PTFH groups. We reported data in a scatter plot graph with mean ± standard deviation (SD). $p < 0.05$ was considered significant.

3. Results

3.1. Radiographic Assessment

According to the ARCO osteonecrosis classification system, patients with NTFH and PTFH displayed different stages of ON. The NTFH group reported three patients with III C stage and two patients with IV C. Patients with III C stages showed clear signs of ON and separation of the subchondral bone from the necrotic cancellous bone. Patients with IV C revealed joint space narrowing following the femoral head collapse. The PTFH group included four patients with IV C and two with IV B, which reported bone fracture and subsequent arthritic changes.

3.2. NTFH and PTFH Groups Displayed Different Histological Features in Cartilage and Bone

The control group showed a regular cartilage surface, adequate cell distribution and rich proteoglycan content. Bone tissue was also well-structured with osteocytes embedded in the bone matrix and trabecular spaces containing bone marrow and blood vessels (Figure 1a). The NTFH group showed a regular cartilage surface with small discontinuities and good proteoglycan content. The extracellular matrix of specimens with radiographic IV C stage displayed a reduced number of cells, some cell clones, and tidemark discontinuities. Bone tissue showed a low number of osteocytes and necrosis of the bone marrow in the trabecular spaces. No inflammatory reactions were, however, present (Figure 1a). The PTFH group exhibited a typical fibrocartilaginous aspect with several cracks in the superficial zone, and an altered cell arrangement with round cells interposed in the extracellular matrix. The tidemark displayed non-continuous areas with cells migrating from the subchondral bone towards the cartilage. The PTFH group showed trabecular spaces containing fibroblasts, blood vessels, and osteoclasts but no inflammatory infiltrate (Figure 1a). The NTFH group showed a higher ICRS-I score than the PTFH group ($p < 0.05$), reporting mean values of 13.1 ± 0.6 and 7.8 ± 0.9 , respectively (Figure 1b). The PTFH group exhibited a worse histological aspect, different from the control group, which reported a mean value of 16.8 ± 0.6 ($p < 0.001$) (Figure 1b). As for the cartilage parameters, the extracellular matrix and the tidemark showed better organization in NTFH rather than in the PTFH group ($p < 0.001$) (data not shown). The Ficat classification system gave evidence of more degenerative changes in the subchondral bone marrow of PTFH group when compared with NTFH group but with no statistical evidence (Figure 1b).

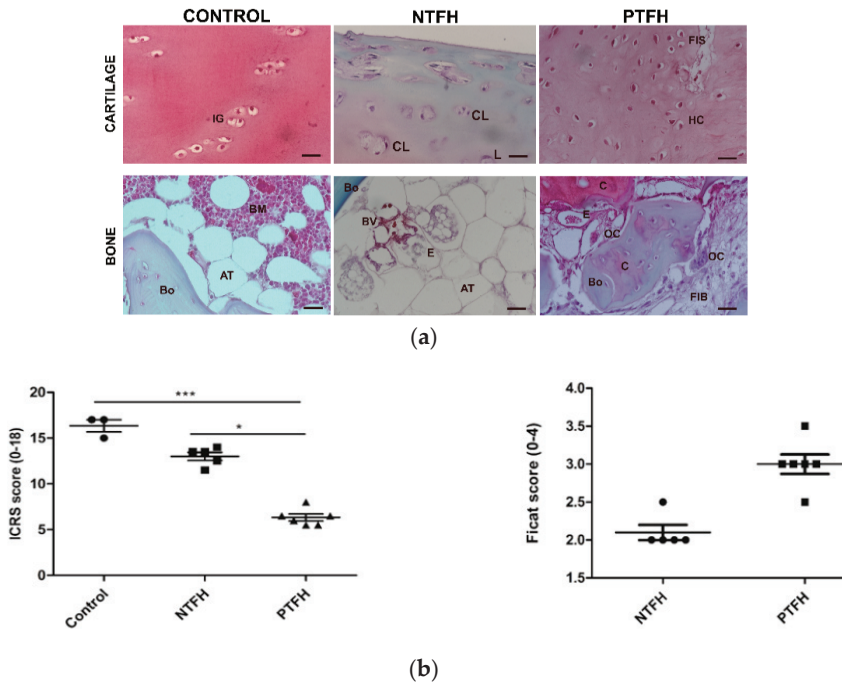


Figure 1. (a) Safranin-O/Fast Green staining of cartilage and subchondral bone from healthy controls, and two groups of patients with non-traumatic femoral head (NTFH) ON ($n = 5$), and post-traumatic femoral head (PTFH) ON ($n = 6$). Red: proteoglycans; green: collagen. Scale bar: 50 μm . IG isogenic groups; CL cell clusters; L: empty lacunae; FIS fibrillation processes; HC hypertrophic chondrocytes; T tears; Bo bone tissue; BM bone marrow; AT adipose tissue; BV blood vessels; FIB fibrous tissue; OC osteoclasts; E erythrocytes. (b) Graphical representation of ICRS and Ficat scores of the osteochondral unit of control, NTFH and PTFH groups. Data are reported in a scatter plot graph with mean \pm standard deviation (SD). * $p < 0.05$: NTFH versus PTFH; *** $p < 0.001$: PTFH versus the control group.

3.3. PTFH Group Displayed a Higher Expression of Fibrotic Markers than NTFH Specimens

The control group showed low protein expression for type I collagen in cartilage, whereas we noticed a high percentage of this marker in the underlying subchondral bone (Figure 2a,b). Fibrosis reactions in terms of the presence of type I collagen were more robust in the cartilage of the PTFH group compared to the NTFH group (Figure 2a,b). This latter group showed higher type I collagen expression compared to the control ($p < 0.05$) and NTFH groups ($p < 0.05$). As for autotaxin, the two ON groups did not show any difference; however, the PTFH group reported a higher amount of this marker compared to the control group ($p < 0.05$). The NTFH group showed mild protein expression for both collagen type I and autotaxin, especially in the articular cartilage.

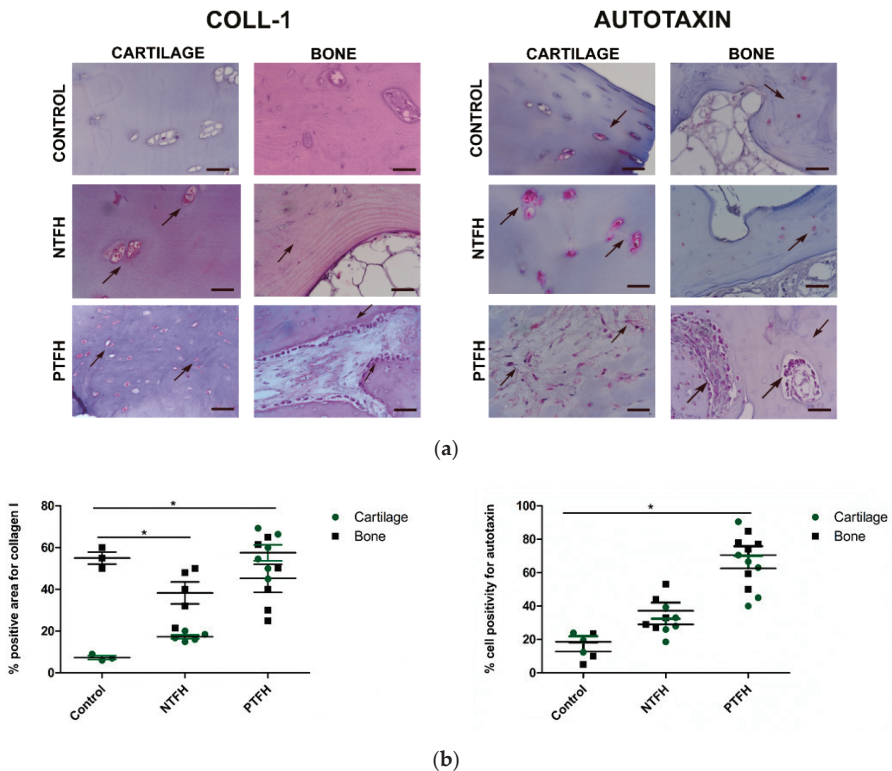


Figure 2. (a) Immunostaining for collagen type I and autotaxin of control, NTFH and PTFH groups. Scale bar: 50 μm . Black arrows: positive areas for markers. (b) Graphical representation of quantitative measurements for collagen type I and autotaxin in control, NTFH and PTFH groups. Data are reported in a scatter plot graph with mean \pm SD. Collagen type I: * $p < 0.05$: Control versus PTFH group; * $p < 0.05$ NTFH versus PTNH group. Autotaxin: * $p < 0.05$: Control versus PTFH group.

We did not find any difference for caspase-3 between the NTFH and PTFH groups. Both specimens displayed higher cell positivity for this marker when compared to the control group (Figure 3a,b). Regarding CB-2, a molecule involved in bone remodelling and pain responses, the control group displayed moderate expression, especially near bone marrow spaces, and at a lesser extent in the osteocytes. The NTFH group revealed higher protein expression for CB-2 in chondrocytes than in osteocytes and bone marrow precursors within the subchondral bone. The PTFH group displayed a similar behaviour (Figure 3a,b).

To assess the breakdown of the extracellular matrix, we analysed ADAMTS-5 and MMP-13 as catabolic markers. All cartilage and bone specimens showed low levels of ADAMTS-5, with no difference between the two ON groups (Figure 4a,b). As for MMP-13, the PTFH group displayed a higher cell positivity in the middle and deep layers of articular cartilage when compared to the control and NTFH groups ($p < 0.05$) (Figure 4a,b).

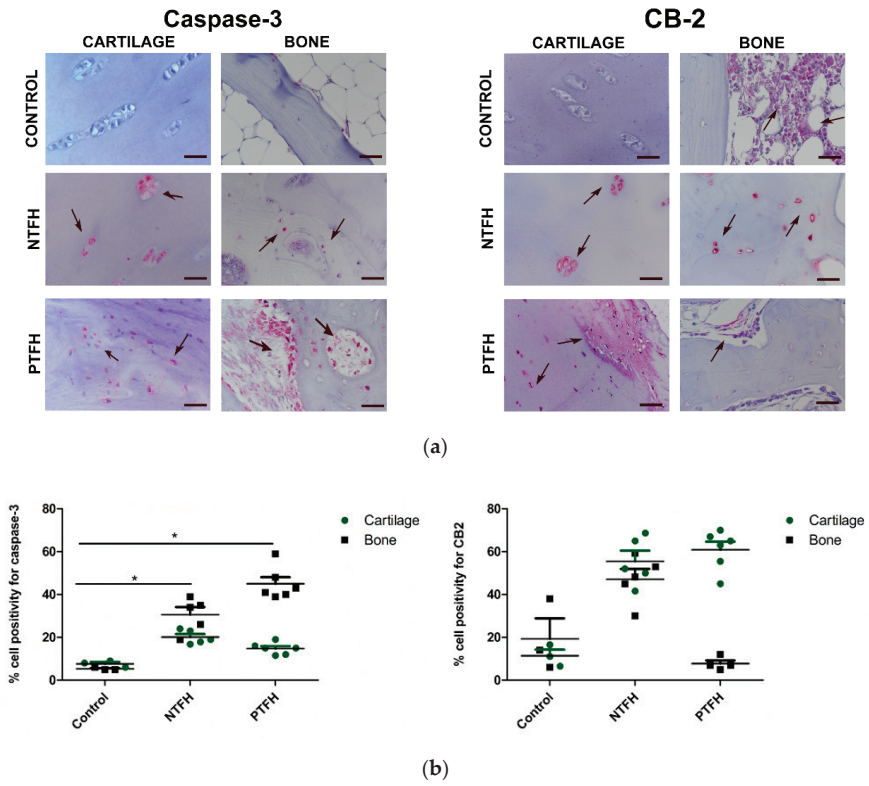


Figure 3. (a) Immunostaining for caspase-3 and CB-2 of the control, NTFH and PTFH groups. Scale bar = 50 μ m. Black arrows show positive cells. (b) Graphical representations of the percentage of positivity for caspase 3 and CB-2. Data are expressed in a scatter plot graph with mean \pm standard deviation (SD). Caspase 3: * $p < 0.05$: Control versus NTFH group; * $p < 0.05$: NTFH versus PTFH group.

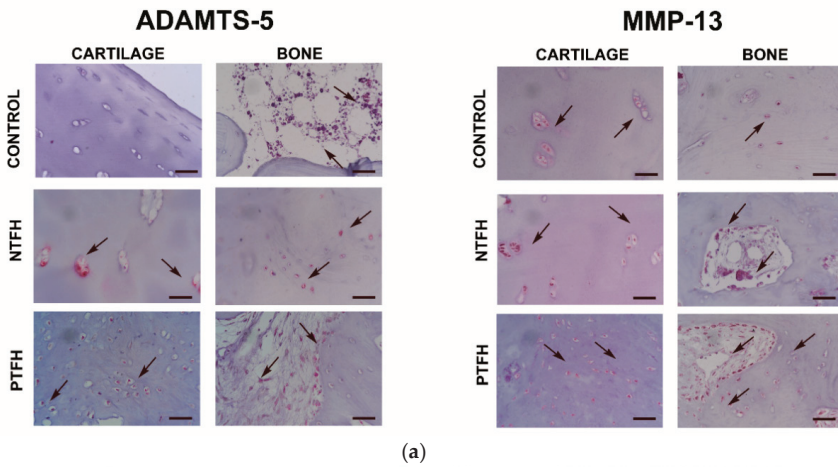


Figure 4. Cont.

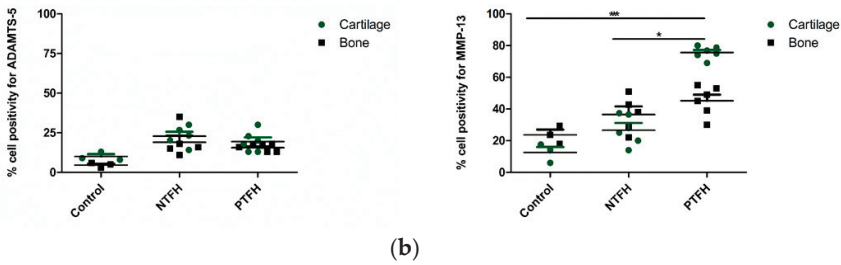


Figure 4. (a) Immunostaining for ADAMTS-5 and MMP-13 in osteochondral tissues from the control, NTFH and PTFH groups. Scale bar = 50 μ m. Black arrows show positive cells. (b) Graphical representations of the percentage of positivity for ADAMTS-5 and MMP-13. Data are expressed in a scatter plot graph with mean \pm standard deviation (SD). MMP-13: ** $p < 0.001$: Control versus PTFH group; * $p < 0.05$: NTFH versus PTFH group.

We analysed NGF and the substance P (SP) nociceptive fibre pattern to test the pain response. Both NTFH and PTFH groups showed higher immunostaining for NGF in the cartilage rather than in the underlying subchondral bone ($p < 0.05$) (Figure 5a,b). Both ON groups displayed an increased SP positivity near cell clones of the articular cartilage and hypercellular and fibrotic areas of the subchondral bone (Figure 5a,b).

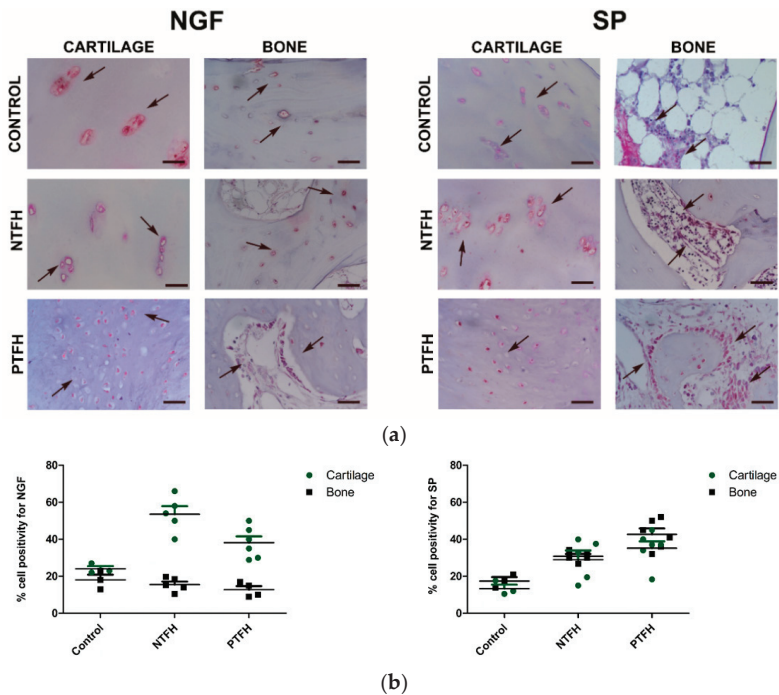


Figure 5. (a) Immunostaining for NGF and SP in osteochondral tissues from control, NTFH and PTFH groups. Scale bar: 50 μ m. Black arrows: positive areas for the selected markers. (b) Graphical representation of quantitative measurements for NGF and SP in control, NTFH and PTFH groups. Data are expressed in a scatter plot graph with mean \pm standard deviation (SD).

4. Discussion

The search for ON therapies capable of controlling the joint microenvironment is a unique challenge [1,2]. A holistic view of biological responses during ON can produce insights for generating efficient strategies [22]. Our pilot study showed different histopathological features in two groups of ON patients by opening up interesting biological perspectives. All specimens with NTFH and PTFH forms displayed basal integration with the underlying bone. However, PTFH samples showed noticeable fibrotic reactions and a reduced stem cell pool in the bone marrow. Interrupting blood supply likely contributed to mediating the death of bone and marrow cells. As the bone supports the exchange of nutrients with cartilage by facilitating joint force distribution, bone alterations might speed up cartilage degeneration [22,45]. The subchondral bone changes may lead to misalignment of the articulating surfaces with consequences on the mechanosensory cells in the bone [45]. Thus, first-line approaches for shifting the bone matrix turn-over are essential to avoid progressive degenerative changes in cartilage tissue. Bisphosphonate treatment could restore the balance between bone resorption and formation [26]. Biopsies from patients with post-traumatic aetiology reported several OA features, including impaired extracellular matrix and vascular infiltration in cartilage because of the mechanical stresses. We determined the relevance of matrix composition and tidemark presence using a semi-quantitative analysis with the ICRS score, by observing different histological scores in the PTFH and NTFH groups. This latter displayed similar results to the control group by reporting intact cartilage but several changes in the subchondral bone. These findings are in line with other studies, which showed intact articular cartilage in the NTFH group with corticosteroid treatments [22]. The two groups even exhibited distinct protein expression for mediators modulating fibrotic and catabolic responses.

Protein assessment for collagen type I and autotaxin corroborated the fibrotic aspect in both cartilage and bone from the PTFH group. The autotaxin-lysophosphatidic acid (LPA) axis is emerging as a critical regulator in various biological responses [46]. Autotaxin exerts a fibrotic activity by catalysing LPA, which promotes fibrosis responses by regulating collagen type I biosynthesis [34,47]. Moreover, autotaxin controls the fusion and bone resorption capacity of osteoclasts [35]. Another peculiar feature observed in the cartilage and bone tissues from the two ON aetiologies was the protein expression for MMP-13. It is a molecule which stimulates collagen and proteoglycan degradation in cartilage and bone [48]. Along this path, Grassel S. et al. provided first evidence of MMPs in the ON setting. ON patients with PTFH showed increased gene expression levels of MMP-2 and a low amount of the tissue inhibitor of metalloproteinases (TIMPs) [49]. The increased protein levels of MMP-13 in the PTFH group may likely depend on the up-regulated activity of chondrocytes in producing MMPs after stress forces. These findings open preliminary biological insights into considering MMPs and fibrotic markers as attractive therapeutic targets by exploiting future technological advances like CRISPR-Cas9 [50]. Combining current ON strategies with small molecule inhibitors to block collagen type I, MMP-13 and ATX could improve the success of PTFH treatment [47,51]. Regardless of the ON aetiology, samples from both groups displayed a moderate positivity for caspase-3, showing higher values than the control. Beyond the classical signalling pathway, we considered the role of CB-2 involved in the endocannabinoid system. Jiang S. et al. reported that this system promotes specific signalling pathways in response to pathogenic events to launch repair processes [52]. In specimens from both groups, we showed positive immunostaining for CB-2, especially in cartilage, with higher values than healthy controls. We noticed a low expression of CB-2 in the bone marrow niche, likely because of the small number of osteoprogenitors in ON patients.

Like in ON disease, femoral heads from patients with the atrophic form of osteoarthritis (OA) display bone marrow lesions with numeric, topographic and functional variations of MSCs [53,54]. Bone marrow perturbations reduce the bone repair and remodelling activities of MSCs and lead to damage of the overlying articular cartilage [55,56]. Targeting both cartilage and bone turn-over and the crosstalk between their cell types may be a valuable approach [56]. In this light, there is abundant evidence of the powerful effects of MSCs for promoting osteochondral repair and inhibiting

inflammatory and fibrotic reactions in the OA environment [57–59]. Optimal therapeutic approaches might envisage several interventions, at varying stages of OA and ON disorders and selecting specific patient features. Restoring the stem cell pool, especially in the PTFH group, through cell-based therapy, could be a feasible intervention. The remarkable bone–cartilage interface imbalance of this patients group, simultaneously with the low stem cell pool, may benefit from the differentiation and paracrine properties of MSCs. Hernigou P et al. reported promising clinical results using autologous bone marrow transplantation in ON cases by highlighting the biological and therapeutic value of this strategy [30]. Along the way, several clinicians have observed the combination of autologous bone marrow concentrate with core decompression contribute in a significant manner to decelerating ON progression by limiting total hip arthroplasty [60,61].

Finally, this study considered pain implications in the biopsy samples from two ON patients focusing on NGF and substance P; this latter is involved in the onset of inflammatory processes and pain transmission [52]. Specimens from both groups manifested pronounced immunostaining for NGF in cartilage. Beyond its role as a neurotrophic factor, NGF impairs the migratory and matrix remodelling activities of cartilage and stem progenitor cells [62,63]. More in-depth investigations are crucial to assess the effect size and produce clinical evidence, as the small number of ON cases and heterogeneity are the major limitations of the present study. However, this pilot study gave indications to enhance the benefit of current ON approaches by merging themselves with fibrotic inhibitors and choosing a multi-disciplinary and targeted strategy to both cartilage and bone in the PTFH group.

5. Conclusions

Sustainable multi-disciplinary strategies can represent valid tools to tackle complex pathologies, with tremendous impact in the clinical decision-making framework. In our pilot study, the different histopathological features of NTFH and PTFH groups would suggest a multi-disciplinary and multi-targeted approach for both cartilage and bone tissues. Hypothetically, restoring the stem cell pool in the subchondral bone from the PTFH group could be fruitful in supporting tissue regeneration. Successful clinical results could be obtained by hindering the fibrotic and catabolic responses at the level of cartilage and bone in the PTFH. Further studies are necessary to measure the effect of size to gain clinical evidence.

Supplementary Materials: The following are available online at <http://www.mdpi.com/2076-3417/10/11/3945/s1>, Figure S1: Scientific diagram.

Author Contributions: Conceptualisation, L.R. and G.D.; methodology, G.D.; C.S. and I.B.; software, G.D.; formal analysis, G.D. and D.D.; investigation, L.R., D.D. and C.S.; data curation, G.D., C.S. and I.B.; writing-original draft preparation, L.R. and G.D.; writing-review and editing, G.D., L.R., I.B., C.S., D.D., and B.G.; supervision, B.G.; project administration, B.G.; funding acquisition, B.G. All authors have read and agreed to the published version of the manuscript.

Funding: This research was funded by the Italian Ministry of Health, 5× 1000 Funds anno 2016. “Malattie osteoarticolari: fisiopatologia e strategie terapeutiche innovative”.

Acknowledgments: The authors wish to thank Patrizia Rappini and Martina Rocchi for their technical and scientific help.

Conflicts of Interest: The authors declare no conflict of interest. The funders had no role in the design of the study; in the collection, analyses, or interpretation of data; in the writing of the manuscript; or in the decision to publish the results.

References

1. Zalavras, C.G.; Lieberman, J.R. Osteonecrosis of the femoral head. *J. Am. Acad. Orthop. Surg.* **2014**, *22*, 455–464. [CrossRef]
2. Banerjee, S.; Issa, K.; Pivec, R.; Kapadia, B.H.; Khanuja, H.S.; Mont, M.A. Osteonecrosis of the hip. *Orthop. Clin. North Am.* **2013**, *44*, 463–476. [CrossRef] [PubMed]

3. Wang, J.; Wang, J.; Zhang, K.; Wang, Y.; Bao, X. Bayesian network meta-analysis of the effectiveness of various interventions for nontraumatic osteonecrosis of the femoral head. *Biomed Res. Int.* **2018**, *2018*, 2790163. [[CrossRef](#)] [[PubMed](#)]
4. Parsons, S.J.; Steele, N. Osteonecrosis of the femoral head: Part 1-Aetiology, pathogenesis, investigation, classification. *Curr. Orthop.* **2007**, *21*, 457–463. [[CrossRef](#)]
5. Mah, W.; Sonkusare, S.K.; Wang, T.; Azeddine, B.; Pupavac, M.; Carrot-Zhang, J.; Hong, K.; Majewski, J.; Harvey, E.J.; Russell, L.; et al. Gain-of-function mutation in *TRPV4* identified in patients with osteonecrosis of the femoral head. *J. Med. Genet.* **2016**, *53*, 705–709. [[CrossRef](#)]
6. Khan, A.M.; Choi, J.; Freiberg, R.A.; Glueck, C.J.; Goldenberg, N.; Wang, P. T786C Mutation in the endothelial nitric oxide synthase gene in patients with primary osteonecrosis. *Orthopedics* **2017**, *40*, e898–e903. [[CrossRef](#)]
7. Assouline-Dayana, Y.; Chang, C.; Greenspan, A.; Shoenfeld, Y.; Gershwin, M.E. Pathogenesis and natural history of osteonecrosis. In *Seminars in Arthritis and Rheumatism*; WB Saunders: Philadelphia, PA, USA, 2002.
8. Zhao, D.W.; Yu, M.; Hu, K.; Wang, W.; Yang, L.; Wang, B.J.; Gao, X.H.; Guo, Y.M.; Xu, Y.Q.; Wei, Y.S.; et al. Prevalence of nontraumatic osteonecrosis of the femoral head and its associated risk factors in the Chinese population: Results from a nationally representative survey. *Chin. Med. J. Engl.* **2015**, *128*, 2843–2850. [[CrossRef](#)]
9. Hwang, Y.; Park, J.; Choi, S.H.; Kim, G. Traumatic and Non-traumatic Osteonecrosis in the Femoral Head of a Rabbit Model. *Lab. Anim. Res.* **2011**, *27*, 127. [[CrossRef](#)]
10. Pivec, R.; Johnson, A.J.; Harwin, S.F.; Mont, M.A. Differentiation, Diagnosis, and Treatment of Osteoarthritis, Osteonecrosis, and Rapidly Progressive Osteoarthritis. *Orthopedics* **2013**, *36*, 118–125. [[CrossRef](#)]
11. Rajpura, A.; Wright, A.C.; Board, T.N. Medical management of osteonecrosis of the hip: A review. *HIP Int.* **2011**, *21*, 385–392. [[CrossRef](#)]
12. Malizos, K.N.; Karantanas, A.H.; Varitimidis, S.E.; Dailiana, Z.H.; Bargiotas, K.; Maris, T. Osteonecrosis of the femoral head: Etiology, imaging and treatment. *Eur. J. Radiol.* **2007**, *63*, 16–28. [[CrossRef](#)]
13. Tripathy, S.K.; Goyal, T.; Sen, R.K. Management of femoral head osteonecrosis: Current concepts. *Indian J. Orthop.* **2015**, *49*, 28–45. [[CrossRef](#)] [[PubMed](#)]
14. Wang, C.; Wang, X.; Xu, X.L.; Yuan, X.L.; Gou, W.L.; Wang, A.Y.; Guo, Q.Y.; Peng, J.; Lu, S.B. Bone microstructure and regional distribution of osteoblast and osteoclast activity in the osteonecrotic femoral head. *PLoS ONE* **2014**, *9*, e96361. [[CrossRef](#)] [[PubMed](#)]
15. Miao, Q.; Hao, S.; Li, H.; Sun, F.; Wang, X. Expression of osteoprotegerin, RANK and RANKL genes in femoral head avascular necrosis and related signaling pathway. *Int. J. Clin. Exp. Pathol.* **2015**, *8*, 10460–10467. [[PubMed](#)]
16. Dimitrova, N.; Zamudio, J.R.; Jong, R.M.; Soukup, D.; Resnick, R.; Sarma, K.; Ward, A.J.; Raj, A.; Lee, J.; Sharp, P.A.; et al. Regulation of bone mass, bone loss and osteoclast activity by cannabinoid receptors. *PLoS ONE* **2017**, *32*, 736–740. [[CrossRef](#)]
17. Ofek, O.; Karsak, M.; Leclerc, N.; Fogel, M.; Frenkel, B.; Wright, K.; Tam, J.; Attar-Namdar, M.; Kram, V.; Shohami, E.; et al. Peripheral cannabinoid receptor, CB2, regulates bone mass. *Proc. Natl. Acad. Sci. USA* **2006**, *103*, 696–701. [[CrossRef](#)]
18. Whyte, L.S.; Ford, L.; Ridge, S.A.; Cameron, G.A.; Rogers, M.J.; Ross, R.A. Cannabinoids and bone: Endocannabinoids modulate human osteoclast function in vitro. *Br. J. Pharmacol.* **2012**, *165*, 2584–2597. [[CrossRef](#)]
19. Xiang, S.; Li, Z.; Weng, X. Changed cellular functions and aberrantly expressed miRNAs and circRNAs in bone marrow stem cells in osteonecrosis of the femoral head. *Int. J. Mol. Med.* **2020**, *45*, 805–815. [[CrossRef](#)]
20. Li, J.; Cheng, L.; Zhao, Y.; Guo, Y.; Liu, Y.; Zhang, W.; Wang, S.; Zhang, Y.; Pan, X.; Nie, L. ADAMTS-7 exhibits elevated expression in cartilage of osteonecrosis of femoral head and has a positive correlation with TNF- α and NF- κ B P65. *Mediat. Inflamm.* **2015**, *2015*, 196702. [[CrossRef](#)]
21. Magnussen, R.A.; Guilak, F.; Vail, T.P. Articular cartilage degeneration in post-collapse osteonecrosis of the femoral head. Radiographic staging, macroscopic grading, and histologic changes. *J. Bone Jt. Surg Am.* **2005**, *87*, 1272–1277. [[CrossRef](#)]
22. Houtpt, J.B.; Pritzker, K.P.; Alpert, B.; Greyson, N.D.; Gross, A.E. Natural history of spontaneous osteonecrosis of the knee (SONK): A Review. In *Seminars in Arthritis and Rheumatism*; WB Saunders: Philadelphia, PA, USA, 1983; Volume 13.

23. Sonoda, K.; Motomura, G.; Kawanami, S.; Takayama, Y.; Honda, H.; Yamamoto, T.; Nakashima, Y. Degeneration of articular cartilage in osteonecrosis of the femoral head begins at the necrotic region after collapse: A preliminary study using T1 rho MRI. *Skeletal Radiol.* **2017**, *46*, 463–467. [[CrossRef](#)] [[PubMed](#)]
24. Chen, C.H.; Chang, J.K.; Lai, K.A.; Hou, S.M.; Chang, C.H.; Wang, G.J. Alendronate in the prevention of collapse of the femoral head in nontraumatic osteonecrosis: A two-year multicenter, prospective, randomized, double-blind, placebo-controlled study. *Arthritis Rheum.* **2012**, *64*, 1572–1578. [[CrossRef](#)] [[PubMed](#)]
25. Lai, K.A.; Shen, W.J.; Yang, C.Y.; Shao, C.J.; Hsu, J.T.; Lin, R.M. The use of alendronate to prevent early collapse of the femoral head in patients with nontraumatic osteonecrosis. *J. Bone Jt. Surg Am.* **2005**, *87*, 2155–2159. [[CrossRef](#)]
26. Chan, K.; Mok, C. Glucocorticoid-Induced Avascular Bone Necrosis: Diagnosis and Management. *Open Orthop. J.* **2012**, *6*, 449–457. [[CrossRef](#)]
27. Choi, H.R.; Steinberg, M.E.; Cheng, E. Osteonecrosis of the femoral head: Diagnosis and classification systems. *Curr. Rev. Musculoskelet Med.* **2015**, *8*, 210–220. [[CrossRef](#)]
28. Jones, L.C.; Hungerford, D.S. Osteonecrosis: Etiology, diagnosis, and treatment. *Curr. Opin. Rheumatol.* **2004**, *16*, 443–449. [[CrossRef](#)]
29. Hernigou, P.; Beaujean, F. Treatment of osteonecrosis with autologous bone marrow grafting. *Clin. Orthop. Relat. Res.* **2002**, *405*, 14–23. [[CrossRef](#)]
30. Hernigou, P.; Trousselier, M.; Roubineau, F.; Bouthors, C.; Chevallier, N.; Rouard, H.; Flouzat-Lachaniette, C.H. Stem cell therapy for the treatment of hip osteonecrosis: A 30-year review of progress. *CiOS Clin. Orthop. Surg.* **2016**, *8*, 1–8. [[CrossRef](#)]
31. Sacco, R.; Leeson, R.; Nissan, J.; Olate, S.; de Castro, C.H.B.C.; Acocella, A.; Lalli, A. A systematic review of oxygen therapy for the management of Medication-Related Osteonecrosis of the Jaw (MRONJ). *Appl. Sci.* **2019**, *9*, 1026. [[CrossRef](#)]
32. Wang, Y.; Ma, X.; Chai, W.; Tian, J. Multiscale stem cell technologies for osteonecrosis of the femoral head. *Stem Cells Int.* **2019**, *2019*, 8914569. [[CrossRef](#)]
33. Mobasheri, A.; Csaki, C.; Clutterbuck, A.L.; Rahmzadeh, M.; Shakibaei, M. Mesenchymal stem cells in connective tissue engineering and regenerative medicine: Applications in cartilage repair and osteoarthritis therapy. *Histol. Histopathol.* **2009**, *24*, 347–366. [[CrossRef](#)] [[PubMed](#)]
34. Wu, L.; Petrigliano, F.A.; Ba, K.; Lee, S.; Bogdanov, J.; McAllister, D.R.; Lin, Y. Lysophosphatidic acid mediates fibrosis in injured joints by regulating collagen type I biosynthesis. *Osteoarthr. Cartil.* **2015**, *23*, 308–318. [[CrossRef](#)] [[PubMed](#)]
35. Flammier, S.; Peyruchaud, O.; Bourguillault, F.; Duboeuf, F.; Davignon, J.; Norman, D.D.; Isaac, S.; Marotte, H.; Tigy, G.; Machuca-Gayet, I. Osteoclast—Derived autotaxin, a distinguishing factor for inflammatory bone loss. *Arthritis Rheumatol.* **2019**, *71*, 1801–1811. [[CrossRef](#)]
36. Troeberg, L.; Nagase, H. Proteases involved in cartilage matrix degradation in osteoarthritis. *Biochim. Biophys. Acta Proteins Proteom.* **2012**, *1824*, 133–145. [[CrossRef](#)]
37. Fan, L.; Li, J.; Yu, Z.; Dang, X.; Wang, K. Hypoxia-inducible factor prolyl hydroxylase inhibitor prevents steroid-associated osteonecrosis of the femoral head in rabbits by promoting angiogenesis and inhibiting apoptosis. *PLoS ONE* **2014**, *9*, e107774. [[CrossRef](#)] [[PubMed](#)]
38. Dunn, S.L.; Wilkinson, J.M.; Crawford, A.; Bunning, R.A.D.; Le Maitre, C.L. Expression of cannabinoid receptors in human osteoarthritic cartilage: Implications for future therapies. *Cannabis Cannabinoid Res.* **2016**, *1*, 3–15. [[CrossRef](#)]
39. Shang, X.; Wang, Z.; Tao, H. Mechanism and therapeutic effectiveness of nerve growth factor in osteoarthritis pain. *Ther. Clin. Risk Manag.* **2017**, *13*, 951–956. [[CrossRef](#)]
40. Li, F.X.Z.; Xu, F.; Lin, X.; Wu, F.; Zhong, J.Y.; Wang, Y.; Guo, B.; Zheng, M.H.; Shan, S.K.; Yuan, L.Q. The role of substance P in the regulation of bone and cartilage metabolic activity. *Front. Endocrinol.* **2020**, *11*, 77. [[CrossRef](#)]
41. Gardeniers, J. A new international classification of osteonecrosis of the ARCO-committee on terminology and classification. *ARCO Newsl.* **1992**, *4*, 41–46.
42. Desando, G.; Bartolotti, I.; Vannini, F.; Cavallo, C.; Castagnini, F.; Buda, R.; Giannini, S.; Mosca, M.; Mariani, E.; Grigolo, B. Repair potential of matrix-induced bone marrow aspirate concentrate and matrix-induced autologous chondrocyte implantation for talar osteochondral repair: Patterns of some catabolic, inflammatory, and pain mediators. *Cartilage* **2017**, *8*, 50–60. [[CrossRef](#)]

43. Hoemann, C.; Kandel, R.; Roberts, S.; Saris, D.B.F.; Creemers, L.; Mainil-Varlet, P.; Méthot, S.; Hollander, A.P.; Buschmann, M.D. International cartilage repair society (ICRS) recommended guidelines for histological endpoints for cartilage repair studies in animal models and clinical trials. *Cartilage* **2011**, *2*, 153–172. [[CrossRef](#)] [[PubMed](#)]
44. Jawad, M.U.; Haleem, A.A.; Scully, S.P. In brief: Ficat classification: Avascular necrosis of the femoral head. *Clin. Orthop. Relat. Res.* **2012**, *470*, 2636–2639. [[CrossRef](#)] [[PubMed](#)]
45. Goldring, S.R.; Goldring, M.B. Changes in the osteochondral unit during osteoarthritis: Structure, function and cartilage-bone crosstalk. *Nat. Rev. Rheumatol.* **2016**, *12*, 632–644. [[CrossRef](#)] [[PubMed](#)]
46. Knowlden, S.; Georas, S.N. The autotaxin-LPA axis emerges as a novel regulator of lymphocyte homing and inflammation. *J. Immunol.* **2014**, *192*, 851–857. [[CrossRef](#)]
47. Thirunavukkarasu, K.; Swearingen, C.A.; Oskins, J.L.; Lin, C.; Bui, H.H.; Jones, S.B.; Pfeifer, L.A.; Norman, B.H.; Mitchell, P.G.; Chambers, M.G. Identification and pharmacological characterization of a novel inhibitor of autotaxin in rodent models of joint pain. *Osteoarthr. Cartil.* **2017**, *25*, 935–942. [[CrossRef](#)]
48. Murphy, G.; Knäuper, V.; Atkinson, S.; Butler, G.; English, W.; Hutton, M.; Stracke, J.; Clark, I. Matrix metalloproteinases in arthritic disease. *Arthritis Res.* **2002**, *4*, S39. [[CrossRef](#)]
49. Grässel, S.; Beckmann, J.; Rath, B.; Vogel, M.; Grifka, J.; Tingart, M. Expression profile of matrix metalloproteinase-2 and -9 and their endogenous tissue inhibitors in osteonecrotic femoral heads. *Int. J. Mol. Med.* **2010**, *26*, 127–133. [[CrossRef](#)]
50. Herm, L.; Haxhia, A.; de Alcantara Camejo, F.; Tayebi, L.; Almeida, L.E. Matrix metalloproteinases and temporomandibular joint disorder: A review of the literature. *Appl. Sci.* **2019**, *9*, 4508. [[CrossRef](#)]
51. Vandenbroucke, R.E.; Libert, C. Is there new hope for therapeutic matrix metalloproteinase inhibition? *Nat. Publ. Gr.* **2014**, *13*, 904–927. [[CrossRef](#)]
52. Jiang, S.; Zagozdzon, R.; Jorda, M.A.; Parmar, K.; Fu, Y.; Williams, J.S.; Groopman, J.E. Endocannabinoids are expressed in bone marrow stromal niches and play a role in interactions of hematopoietic stem and progenitor cells with the bone marrow microenvironment. *J. Biol. Chem.* **2010**, *285*, 35471–35478. [[CrossRef](#)]
53. Roemer, F.W.; Neogi, T.; Nevitt, M.C.; Felson, D.T.; Zhu, Y.; Zhang, Y.; Lewis, C.E. Subchondral bone marrow lesions are highly associated with, and predict subchondral bone attrition longitudinally: The MOST study. *Osteoarthr. Cart.* **2010**, *18*, 47. [[CrossRef](#)] [[PubMed](#)]
54. Bellido, M.; Lugo, L.; Roman-Blas, J.A.; Castañeda, S.; Calvo, E.; Largo, R.; Herrero-Beaumont, G. Improving subchondral bone integrity reduces progression of cartilage damage in experimental osteoarthritis preceded by osteoporosis. *Osteoarthr. Cartil.* **2011**, *19*, 1228–1236. [[CrossRef](#)]
55. Campbell, T.M.; Churchman, S.M.; Gomez, A.; McGonagle, D.; Conaghan, P.G.; Ponchel, F.; Jones, E. Mesenchymal stem cell alterations in bone marrow lesions in patients with hip osteoarthritis. *Arthritis Rheumatol.* **2016**, *68*, 1648–1659. [[CrossRef](#)] [[PubMed](#)]
56. Karsdal, M.A.; Bay-Jensen, A.C.; Lories, R.J.; Abramson, S.; Spector, T.; Pastoureau, P.; Christiansen, C.; Attur, M.; Henriksen, K.; Goldring, S.R.; et al. The coupling of bone and cartilage turnover in osteoarthritis: Opportunities for bone antiresorptives and anabolics as potential treatments? *Ann. Rheum. Dis.* **2014**, *73*, 336–348. [[CrossRef](#)]
57. Desando, G.; Cavallo, C.; Sartoni, F.; Martini, L.; Parrilli, A.; Veronesi, F.; Fini, M.; Giardino, R.; Facchini, A.; Grigolo, B. Intra-articular delivery of adipose derived stromal cells attenuates osteoarthritis progression in an experimental rabbit model Intra-articular delivery of adipose derived stromal cells attenuates osteoarthritis progression in an experimental rabbit model. *Arthritis Res. Ther.* **2013**, *15*, R22. [[CrossRef](#)]
58. Perdisa, F.; Gostyrńska, N.; Roffi, A.; Filardo, G.; Marcacci, M.; Kon, E. Adipose-derived mesenchymal stem cells for the treatment of articular cartilage: A systematic review on preclinical and clinical evidence. *Stem Cells Int.* **2015**, *2015*, 597652. [[CrossRef](#)]
59. Murphy, M.B.; Moncivais, K.; Caplan, A.I. Mesenchymal stem cells: Environmentally responsive therapeutics for regenerative medicine. *Exp. Mol. Med.* **2013**, *45*, e54. [[CrossRef](#)] [[PubMed](#)]
60. Zhao, D.; Cui, D.; Wang, B.; Tian, F.; Guo, L.; Yang, L.; Liu, B.; Yu, X. Treatment of early stage osteonecrosis of the femoral head with autologous implantation of bone marrow-derived and cultured mesenchymal stem cells. *Bone* **2012**, *50*, 325–330. [[CrossRef](#)]
61. Liu, Y.; Liu, S.; Su, X. Core decompression and implantation of bone marrow mononuclear cells with porous hydroxylapatite composite filler for the treatment of osteonecrosis of the femoral head. *Arch. Orthop. Trauma Surg.* **2013**, *133*, 125–133. [[CrossRef](#)]

62. Jiang, Y.; Hu, C.; Yu, S.; Yan, J.; Peng, H.; Ouyang, H.W.; Tuan, R.S. Cartilage stem/progenitor cells are activated in osteoarthritis via interleukin-1 β /nerve growth factor signaling. *Arthritis Res. Ther.* **2015**, *17*, 327. [[CrossRef](#)]
63. Chartier, S.R.; Mitchell, S.A.T.; Majuta, L.A.; Mantyh, P.W. Immunohistochemical localization of nerve growth factor, tropomyosin receptor kinase A, and p75 in the bone and articular cartilage of the mouse femur. *Mol. Pain* **2017**, *13*, 1744806917745465. [[CrossRef](#)] [[PubMed](#)]



© 2020 by the authors. Licensee MDPI, Basel, Switzerland. This article is an open access article distributed under the terms and conditions of the Creative Commons Attribution (CC BY) license (<http://creativecommons.org/licenses/by/4.0/>).

Review

New Insights on Mechanical Stimulation of Mesenchymal Stem Cells for Cartilage Regeneration

Silvia Ravalli ¹, Marta Anna Szychlinska ¹, Giovanni Lauretta ¹ and Giuseppe Musumeci ^{1,2,3,*}

¹ Department of Biomedical and Biotechnological Sciences, Anatomy, Histology and Movement Sciences Section, School of Medicine, University of Catania, 95123 Catania, Italy; silviaravalli@gmail.com (S.R.); mszychlinska@unict.it (M.A.S.); gio.lau.gl@gmail.com (G.L.)

² Research Center on Motor Activities (CRAM), University of Catania, 95123 Catania, Italy

³ Department of Biology, Sbarro Institute for Cancer Research and Molecular Medicine, College of Science and Technology, Temple University, Philadelphia, PA 19122, USA

* Correspondence: g.musumeci@unict.it; Tel.: +39-095-3782043

Received: 6 April 2020; Accepted: 22 April 2020; Published: 23 April 2020

Abstract: Successful tissue regeneration therapies require further understanding of the environment in which the cells are destined to be set. The aim is to structure approaches that aspire to a holistic view of biological systems and to scientific reliability. Mesenchymal stem cells represent a valuable resource for cartilage tissue engineering, due to their chondrogenic differentiation capacity. Promoting chondrogenesis, not only by growth factors but also by exogenous enhancers such as biomechanics, represents a technical enhancement. Tribological evaluation of the articular joint has demonstrated how mechanical stimuli play a pivotal role in cartilage repair and participate in the homeostasis of this tissue. Loading stresses, physiologically experienced by chondrocytes, can upregulate the production of proteins like glycosaminoglycan or collagen, fundamental for articular wellness, as well as promote and preserve cell viability. Therefore, there is a rising interest in the development of bioreactor devices that impose compression, shear stress, and hydrostatic pressure on stem cells. This strategy aims to mimic chondrogenesis and overcome complications like hypertrophic phenotyping and inappropriate mechanical features. This review will analyze the dynamics inside the joint, the natural stimuli experienced by the chondrocytes, and how the biomechanical stimuli can be applied to a stem cell culture in order to induce chondrogenesis.

Keywords: mesenchymal stem cells; tissue engineering; chondrogenesis; osteoarthritis; bioreactor; mechanical stimuli; physical stimulation; compression; shear stress; hydrostatic pressure

1. Introduction

Scientific minds have always expressed a stubborn yearn to master the creation of artificial biological elements in order to emulate the delicate machinery of the human body. The idea of being able to control cell destiny and replace malfunctioning parts of the body with brand new tissues and organs has led to remarkable progress in biological fields such as tissue engineering and regenerative medicine. A promising application of this concept relies on the use of stem cells to originate functional and specialized tissues [1]. Mesenchymal stem cells (MSCs) constitute a specific subtype of multipotent stem cells, which can differentiate into a variety of cell types and offer the advantage of obtaining pure stem cell populations [2]. One of the most challenging ambitions in regenerative biomedicine is to restore damaged articular cartilage, as it is one of the most challenging tissue types to heal by virtue of its anatomical and structural complexity. More precisely, the avascular, alymphatic, and aneural nature of the cartilage, combined with the fact that it is characterized by the chondrocyte cell type only, limits its ability to self-repair [3].

Conventional treatment and modern therapies to treat this singular tissue, ranging from injections to surgical procedures, still suffer, in many instances, from wide variation in clinical outcome, complications, specificity, and effectiveness and a lack of well-grounded long-term reliability [4]. Joint injection is an easy and minimally invasive procedure for the delivery of MSCs as anti-inflammatory mediators and immune-modulating factors [5]. Pain relief, improvement in articular function, and regeneration of cartilage following this treatment have been observed in a growing number of studies [6–8]. However, the efficacy of this procedure is controversial, since after injection, cells might not survive or remain in situ in the long term [9,10]. Satué et al., observed MSCs migrating and engrafting into the damaged cartilage as early as the first day after injection [11]; in contrast, in another recent study, MSCs were mostly found in the synovium but not in the cartilage surrounding the defect [12]. Disappearance of the injected cells within the joint may be due to failure in the extracellular matrix (ECM) attachment mechanism [12]. Although intra-articular injection of MSCs appears to be safe during the short term [13], further investigations, such as randomized controlled trials, are necessary to explore long-term adverse events and reduce the heterogeneous nature of the studies in terms of design, cell number, exogenous factors, and administration protocols.

Tissue engineering has raised interest as a reasonable approach to manage pathologies like osteoarthritis [1]. The latter is a degenerative disease characterized by progressive loss of articular cartilage, synovial inflammation, osteophyte formation, and joint space narrowing that lead to overall stiffness, pain, and loss of mobility of the affected joint. The bases of this escalating damage rely on a compromised balance between anabolic and catabolic mechanisms, which can be consequent to several risk factors like ageing, muscle atrophy, metabolic disorders, inflammatory conditions, injuries and overload, or wrong biomechanics of the joint [14]. This review aims to explore cartilage dynamics and understand what kind of biophysical principles will be beneficial for the engineering-based treatment of degenerative and rheumatic diseases of the joints.

2. Chondrogenesis In Vitro

The essence of regenerative therapy lies in the use of stem cells, bioactive molecules, biomaterials, and their combinations [15]. Physiological chondrogenesis is regulated by specific cytokines and transcription factors, such as the transforming growth factor beta (TGF- β), fibroblast growth factor (FGF), and insulin-like growth factor 1 (IGF-1) [16]. As another example, SRY-related high-mobility group box gene 9 (SOX-9) is a transcription factor essential for chondrogenesis processes [17] and also to avoid dysregulated chondrocyte hypertrophy [18]. Commonly, MSCs undergo chondrogenic differentiation, recognizable by increasing in specific ECM components, when in the presence of TGF- β . This pathway consists of the proper formation of the receptor complex that requires type I and type II serine/threonine kinase receptors and intracellular effectors. The type I receptor family counts seven members which phosphorylate different small mother against decapentaplegic (SMAD) proteins. Transcriptional activation of chondrogenic genes, like those encoding type II collagen and aggrecan, is mediated by the involvement of the type I receptor 5 (ALK 5) and subsequent phosphorylation of SMAD 2/3. Otherwise, TGF- β could bind ALK 1 and activate the SMAD 1/5/8 pathways, resulting in hypertrophy-related gene expression [19]. Nevertheless, one of the clinical limits of this kind of chondrogenic differentiation, based on the TGF- β pathway, relies on the risk of incurring undesired and premature hypertrophy entrance of MSCs [20]. Considering this scenario, a more sophisticated and authentic approach to differentiation is offered by understanding the mechanical forces naturally experienced by chondrogenic progenitors and applying them, even in the absence of exogenous growth factors, to stem cells in order to mimic the same environment within the joint.

3. Influencing the Mechanical Environment

The characteristic structure of the articular cartilage is the result of the dynamic processes that occur within the joint. Chondrocytes experience biomechanical stimuli like compression, shear stress, and hydrostatic pressure [19]. These forces are perceived as a shifting of currents, electrical fields,

or changes in osmolarity and so converted into intracellular signals, influencing mechanisms like transcription, exocytosis, and activity of Na⁺/K⁺-ATPase [21]. Growth factors such as TGF-β, IGF, and bone morphogenetic proteins (BMP)-2,-4,-7 are necessary to stimulate chondrogenic processes and require the presence of calcium ions (Ca²⁺) to regulate cell functions, such as the synthesis of extracellular matrix components. Physical stimuli have been associated with the regulation of Ca²⁺ entry, primarily through voltage-operated calcium channels (VOCCs), transient receptor potential (TRP) channels, and purinergic receptors [22]. Furthermore, VOCC inhibitors have shown to reduce cartilage degradation and the progression of osteoarthritis [23], suggesting their importance in both physiological and pathological milieu. TRP channels, such as TRP vanilloid 4 (TRPV4), which have been linked to upregulation of the SOX9 pathway, or TRPC1, able to guide chondrogenesis in stem cells and regulate the activity of other voltage-dependent ion channels, are also highly involved. Inhibitors for these two receptors, 2-aminoethoxydiphenylborane (2-APB) and Ruthenium Red, have been shown to prevent MSC chondrogenesis induced by pulsed electromagnetic fields (PEMFs) [24]. The structure of the articular cartilage comprises several layers: First, a thin superficial zone, where the collagen fibers are aligned parallel to the surface and the chondrocytes are numerous and flattened. This layer is in tight contact with the synovial fluid, and it can resist shear stresses. Under the first zone, there is a transitional zone which contains especially proteoglycans (PGs) employed for compressive resistance. Here, the collagen is arranged obliquely. Just below, the deep zone can cushion the compressions and presents collagen fibers organized perpendicular to the surface, high concentrations of proteoglycans, and columns of cells. Lastly, the tide mark separates this last zone from the calcified cartilage [25] (Figure 1).

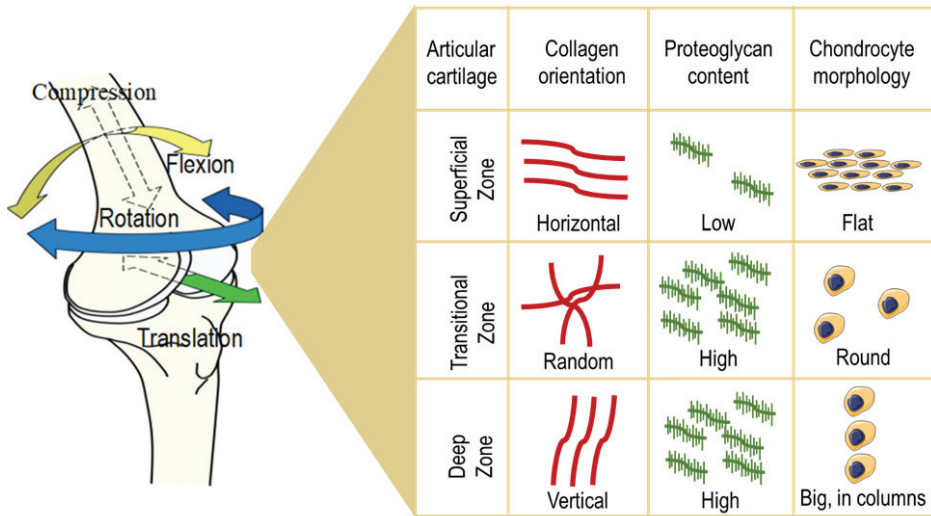


Figure 1. Structure of the articular cartilage. The structure of the articular cartilage comprises several layers: First, a superficial zone, where the collagen fibers are aligned horizontally, the chondrocytes are numerous and flattened, and the proteoglycan content is low. Under the first zone, there is a transitional zone which contains high levels of proteoglycans, randomly arranged collagen, and round-shaped cells. Just below, the deep zone presents vertically aligned collagen fibers, a high concentration of proteoglycans, and columns of cells.

For the sake of simplicity, this tissue could be imagined like a biphasic model: one phase is represented by the interstitial water that permeates the other phase, made up of the solid components of the ECM (collagen, PGs and other proteins). These two phases are extremely interdependent in terms of functionality and biomechanics. Compression is one of the forces experienced by cartilage,

which leads to an internal increase of hydrostatic pressure of the aqueous phase. As a result, the water leaks from the ECM towards the capsule, but the structure of the cartilage will remain unaltered thanks to the PG component. More precisely, the effect of uniaxial compression will be compensated by the tensile stiffness generated by the repulsive forces between the negatively charged carboxylic or sulfonic groups of the glycosaminoglycans (GAGs). When the pressure ceases, the water is again attracted inside the interstices. Tissue compressibility under load reaches even a millimeter, but, when the spring back is not able to compensate hard and long compressions, the structure can be damaged [26]. Shear or rotational stress, which could be defined by the change in thickness with respect to the original height, is another force generated by joint movement and is caused by the tangential friction of synovial fluid on the surface. This movement allows synovial fluid to nourish the cartilage, transport waste materials, and keep the chondrocytes metabolically active with a mechanism of diffusion and fluid convection [27]. Under this condition, the collagen network is the viscoelastic component of the tissue that exhibits cushioning ability. The collagen concentration is directly proportional to resistance to shifting [28]. Weight-bearing articular cartilage of the hip and knee daily experience stress amplitudes from 0.5 to 7.7 MPa and average compression of 13% [29–31]. Chondrocytes show selective responses to various mechanical stimuli. Indeed, dynamic stresses are able to improve the production of ECM components, while static compressions do not lead to great achievements in tissue engineering constructs. Mechanical stimulation triggers those pathways that culminate in maintaining functional ECM in order to provide substantial physical stability against the stresses to which the cartilage is subjected. It is a feedback cycle in which the mechanical stress influences the production of those components which sustain the stress itself. It is not surprising that, in fact, an unbalanced step in this cycle could pave the way to a pathological mechanism which could, in the end, lead to the onset of osteoarthritic features. If physiological stimulation fails, following, for example, sedentary habits, or it exceeds the ability of the tissue to sustain it, e.g., excessive mechanical loading [32], the chondrocytes will miss most of the input to produce the new ECM, resulting in unbalanced homeostasis. It is highly recommended to patients who suffer from early osteoarthritis, who are able to conduct physical exercise, to encourage the movement of the diseased articulation in order to stimulate the restoration of the physiological cycle, which may lead to improvements in biochemical disorders. This dynamic environment should be considered in tissue engineering approaches in order to realize as realistic a construct as possible. The challenge proposed is to move from a purely biological view of the natural cell to an engineered one.

Stem cells are studied as structures able to sense and transmit physical stimuli, translating them into biological and mechanical responses, since they have greater mechanical sensitivity than adult cells [33,34]. As already mentioned, ion channels are paramount in triggering those signaling pathways which lead to matrix turnover and homeostasis, and an intracellular increase of Ca^{2+} levels has been considered as one of the stem cell responses to mechanical load. Sequestration of calcium ions and inhibition of VOCCs and other channels have been shown to attenuate the effects of mechanical stimulation. More specifically, during physical stimulation of MSCs, Ca^{2+} is known to be involved in the activation of pivotal transcription factors leading to chondrogenic differentiation [20]. In the next section, some interesting works on the topic are presented. In some of those, no exogenous growth factors were added during the experiment. Hence, chondrogenic differentiation was achieved exclusively as a result of load applications. Figure 2 illustrates the different types of mechanical forces applied in these experiments.

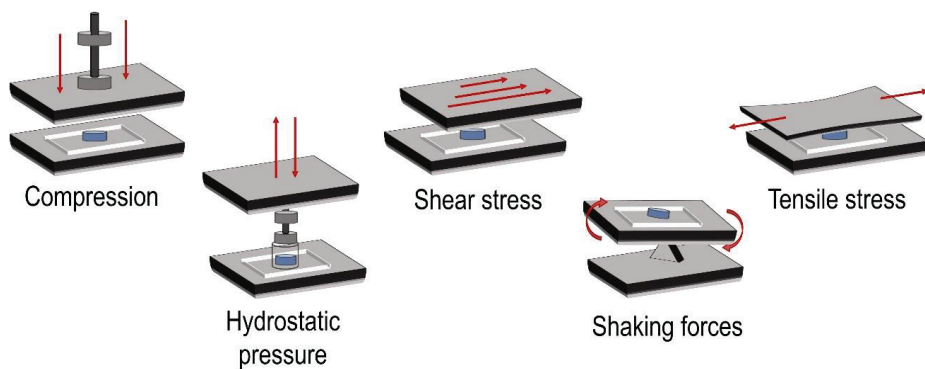


Figure 2. Types of mechanical stimuli experienced by the cells. Stem cell cultures, used in tissue engineering, undergo biophysical stimulation in order to promote chondrogenesis and recreate the dynamic environment within the joint.

4. Practical Applications

To reveal the physiological effect of mechanical stimulation on stem cells, loading machines were designed to be able to apply different types of mechanical forces with different intensity, duration, and frequency.

Cochis et al. [35] cultivated MSCs in a methylcellulose solution retained within a porous polyurethane matrix to evaluate the suitability of the matrix in supporting mechanically induced chondrogenesis of the cells in the absence of exogenous factors. The composite underwent a combination of compression and shear forces by the use of a bioreactor which applied compressive and rolling movements through a ceramic ball. This ball compressed the scaffold dynamically at 1 Hz, resulting in a strain amplitude of 10–20% of its height, and provided shear stress with oscillations perpendicular to the scaffold axis of $\pm 25^\circ$ at 1 Hz. After 21 days, the samples were analyzed by reverse transcription polymerase chain reaction (RT-PCR), biochemical, histochemical, and immunofluorescent assays, and the authors concluded that the physical stimulation led to the activation of TGF- β and to accumulation in the surrounding matrix of glycosaminoglycans and type II collagen, confirming the chondrogenesis process.

Another study on the involvement of mechanical forces in the destiny of adipose-derived mesenchymal stem cells (ADSCs) by Zhang et al. [16] highlights the role of dynamic compression in combination with exogenous SOX-9 on chondrogenesis. ADSCs were seeded in 3D porous poly(lactic-co-glycolic acid) (PLGA) scaffolds. Gradual, meaning with a unique structure at each level, and uniform scaffolds were subjected, with the use of a bioreactor, to sequential uniaxial compressions of 5–10% strain amplitude and frequency of 0.1 Hz. The authors analyzed the morphology of the ADSCs and the ECM deposition within the scaffolds by scanning electron microscopy (SEM), noticing that ECM accumulation by ADSCs, on gradual scaffolds and in the presence of SOX-9, was higher than that in uniform scaffolds or in gradual scaffolds without SOX-9. RT-PCR analysis also showed the highest expressions of Proteoglycan 4 (PRG4), Parathyroid hormone-related protein (PTHrP), type II collagen, aggrecan, SOX-9, and Hypoxia-inducible factor 1- α (HIF-1 α) in the group of SOX-9 gradual scaffolds.

To better understand the single contributions of compression and shear forces in chondrogenic induction, Schatti et al. [27] analyzed these two stimuli, both alone and in combination. MSCs were seeded onto polyurethane scaffolds and underwent either compression at 1 Hz, in a strain amplitude of 10–20%, or oscillation of $\pm 25^\circ$ at 1 Hz, or a combination of both loads. Oscillation was imposed through the shifting of a ball perpendicularly to the scaffold axis. Superimposed compression was applied along the axis of the scaffold as well. The results suggested that stimulation by combined

strains, instead of the application a single stimulus alone, is the best way to assure a chondrogenic phenotype in the absence of exogenous growth factors. The authors gave evidence of significant upregulation, in comparison to the control group, of the chondrogenesis markers (type II collagen, Aggrecan (AGG), Cartilage oligomeric matrix protein (COMP), SOX-9) only in the samples loaded with both compression and shear. Also, this last group was the only one in which type II collagen immunostaining was detected and that seemed to maintain a constant release of GAG in medium.

Cheng et al. [36] developed a novel construct made up by platelet-rich fibrin (PRF) membrane, which functions as a growth-factor-rich scaffold for bone-marrow-derived stem cells (BMSCs), for transplantation in cartilage defects. Flexibility of the neo-formed cartilage and differentiation of the stem cells were achieved through stimulation by hydrostatic pressure, in order to achieve boundaryless tissue consistency between the formed neocartilage and the damaged host cartilage in the temporomandibular joint (TMJ). TMJ offers an interesting environment for evaluating the integration of a cartilage construct within the damaged surface and to compare the behavioral differences of fibrocartilage in comparison to hyaline cartilage of the knee joint. In TMJ, the control of applied loads is difficult because of the impossibility to immobilize this joint, so the adaptation and responses of the construct to biophysical stimuli are more consistent and are extremely suitable to be studied as a model for cartilage regeneration approaches [37]. The hydrostatic pressure device, in this experiment, applied compression ranging from 90 to 150 kPa, revealing that proliferation and chondrogenic markers of the BMSC/PRF constructs were highest during the first days and gradually decreased at 6 days, suggesting that BMSCs could have limited chondrogenic capacity in relation to decreased growth factor release from the PRF. The authors concluded that pressure is an indispensable stimulus in order to promote cell proliferation, tissue regeneration, and repair mechanisms and to obtain a physiologic hierarchical and polar arrangement of the neoformed tissue.

4.1. Influence of Cell Distribution

Gardner et al. [38] simulated the multiaxial mechanical loads that characterize the articular joint and observed the results derived from applying these forces on fibrin–poly(ester-urethane) scaffolds seeded with MSCs. The constructs were divided into three groups, represented in Figure 3: in the first group, the cells were evenly dispersed throughout the scaffold (Uniform); in the second group, the cells were asymmetrically disseminated within the matrix, forming a thin layer on the surface (Asymmetric); and in the third group, the cells were allowed to adhere only to the upper face of the scaffold (Surface Only). These different distributions were investigated in terms of matrix deposition in response to mechanical stress. The protocol employed 20 cycles of 10% compression, achieved by the raising and lowering of a ball onto the scaffold. The rotation on the ball generated shear friction of $\pm 25^\circ$ at 1 Hz. Histological and immunohistochemical analysis showed that there was an increase in glycosaminoglycans and type II collagen levels in the Asymmetric group in comparison to the other two groups. Besides this, the cells in the Surface Only group produced a small amount of matrix, suggesting a hypertrophic-like phenotype. In conclusion, the pattern of cell distribution within the scaffold is a critical parameter to take into consideration, and matrix deposition could be enhanced by considering the anisotropic properties of the materials.

Cell distribution can also be controlled by physiological mobilization of the cells, from their niches to different areas of the scaffold, employing biomechanical stimulation. Long-lasting regeneration of articular cartilage after surgical techniques like autologous chondrocyte implantation (ACI), mosaicplasty, and microfracture can be hampered by failure to attract progenitor cells, leading to the formation of fibrocartilage. In vitro loading compression provided by a bioreactor, such as 10% strain at 0.3 Hz frequency, applied intermittently for 24 hours, was shown to induce the mobilization of MSCs from a reservoir to an alginate scaffold located above it [39]. This experiment aimed to provide a model of a cartilage defect in the tibial plateau in order to evaluate the possible effect of biomechanical loading on cell recruitment from the subchondral bone. The mobilization of the stem cells from the reservoir required the supporting effect of laminin-521 (LN-521), as it is a basement

membrane protein which exerts a pivotal role in cell adhesion and migration mechanisms. The processes involved in antigravity migration within the scaffold are still the object of study and could imply extracellular signals between the cells and also physical fluidic movements induced by the stimulation of the bioreactor.

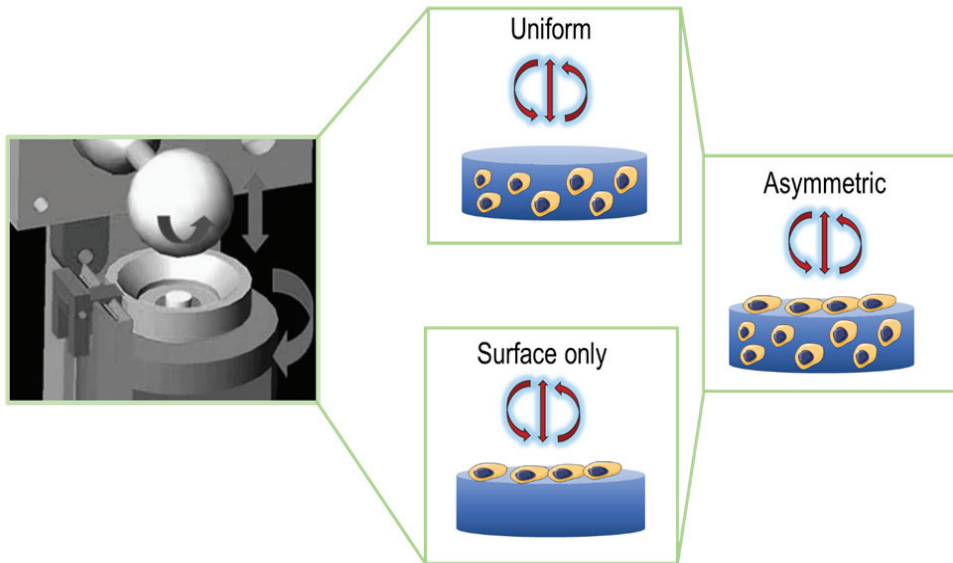


Figure 3. Different distributions of mesenchymal stem cells (MSCs) in fibrin–polyurethane composite scaffolds. Gardner et al., imposed a protocol of mechanical loads on scaffolds seeded with MSCs. The study comprised three types of distribution: cells evenly dispersed throughout the scaffold (Uniform), cells asymmetrically disseminated, forming a thin layer on the surface (Asymmetric), and cells allowed to adhere only to the upper face of the scaffold (Surface Only).

4.2. Osteogenic Involvement

Another recent study by Carrol et al., presented the role of mechanical stimulation in MSC osteogenic differentiation [40]. This work explains about the ability of cyclic tensile strain (CTS) to regulate the initiation of MSC differentiation and, more specifically, their involvement in the endochondral pathway. MSCs embedded in fibrin hydrogels experienced uniaxial tensile deformation in a novel bioreactor system. The authors found out that CTS, in the absence of differentiation factors, can enhance the expression of tenogenic and osteogenic markers. The lack of evident chondrogenesis suggests that CTS could take part in directly initiating intramembranous ossification. When in the presence of chondrogenic growth factor (TGF- β 3), instead, CTS induced increased proteoglycan and collagen production and enhanced upregulation of the markers of endochondral ossification (Bone morphogenetic protein 2 (BMP2), Runt-related transcription factor 2 (RUNX2), (Alkaline phosphatase) ALP, Osteopontin (OPN), Collagen Type X Alpha 1 Chain (COL10A1)). The authors concluded that CTS is an inducer of both endochondral and intramembranous ossification of stem cells, depending on the environment.

Endochondral ossification-based engineering techniques are promising strategies to provide regeneration of large defects. Hybrids of bone and cartilage tissue from induced pluripotent stem cells (iPSCs) have been achieved by the combined use of osteogenic and chondrogenic media in addition to mechanical stimulation, by means of shaking forces [41]. iPSCs offer the advantage of self-organizing in culture medium into cell aggregates, known as embryoid bodies (EB), without the support of scaffolds, providing a model to examine mechanisms of tissue differentiation and organ development. In this

experiment, the aggregates, when maintained in osteogenic medium culture, underwent osteogenic induction, reaching mineralization; when, instead, the aggregates were set first in osteogenic and later in chondrogenic medium, they were able to originate both tissues by expressing osteogenic and chondrogenic marker genes. The percentages of bone and cartilage composition seem to be subject to variations in culture periods, medium components, and shaking frequency, allowing the generation of easily manipulated osteochondral organoids.

4.3. Co-Cultures

Co-cultures of articular chondrocytes (ACs) and MSCs have been proposed to overcome problems associated with the dedifferentiation of chondrocytes during *in vitro* expansion or to the tendency of MSCs to acquire hypertrophic features [42,43]. In co-cultures, the milieu created by the chondrocytes can, in fact, stimulate stem cell differentiation, which, in turn, acts as an enhancer of phenotype stability and the proliferation of chondrocytes by stimulating cell–cell adhesion mechanisms and by secreting several paracrine factors like growth factors and cytokines. Proper mechanical stress, in the form of cyclic sinusoidal dynamic tensile mechanical stimulation, can stimulate the co-culture by improving the deposition of ECM (GAGs, type II collagen) and the expression of regulatory factors (TGF β , SOX9) and promoting the exchange of molecules between MSCs and chondrocytes [44].

Co-cultures offer the advantage of overcoming the tissue engineering challenge of maintaining a sufficient number of functional chondrocytes which will provide structural reliability with the right amount of ECM. Scaffolds embedded with ADSCs, subjected to cyclic compression in bioreactors, could benefit from the presence of chondrocytes, since they are able to release paracrine factors (i.e., TGF- β 1 and IGF-1), guiding stem cells towards chondrogenic differentiation. This approach has been used to reduce the use of exogenous growth factors, which can instead be synthesized by a proper number of chondrocytes during *in vitro* expansion [35]. Even though similar production of type II collagen and GAGs was observed in single and co-cultures, the latter were shown to be able to suppress the expression of Col I, Col X, and Tumor necrosis factor alpha (TNF- α) markers [45].

4.4. Computational Approach

The spreading use of bioreactors has offered the possibility to observe, in a feasible and controlled way, the process of differentiation of stem cells under mechanical stresses, leading to expanded understanding of the mechanisms underpinning the relationship between physical stimulation and biological responses. The outcome of these kinds of stimulation is strongly dependent on the design of the machine, the type of mechanical forces, their intensity and frequency, and the times of stimulation, not to mention the variables related to the scaffolds and the cells. Therefore, the results coming from different studies lead to high heterogeneity and difficulties in providing a uniform consensus about the best protocol to induce processes of differentiation. For this reason, computational models can help, since they have been suggested and used to further investigate tissue engineering strategies. These approaches could be employed to characterize the mechanical stresses imposed by the bioreactors, refine scaffold geometry, and analyze physiobiological dynamics and cell behavior [46]. *In silico* experiments complement *in vitro* and *in vivo* analysis, addressing some complex questions which can be difficult to answer through more traditional approaches. Theoretical assumptions, simplifications in the conceptual framework, and the need to operate consistent validations could limit their use. Koh et al. [47] investigated the mechanisms of cartilage regeneration in osteochondral defects by using 3D medical imaging of the knee joint and analyzing the mechano-regulation processes underlying MSC differentiation. Two computational finite element (FE) models were employed to investigate the effects of physical stresses on cell regenerative mechanisms, as well as physiological processes like mitosis and cell death. The aim of the models was to provide predictions of the influence of different loading conditions on the whole system. The results indicated that simulation of a stance-phase gait cycle performed according to the ISO14,243-1 standard [48] induces more consistent cartilage regeneration than simulation of a vertical loading. This is because when the vertical loading was simulated, it

was predicted that endochondral ossification would sustain bone development and that hydrostatic pressure would induce the formation of fibrocartilage.

5. Conclusions

Designing tissue engineering strategies for articular cartilage requires a thorough control of stem cell fate. The latter can be achieved through a more traditional approach using growth factors or, as suggested by the studies discussed above, by applying precise extrinsic mechanical loads, able to mimic the environment within the joint. Therefore, mechanical loading has been proposed as an alternative strategy to induce MSC chondrogenesis without the use of exogenous factors. Depending on the stimulus applied, promotion of specific tissue-related elements can be achieved. It can be concluded that shear stress and hydrostatic pressure, which exert their maximum effect on the superficial zone of the tissue, can increase type II collagen synthesis. Superimposed compression is, instead, the leading promoter of glycosaminoglycan production, since these components are directly involved in structural maintenance following perpendicular stresses. As a future perspective, functionalized bioengineering needs to take into account that de novo tissues should not lack the excellent organization of the cartilage that is critical for their role. A more in-depth study of the effects of different forces imposed on MSC cultures could represent a possible key to creating the original cartilage disposition with parallel collagen fibers in the superficial zone and perpendicular alignment in the thicker layer. Another aspect that should be investigated is the exact biomolecular mechanism by which the cells respond positively to friction and pressure. Tribology offers paramount principles to follow in order to understand and truly benefit the regenerative sciences.

Author Contributions: Conceptualization, S.R. and G.M.; writing—original draft preparation, S.R.; G.L.; writing—review and editing, M.A.S.; visualization, S.R.; supervision, G.M. All authors have read and agreed to the published version of the manuscript.

Funding: This work was supported by the University Research Project Grant (Triennial Research Plan 2016-2018), Department of Biomedical and Biotechnological Sciences (BIOMETEC), University of Catania, Italy.

Conflicts of Interest: The authors declare no conflict of interest.

References

1. Szychlinska, M.A.; Castrogiovanni, P.; Nsir, H.; Di Rosa, M.; Guglielmino, C.; Parenti, R.; Calabrese, G.; Pricoco, E.; Salvatorelli, L.; Magro, G.; et al. Engineered cartilage regeneration from adipose tissue derived-mesenchymal stem cells: A morphomolecular study on osteoblast, chondrocyte and apoptosis evaluation. *Exp. Cell. Res.* **2017**, *357*, 222–235. [[CrossRef](#)]
2. Rosenbaum, A.J.; Grande, D.A.; Dines, J.S. The use of mesenchymal stem cells in tissue engineering: A global assessment. *Organogenesis* **2008**, *4*, 23–27. [[CrossRef](#)] [[PubMed](#)]
3. Archer, C.W.; Francis-West, P. The chondrocyte. *Int. J. Biochem. Cell. Biol.* **2003**, *35*, 401–404. [[CrossRef](#)]
4. Ashammakhi, N.; Ahadian, S.; Darabi, M.A.; El Tahchi, M.; Lee, J.; Suthiwanich, K.; Sheikhi, A.; Dokmeci, M.R.; Oklu, R.; Khademhosseini, A. Minimally Invasive and Regenerative Therapeutics. *Adv. Mater.* **2018**, *31*, 1804041. [[CrossRef](#)]
5. Wang, Y.; Yuan, M.; Guo, Q.-Y.; Lu, S.-B.; Peng, J. Mesenchymal Stem Cells for Treating Articular Cartilage Defects and Osteoarthritis. *Cell. Transplant.* **2015**, *24*, 1661–1678. [[CrossRef](#)]
6. Li, L.; Duan, X.; Fan, Z.; Chen, L.; Xing, F.; Xu, Z.; Chen, Q.; Xiang, Z. Mesenchymal Stem Cells in Combination with Hyaluronic Acid for Articular Cartilage Defects. *Sci. Rep.* **2018**, *8*, 9900. [[CrossRef](#)]
7. ter Huurne, M.; Schelbergen, R.; Blattes, R.; Blom, A.; de Munter, W.; Grevers, L.C.; Jeanson, J.; Noël, D.; Casteilla, L.; Jorgensen, C.; et al. Antiinflammatory and chondroprotective effects of intraarticular injection of adipose-derived stem cells in experimental osteoarthritis. *Arthritis Rheum.* **2012**, *64*, 3604–3613. [[CrossRef](#)] [[PubMed](#)]
8. Vega, A.; Martín-Ferrero, M.A.; Del Canto, F.; Alberca, M.; García, V.; Munar, A.; Orozco, L.; Soler, R.; Fuentes, J.J.; Huguet, M.; et al. Treatment of Knee Osteoarthritis With Allogeneic Bone Marrow Mesenchymal Stem Cells: A Randomized Controlled Trial. *Transplantation* **2015**, *99*, 1681–1690. [[CrossRef](#)] [[PubMed](#)]

9. Pas, H.I.; Winters, M.; Haisma, H.J.; Koenis, M.J.; Tol, J.L.; Moen, M.H. Stem cell injections in knee osteoarthritis: A systematic review of the literature. *Br. J. Sports Med.* **2017**, *51*, 1125–1133. [[CrossRef](#)]
10. Zwolaneck, D.; Satué, M.; Proell, V.; Godoy, J.R.; Odörfer, K.I.; Flicker, M.; Hoffmann, S.C.; Rütlicke, T.; Erben, R.G. Tracking mesenchymal stem cell contributions to regeneration in an immunocompetent cartilage regeneration model. *JCI Insight* **2017**, *2*, 87322. [[CrossRef](#)] [[PubMed](#)]
11. Satué, M.; Schüler, C.; Ginner, N.; Erben, R.G. Intra-articularly injected mesenchymal stem cells promote cartilage regeneration, but do not permanently engraft in distant organs. *Sci. Rep.* **2019**, *9*, 10153. [[CrossRef](#)] [[PubMed](#)]
12. Enomoto, T.; Akagi, R.; Ogawa, Y.; Yamaguchi, S.; Hoshi, H.; Sasaki, T.; Sato, Y.; Nakagawa, R.; Kimura, S.; Ohtori, S.; et al. Timing of Intra-Articular Injection of Synovial Mesenchymal Stem Cells Affects Cartilage Restoration in a Partial Thickness Cartilage Defect Model in Rats. *Cartilage* **2020**, *11*, 122–129. [[CrossRef](#)] [[PubMed](#)]
13. Lee, W.S.; Kim, H.J.; Kim, K.I.; Kim, G.B.; Jin, W. Intra-Articular Injection of Autologous Adipose Tissue-Derived Mesenchymal Stem Cells for the Treatment of Knee Osteoarthritis: A Phase IIb, Randomized, Placebo-Controlled Clinical Trial. *Stem Cells Transl. Med.* **2019**, *8*, 504–511. [[CrossRef](#)] [[PubMed](#)]
14. Di Rosa, M.; Szychlińska, M.A.; Tibullo, D.; Malaguarnera, L.; Musumeci, G. Expression of CHI3L1 and CHIT1 in osteoarthritic rat cartilage model. A morphological study. *Eur. J. Histochem.* **2014**, *58*, 2423. [[CrossRef](#)] [[PubMed](#)]
15. Szychlińska, M.A.; Calabrese, G.; Ravalli, S.; Parrinello, N.L.; Forte, S.; Castrogiovanni, P.; Pricoco, E.; Imbesi, R.; Castorina, S.; Leonardi, R.; et al. Cycloastragenol as an Exogenous Enhancer of Chondrogenic Differentiation of Human Adipose-Derived Mesenchymal Stem Cells. A Morphological Study. *Cells* **2020**, *9*, 347. [[CrossRef](#)] [[PubMed](#)]
16. Zhang, Y.; Tang, C.L.; Chen, W.J.; Zhang, Q.; Wang, S.L. Dynamic compression combined with exogenous SOX-9 promotes chondrogenesis of adipose-derived mesenchymal stem cells in PLGA scaffold. *Eur. Rev. Med. Pharmacol. Sci.* **2015**, *19*, 2671–2678.
17. Ikeda, T.; Kawaguchi, H.; Kamekura, S.; Ogata, N.; Mori, Y.; Nakamura, K.; Ikegawa, S.; Chung, U. Distinct roles of Sox5, Sox6, and Sox9 in different stages of chondrogenic differentiation. *J. Bone Miner. Metab.* **2005**, *23*, 337–340. [[CrossRef](#)]
18. Cucchiari, M.; Thurn, T.; Weimer, A.; Kohn, D.; Terwilliger, E.F.; Madry, H. Restoration of the extracellular matrix in human osteoarthritic articular cartilage by overexpression of the transcription factor SOX9. *Arthritis Rheum.* **2007**, *56*, 158–167. [[CrossRef](#)]
19. Fahy, N.; Alini, M.; Stoddart, M.J. Mechanical stimulation of mesenchymal stem cells: Implications for cartilage tissue engineering. *J. Orthop. Res.* **2018**, *36*, 52–63. [[CrossRef](#)]
20. Hellingman, C.A.; Koevoet, W.; Kops, N.; Farrell, E.; Jahr, H.; Liu, W.; Baatnburg de Jong, R.J.; Frenz, D.; van Osch, G. Fibroblast Growth Factor Receptors in in-Vitro and in-Vivo Chondrogenesis: Relating Tissue Engineering Using Adult Mesenchymal Stem Cells To Embryonic Development. *Tissue Eng. Part A* **2010**, *16*, 545–556. [[CrossRef](#)]
21. Schulz, R.M.; Bader, A. Cartilage tissue engineering and bioreactor systems for the cultivation and stimulation of chondrocytes. *Eur. Biophys. J.* **2007**, *36*, 539–568. [[CrossRef](#)] [[PubMed](#)]
22. Uzielienė, I.; Bernotas, P.; Mobasher, A.; Bernotienė, E. The Role of Physical Stimuli on Calcium Channels in Chondrogenic Differentiation of Mesenchymal Stem Cells. *Int. J. Mol. Sci.* **2018**, *19*, 2998. [[CrossRef](#)]
23. Matta, C.; Zákány, R.; Mobasher, A. Voltage-Dependent Calcium Channels in Chondrocytes: Roles in Health and Disease. *Curr. Rheumatol. Rep.* **2015**, *17*, 43. [[CrossRef](#)]
24. Parate, D.; Franco-Obregón, A.; Fröhlich, J.; Beyer, C.; Abbas, A.A.; Kamarul, T.; Hui, J.H.P.; Yang, Z. Enhancement of mesenchymal stem cell chondrogenesis with short-term low intensity pulsed electromagnetic fields. *Sci. Rep.* **2017**, *7*, 1–13. [[CrossRef](#)]
25. Sophia Fox, A.J.; Bedi, A.; Rodeo, S.A. The basic science of articular cartilage: Structure, composition, and function. *Sports Health* **2009**, *1*, 461–468. [[CrossRef](#)] [[PubMed](#)]
26. Jackson, A.; Gu, W. Transport Properties of Cartilaginous Tissues. *Curr. Rheumatol. Rev.* **2009**, *5*, 40–50. [[CrossRef](#)] [[PubMed](#)]
27. Schätti, O.; Grad, S.; Goldhahn, J.; Salzmann, G.; Li, Z.; Alini, M.; Stoddart, M.J. A combination of shear and dynamic compression leads to mechanically induced chondrogenesis of human mesenchymal stem cells. *Eur. Cell. Mater.* **2011**, *22*, 214–225. [[CrossRef](#)] [[PubMed](#)]

28. Cohen, N.P.; Foster, R.J.; Mow, V.C. Composition and Dynamics of Articular Cartilage: Structure, Function, and Maintaining Healthy State. *J. Orthop. Sport Phys. Ther.* **1998**, *28*, 203–215. [[CrossRef](#)]
29. Afoke, N.Y.; Byers, P.D.; Hutton, W.C. Contact pressures in the human hip joint. *J. Bone Joint. Surg. Br.* **1987**, *69*, 536–541. [[CrossRef](#)]
30. Mow, V.C.; Wang, C.C. Some bioengineering considerations for tissue engineering of articular cartilage. *Clin. Orthop. Relat. Res.* **1999**, *367*, S204–S223. [[CrossRef](#)]
31. Eisenhart, R.; Adam, C.; Steinlechner, M.; Muller-Gerbl, M.; Eckstein, F. Quantitative determination of joint incongruity and pressure distribution during simulated gait and cartilage thickness in the human hip joint. *J. Orthop. Res.* **1999**, *17*, 532–539. [[CrossRef](#)]
32. Chang, S.H.; Mori, D.; Kobayashi, H.; Mori, Y.; Nakamoto, H.; Okada, K.; Taniguchi, Y.; Sugita, S.; Yano, F.; Chung, U.I.; et al. Excessive mechanical loading promotes osteoarthritis through the gremlin-1-NF- κ B pathway. *Nat. Commun.* **2019**, *10*, 1442. [[CrossRef](#)]
33. Cheng, B.; Liu, Y.; Zhao, Y.; Li, Q.; Liu, Y.; Wang, J.; Chen, Y.; Zhang, M. The role of anthrax toxin protein receptor 1 as a new mechanosensor molecule and its mechanotransduction in BMSCs under hydrostatic pressure. *Sci. Rep.* **2019**, *9*, 12642. [[CrossRef](#)] [[PubMed](#)]
34. Chowdhury, F.; Na, S.; Li, D.; Poh, Y.C.; Tanaka, T.S.; Wang, F.; Wang, N. Material properties of the cell dictate stress-induced spreading and differentiation in embryonic stem cells. *Nat. Mater.* **2010**, *9*, 82–88. [[CrossRef](#)]
35. Cochis, A.; Grad, S.; Stoddart, M.J.; Farè, S.; Altomare, L.; Azzimonti, B.; Alini, M.; Rimondini, L. Bioreactor mechanically guided 3D mesenchymal stem cell chondrogenesis using a biocompatible novel thermo-reversible methylcellulose-based hydrogel. *Sci. Rep.* **2017**, *7*, 45018. [[CrossRef](#)]
36. Cheng, B.; Tu, T.; Shi, X.; Liu, Y.; Zhao, Y.; Zhao, Y.; Li, C.; Chen, H.; Chen, Y.; Zhang, M. A novel construct with biomechanical flexibility for articular cartilage regeneration. *Stem. Cell. Res. Ther.* **2019**, *10*, 298. [[CrossRef](#)]
37. Kuo, J.; Zhang, L.; Bacro, T.; Yao, H. The region-dependent biphasic viscoelastic properties of human temporomandibular joint discs under confined compression. *J. Biomech.* **2010**, *43*, 1316–1321. [[CrossRef](#)] [[PubMed](#)]
38. Gardner, O.F.W.; Musumeci, G.; Neumann, A.J.; Eglin, D.; Archer, C.W.; Alini, M.; Stoddart, M.J. Asymmetrical seeding of MSCs into fibrin–poly(ester-urethane) scaffolds and its effect on mechanically induced chondrogenesis. *J. Tissue Eng. Regen. Med.* **2017**, *11*, 2912–2921. [[CrossRef](#)] [[PubMed](#)]
39. Gamez, C.; Schneider-Wald, B.; Schuette, A.; Mack, M.; Hauk, L.; Khan, A.U.M.; Gretz, N.; Stoffel, M.; Bieback, K.; Schwarz, M.L. Bioreactor for mobilization of mesenchymal stem/stromal cells into scaffolds under mechanical stimulation: Preliminary results. *PLoS ONE* **2020**, *15*, 0227553. [[CrossRef](#)]
40. Carroll, S.F.; Buckley, C.T.; Kelly, D.J. Cyclic Tensile Strain Can Play a Role in Directing both Intramembranous and Endochondral Ossification of Mesenchymal Stem Cells. *Front. Bioeng. Biotechnol.* **2017**, *5*, 73. [[CrossRef](#)] [[PubMed](#)]
41. Limraksasin, P.; Kondo, T.; Zhang, M.; Okawa, H.; Osathanon, T.; Pavasant, P.; Egusa, H. In Vitro Fabrication of Hybrid Bone/Cartilage Complex Using Mouse Induced Pluripotent Stem Cells. *Int. J. Mol. Sci.* **2020**, *21*, 581. [[CrossRef](#)] [[PubMed](#)]
42. Meretoja, V.V.; Dahlin, R.L.; Kasper, F.K.; Mikos, A.G. Enhanced chondrogenesis in co-cultures with articular chondrocytes and mesenchymal stem cells. *Biomaterials* **2012**, *33*, 6362–6369. [[CrossRef](#)] [[PubMed](#)]
43. Mueller, M.B.; Tuan, R.S. Functional characterization of hypertrophy in chondrogenesis of human mesenchymal stem cells. *Arthritis Rheum.* **2008**, *58*, 1377–1388. [[CrossRef](#)] [[PubMed](#)]
44. Ouyang, X.; Xie, Y.; Wang, G. Mechanical stimulation promotes the proliferation and the cartilage phenotype of mesenchymal stem cells and chondrocytes co-cultured in vitro. *Biomed. Pharmacother.* **2019**, *117*, 109146. [[CrossRef](#)] [[PubMed](#)]
45. Chen, C.H.; Kuo, C.Y.; Chen, J.P. Effect of Cyclic Dynamic Compressive Loading on Chondrocytes and Adipose-Derived Stem Cells Co-Cultured in Highly Elastic Cryogel Scaffolds. *Int. J. Mol. Sci.* **2018**, *19*, 370. [[CrossRef](#)]
46. Pearce, D.; Fischer, S.; Huda, F.; Vahdati, A. Applications of Computer Modeling and Simulation in Cartilage Tissue Engineering. *Tissue Eng. Regen. Med.* **2020**, *17*, 1–13. [[CrossRef](#)]

47. Koh, Y.-G.; Lee, J.-A.; Lee, H.-Y.; Kim, H.-J.; Kang, K.-T. Biomechanical Evaluation of the Effect of Mesenchymal Stem Cells on Cartilage Regeneration in Knee Joint Osteoarthritis. *Appl. Sci.* **2019**, *9*, 1868. [[CrossRef](#)]
48. International Organization for Standardization (ISO). *Implants for Surgery—Wear of Total Knee-Joint Prostheses—Part 1: Loading and Displacement Parameters for Wear-Testing Machines with Load Control and Corresponding Environmental Conditions for Test*; ISO 14243-1:2009; ISO: Geneva, Switzerland, 2009.



© 2020 by the authors. Licensee MDPI, Basel, Switzerland. This article is an open access article distributed under the terms and conditions of the Creative Commons Attribution (CC BY) license (<http://creativecommons.org/licenses/by/4.0/>).

MDPI
St. Alban-Anlage 66
4052 Basel
Switzerland
Tel. +41 61 683 77 34
Fax +41 61 302 89 18
www.mdpi.com

Applied Sciences Editorial Office
E-mail: appls@mdpi.com
www.mdpi.com/journal/appls



MDPI
St. Alban-Anlage 66
4052 Basel
Switzerland

Tel: +41 61 683 77 34
Fax: +41 61 302 89 18

www.mdpi.com



ISBN 978-3-0365-3940-9